Degradation Modeling and Reliability Analysis of Bridge Rebar Corrosion

By Zhanhang Li

A thesis submitted to the

School of Graduate Studies

Rutgers, The State University of New Jersey

In partial fulfillment of the requirements

For the degree of

Master of Science

Graduate Program in Industrial and Systems Engineering

Written under the Direction of

Dr. David Coit

And approved by

———————————————

———————————————

———————————————

———————————————

New Brunswick, New Jersey

October 2020

ABSTRACT OF THE THESIS

Degradation Modeling and Reliability Analysis of Bridge Rebar Corrosion

By ZHANHANG LI

Thesis Director:

David Coit

In this thesis, different models of steel rebar degradation of bridges are established, and machine learning approaches are applying to give forecasts to the rebar degradation level. Reinforced concrete is a kind of building materials which is widely used in the world. It has many advantages such as firm, durable, good fire resistance, lower cost, and saving steel than ordinary steel structure. However, as the concrete structure ages, the concrete surface may crack. This can cause the chloride ions to penetrate the concrete and then touch and react with the steel bars, which can lead to corrosion. The corrosion of bridge rebar is one of the main factors affecting the reliability and stability of bridges, and the maintenance of reinforced concrete costs a lot of resource and efforts. United States spends $8.3 billion each year for mitigation and rehabilitation of bridge decks. Therefore, it is necessary to obtain the best maintenance strategy through research on the degradation process of bridge rebar, to reduce the risk and save maintenance cost. There have been many studies on the degradation process of concrete, which have involved in-depth analysis on the degradation of rebars embedded in concrete. However, when applied to real situations, the results of these studies either focus too much on physical and chemical processes and make the model too complex or are not specific enough to take the real situation into account.

Since the corrosion process is irreversible and uncertain, the degradation process can be expressed as a gamma process. The influence of concrete crack width, concrete crack depth, and chloride ion concentration on the corrosion of bridge reinforcement was considered in the degradation process model. Considering the above situation, different degradation models for steel corrosion are proposed in this research, including a degradation model for linear gamma process affected by multiple factors, an accelerated experimental degradation model for linear gamma degradation process, and a two-stage degradation model. Based on the experimental data, the maximum likelihood estimation method is used to give the parameter values of different degradation models. The influence of crack width, crack depth and chloride ion concentration on concrete covered rebar degradation under different models is also analyzed. The degradation of rebar in two stages is studied from two aspects of degradation latency and degradation increment. The corresponding reliability function are derived and applied to evaluate the impact of the environmental stress. Besides, machine learning approaches help to give forecasts and the performance are analyzed. In this thesis, linear regression model and BP-ANN are applied to forecast the rebar degradation levels. The forecast results are compared between different materials and different approached. In the end, the Bi-LSTM network combined with gamma-gamma two stage degradation model is applied to give forecasts of the rebar degradation level. This research is helpful to determine the degree of concrete covered rebar degradation and provides a reference for the research on concrete covered rebar corrosion and reinforcement of bridges and buildings. At the same time, the model proposed in this study can also be applied to the modeling and analysis of other product degradation processes.

Contents

List of Figures

List of Tables

Nomenclature

The notation used in formulating the reliability and cost rate models in Sections 3 and 4 is now listed. CDF means cumulative distribution function, while PDF means probability density function.

$X(t)$ = Degradation level at time t

α_0 = Shape parameter of a gamma distribution

a = Pre-cracking size on the concrete surface

β = Scale parameter of a gamma distribution

β_0 = Inherent factor for each rebar in scale parameter

$\beta(\mathbf{u})$ = Scale parameter of gamma distribution when given $\mathbf{u}$

$\alpha(t)$ = Shape parameter of gamma distribution at time t for a gamma process

$g(\cdot)$ = Gamma distribution probability density function

u_1 = Parameter determines whether there is artificial crack on the concrete

u_2 = Artificial crack width on the concrete

u_3 = Artificial crack depth on the concrete

u_4 = Chloride solution concentration

$\mathbf{u_1}$ = Vector of $[u_2, u_3, u_4]$

$\mathbf{u_2}$ = Vector of $[u_4]$

t_{F_0} = Time when degradation path of BS reaches 500mv as degradation level, under condition, which is no crack, chloride concentration is 15%

t_{F_1} = Time when degradation path of BS reaches 500mv as degradation level, under condition which is crack width is 0.035, crack depth is 0.5, chloride concentration is 15%

t_{F_2} = Time when degradation path of BS reaches 500mv as degradation level, under condition which is crack width is 0.035, crack depth is 0.5, chloride concentration is 15%

t_L = Degradation latency.

k = Acceleration exponent

x_0	= Alarm threshold for rebar degradation
A	= Acceleration ratio compared with the benchmark degradation process
A_F	= Acceleration factor
C	= Chloride solution concentration
$G(\cdot)$	= CDF of gamma distribution
H	= Failure threshold of bridge rebar
$\Gamma(\cdot)$	= Gamma function
$E[X(t)]$	= Expected degradation rate
$F_T(v)$	= Probability that the component fails during a time interval 0 to v
$F_{X(t)}(H)$	= Cumulative distribution function for $X(t)$ evaluated at H, i.e., Probability that $X(t) < H$ at time t
$L(\cdot)$	= Likelihood function
T_1	= The time span of the first degradation stage
T_2	= The time span of the second degradation stage
T	= The time span of the entire degradation stage

1. Introduction

In this research, three degradation models are established based on the actual experimental data. The experiment considered the effects of crack width, crack depth, and chloride ions concentration. The data of concrete covered rebar degradation process under different conditions is obtained by tracking the different corrosion samples in a three-year experiment. The samples are rebars embedded in concrete. Above those concrete samples, there are artificial cracks with different sizes and a dam over the crack which contains solutions with different salt concentrations. By detecting the voltage between the corroded rebar and the normal rebar, the potential possibility of corroded rebar can be obtained. In order to facilitate the study, this research equates the corrosion potential of rebars with the degradation level of rebars.

Through the study of the degradation process of concrete-covered rebars, five models for rebar degradation are established, namely the general rebar degradation model in Section 3, the accelerated test degradation model, the preliminary two-stage degradation model, gamma-gamma two-stage degradation model and Weibull-gamma two stage degradation model. Due to the randomness and irreversibility of the steel corrosion process, the above models are established based on the gamma process and Weibull distribution. The general rebar degradation model considers the degradation of different rebars under different conditions independently. The acceleration test degradation model takes the rebar corrosion process under non-artificial-crack condition as the benchmark. By introducing the acceleration ratio parameter, A_F, the different artificial crack conditions are regarded as acceleration experiments for the benchmark degradation process.

A two-stages degradation model is used for each rebar, where the stage 1 is the time until the corrosion reaches a certain level and then it will switch to another linear degradation stage as stage 2. The two-stage degradation model holds that there is a degradation latency stage namely as stage 1 for each kind of rebar, and when the corrosion reaches a certain level, it will switch to another linear degradation stage as stage 2 which is different with the stage 1. Degradation rate during the stage 1 can be small, however, after the switch level, it can become large. Gamma-gamma degradation model is based on gamma process and is more consistent with the physical mechanism, which is, in the first degradation stage of rebar, the pre-cracking size and chloride concentration can both effect the degradation process. In the second degradation stage, only the chloride concentration will impact the corrosion.

Weibull-gamma two-stage degradation holds the same physical idea. In the Weibull-gamma two-stage degradation model, the time of the first degradation stage T_1 follows the Weibull distribution. The second degradation stage is a gamma process. Through the model parameter's maximum likelihood estimation result and linear regression analysis, the effects of crack width, crack depth, and chloride concentration on the degradation process under different models are also

analyzed. The acceleration factor A_F for each material are also calculated in the gamma-gamma and Weibull-gamma two-stage degradation model.

Reinforced concrete is wildly used in roads, bridges, and buildings. Reinforced concrete refers to a structure made with concrete and rebars, which has excellent compressive and tensile strength. However, in practical situations, the cycle of freezing and thawing may cause small cracks in the concrete. When water penetrates the surface of concrete and enters the interior, the volume of frozen water expands. After repeatedly freezing and thawing cycle, cracks in concrete are generated and deepened on the micro level, which makes concrete crack and causes permanent and irreversible damage to concrete. Chloride ions from the outside environment, such as from snow-dissolving agents, will penetrate these small cracks and react with the rebars embedded in the concrete. It will lead to the rust of the rebar, which can expand 3 to 4 times in volume after corroded. The corroded rebar will enlarge the crack size and let water penetrate deeper into the concrete to aggravate the situation.

Corrosion is one of the most aggressive factors that diminish the structural reliability and stability. The annual rehabilitation cost of corrosion is about $8.3 billion just for the highway bridges in the United States of America. Therefore, it is of great importance to analyze the bridge rebar degradation and determine the deterioration level or rebars to guide the maintenance management strategy. Figure 1 shows the samples of corrosion tests in the rebar corrosion experiment.

Figure 1 Samples of Corrosion Tests

The degradation process models proposed in this proposal are based on gamma processes. The gamma process is a monotonous random process which can be described as arising from a compound Poisson process of gamma-distributed increments in which the Poisson rate tends to infinity while the sizes of the increments tend to zero in proportion [1].

Consider a non-negative stochastic process $\{X(t); t > 0\}$. $X(t)$ represents the value of the degradation process at each independent time t. A gamma process has following properties:

i.   The increments $\Delta X(t) = X(t + \Delta t) - X(t)$ follows gamma distribution

$$X(t+\Delta t) - X(t) \sim g(x; \; \alpha(t+\Delta t)\text{-}\alpha(t), \; \beta)$$

(1.1)

$$g(x; \alpha(t+\Delta t) - \alpha(t), \beta) = \frac{\beta^{\alpha(t+\Delta t)-\alpha(t)} x^{\alpha(t+\Delta t)-\alpha(t)-1} \exp(-\beta x)}{\Gamma(\alpha(t+\Delta t) - \alpha(t))}$$

where $\alpha(t)$ and β are the shape parameter and scale parameter.

ii.   The increments $\Delta X(t)$ are independent.

In this proposal, Δt is always equal to 1 month. Considering the independent increments property, when $\alpha(t) = \alpha_0 t$ all the increments in the gamma process are i.i.d.

Maximum likelihood estimation is applied to estimate the parameters of the gamma process.

Maximum likelihood estimation is one of the methods of parameter estimation. It is known that a random sample satisfies a certain probability distribution, but the specific parameters are unknown. Parameter estimation is the reverse derivation of approximate values of parameters through the results of several trials. Maximum likelihood estimation is based on the idea that given a parameter which can maximizes the probability of the occurrence of the sample, then the parameter is taken as the true value of the estimation. The principle of maximum likelihood estimation is as follows:

Given a probability distribution D, the probability density function (continuous distribution) or probability mass function (discrete distribution) of D is $f_D(\cdot)$. The distribution parameter is θ. A sample $\{X_1, X_2, ..., X_n\}$ with n values can be extracted from this distribution. The likelihood function can be calculated by using $f_D(\cdot)$:

$$L(\theta \mid x_1, x_2, ..., x_n) = f_\theta(x_1, x_2, ..., x_n) \tag{1.2}$$

If D is a discrete distribution, $f_\theta(\cdot)$ is the probability of observing this sample when the parameter is θ. If D is a continuous distribution, $f_\theta(\cdot)$ is the value of the probability density function to the joint distribution at the observed sample point. So the value of $\{X_1, X_2, ..., X_n\}$ can give an estimate of θ, by maximizing the likelihood function L. Maximum likelihood estimation for θ does not necessarily exist, nor is it necessarily unique.

2. Background and Literature Review

Reinforced concrete is the most wildly used construction material all over the word. The durability and reliability are also important problems which are significantly impacted by the corrosion of the rebar embedded inside [1]. The degradation of reinforced concrete in the slab of bridge can cause the entire cascade failure [32] of the entire bridge. The degradation of reinforced concrete also leads to an annual cost of about $8.3 billion for mitigation and rehabilitation of bridge decks in the United States of America [2]. There have been many research studies on the corrosion

of steel reinforcement in concrete, that thoroughly discuss the physicochemical model for the corrosion of rebars embedded in the concrete, analyze the process of rebar corrosion and the effect on it [3]. However, most of these studies are conducted for experimental study of the mechanism in rebar's corrosion. Randomness is one of the factors which is ignored in modeling the rebar degradation process of the previous studies. Moreover, the variability of environmental conditions may also have effects on the rebar degradation which is not considered in the previous studies. The purpose of this study is to establish a model for the degradation process, which considers the randomness of the degradation process and the variability of input conditions. The proposed model predicts the corrosion degree of rebar embedded in concrete and provides a guidance for the reliability evaluation and maintenance of reinforced concrete structures.

Reinforced concrete structures have excellent mechanical properties, but they are not completely solid. Park et al [4] described the behavior of chloride ions and the equivalent diffusion of chloride ions in concrete. They proposed a corresponding model showing the effect of concrete cracks on chloride ion diffusion.
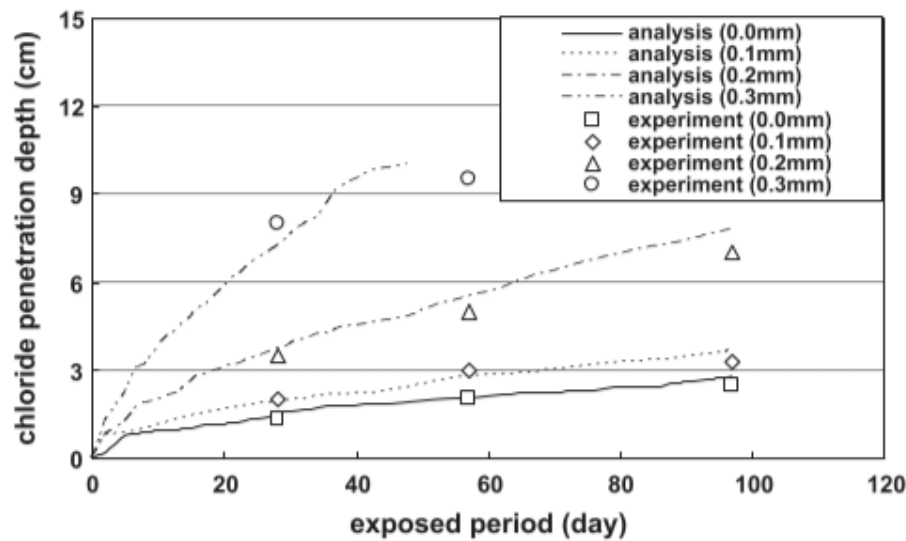
Figure 2 Variation of chloride penetration depth with age for different crack widths [4].

Figure 2 shows the chloride penetration depth in concrete over time under different crack conditions. As it is shown in the initial stage of diffusion, the cracks greatly help chloride ions penetrate the concrete. Park et al [4]. concluded that the wider the crack is, the faster the chloride

ions spread. When the crack width is greater than 0.2mm, the diffusion of chlorine ions will be greatly accelerated. Phares et al. [5] also develops the experiment to exam the rebar corrosion and concludes the similar result, which is, the ingress of chloride ions through the cracked deck is faster than that of un-cracked deck. Considering the experimental samples of the data source in this proposal, the width for different artificial cracks is all greater than 0.2mm. Therefore, these artificial cracks significantly accelerate the diffusion of chloride ions in these sample concrete.

Chloride penetration can cause corrosion of steel reinforcement, but this is not a one-direction behavior. In fact, the corrosion of rebars causes them to expand, which makes cracks in the concrete, and accelerates the chloride penetration reversely. Fenghua et al [6] studied the effect of corrosion of steel in concrete. They mentioned that the corrosion and expansion of rebars in concrete would lead to the increase of internal micro-cracks in concrete, which would lead to cracks in concrete. Moreover, the corrosion of rebars will lead to the reduction of the bonding capacity between concrete and rebars and decrease the effective load-carrying area of steel bars [7].

(a) semiellipse   (b) semiellipse+semicircle

(c) circle
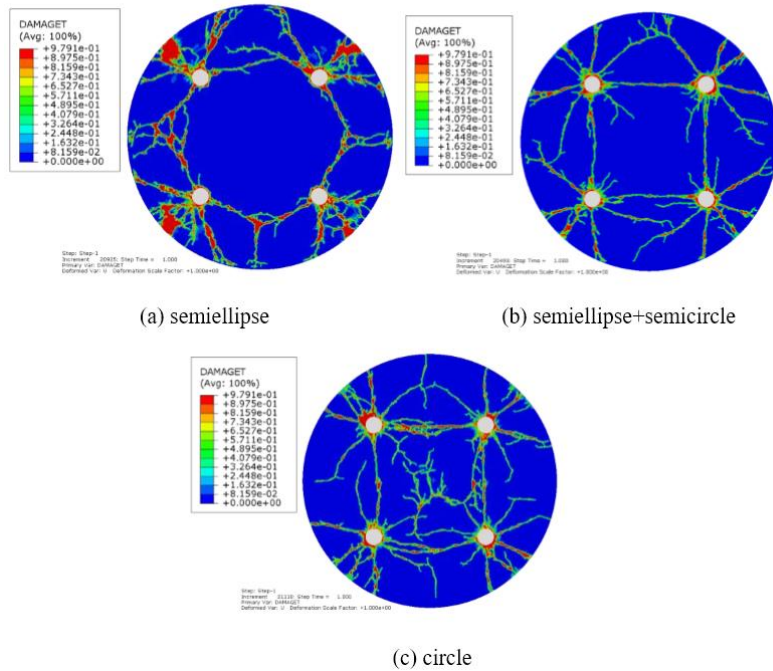
Figure 3 Corrosion damage distribution of concrete when corrosion rate is 10% and the number of

reinforcements is four [6]

Figure 3 shows the damage to concrete caused by the distribution of corrosion products at a corrosion rate of 10%. Another message from this figure is that no matter how cracks are distributed inside the concrete, they will always spread to the concrete surface.

The data in this thesis are obtained from the tracking records of four different kinds of rebar, which are Black Steel, Epoxy Coated Steel, Stainless Steel, and MMFX Steel. Black steel is made of steel that has not been galvanized. Its name comes from the scaly, dark-colored iron oxide coating on its surface. It is used in the applications that do not require galvanized steel. Epoxy Coated Steel was introduced to the market around 1970. The epoxy coating on its surface can effectively prevent corrosion of rebar [7]. Mohamed et al [8] described the chemical reaction mechanism of steel corrosion, and mentioned that the products of steel corrosion, hydrated ferric oxide, are 3-6 times the volume of the original material, which can lead to cracking and peeling of cement. They also introduced Stainless Steel (SS) and MMFX, in which Stainless Steel is an uncoated alloy steel with a higher content of chromium (Cr~18%) and nickel (Ni~10%), as well as a lower carbon content (C<0.015). This can be the reason that SS rebar obtained much better corrosion resistance than ordinary rebar. MMFX is an alloy containing about 9% of chromium, and according to its manufacturer's tests [9], some models of MMFX and SS can provide more than 100 years of service in a bridge, as shown in Table 1.

Table 1: Reinforcing Steel Comparative Durability Assessment and 100-year Service Life Cycle Cost Analysis Report, Tourney Consulting Group LLC. June 2016 [9]

COMPARATIVE TABLE OF SERVICE IN LIFE IN YEARS FOR VARIOUS REINFORCEMENT & ENVIRONMENTS			
Application	Bridge	Marine Piles	Severe Soils
Concrete Type	Bridge LP	Pile Mix LP	Pile Mix LP
Minimum Cover	1.5 in (37.5 mm)	2.0 in (50.0 mm)	1.5 in (37.5 mm)
Reinforcement Type			
Black Bar (BB)	25 yrs.	26 yrs.	18 yrs.

Epoxy Coated (ECR)	34 yrs.	35 yrs.	18 yrs.
Galvanized (GS)	76 yrs.	64 yrs.	57 yrs.
ChromX 4100	61 yrs.	65 yrs.	42 yrs.
ChromX 4100 with 2 Gpy CNI	>100 yrs.	94 yrs.	98 yrs.
ChromX 9100 (ASTM A1035)	>100 yrs.	>100 yrs.	>100 yrs.
UNS S32304 (Stainless Steel)	>100 yrs.	>100 yrs.	>100 yrs.

Mohammed et al [8] also reviewed the corrosion model of Tuutti et al [10] and concluded that the corrosion of steel bars in concrete can be divided into two stages, the initiation stage and the propagation stage, and illustrated the model with a diagram shown as Figure 4. Mohammed et al [8] illustrated that the loss of steel rebar in relation to time is also related to the thickness of the concrete, the material of the concrete, and the material of the steel itself.
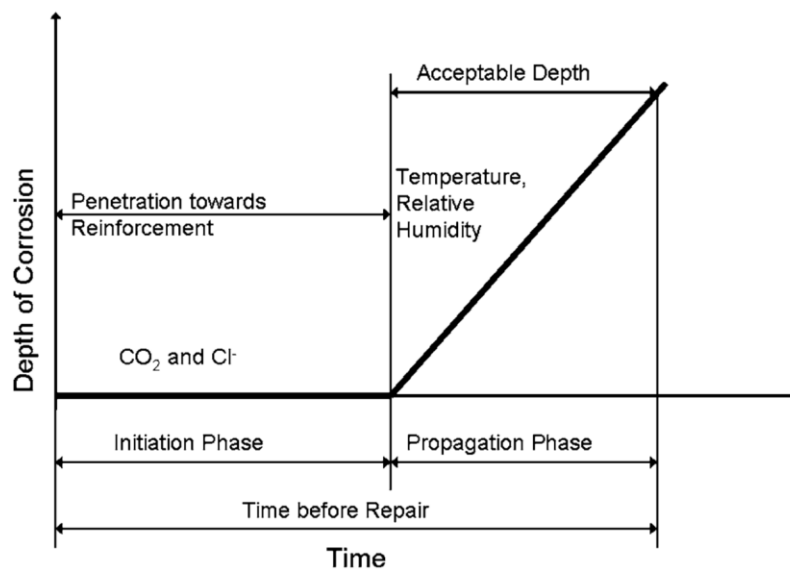
Figure 4 Schematic of Tuuttis model of the consequent phases of steel corrosion inside concrete [10]

The degradation is the reduction of system or component performance cause by cumulative

damages applied. When the degradation reaches a specific threshold, the system fails. There are significant number of research studies about the degradation process effected system reliability [11]. To be specific, many system degradation models have been proposed and used for the estimation of failure time distribution [12], remaining useful life prediction [13] and condition-based inspection or maintenance [14, 15]. Stochastic degradation processes are widely used to model the degradation process of systems considering the uncertainty in the deterioration process.

The stochastic process is a whole series of random variable which depends on the parameters, mainly the time. A random variable is a quantitative representation of a random phenomenon whose value changes with the influence of contingent factors. The stochastic processes commonly used in the degradation process are the inverse Gaussian (IG) process [38], gamma process [16-18] and Wiener process [19,20]. The IG process and gamma process are preferentially considered if the degradation paths are monotonic while the Wiener process is effective to describe the nonmonotonic degradation path [21-23]. Park and Padgett [24] reviewed the most common stochastic degradation models. They described that the general degradation model based on the random process is:

$$c(X_{n+1}) = c(X_n) + D_n h(X_n) \qquad (2.1)$$

Where X_{n+1} is the damage after $n+1$ increments of stress. D_n is the damage incurred at the $(n+1)^{th}$ increment, $c(\cdot)$ is damage accumulation function, and $h(\cdot)$ is the damage model function. Their paper shows a common research concern of degradation processes, which is, focusing on the increments of degradation processes at each time period. At the same time, different settings are used for $c(u), h(\cdot),$ and $D(\cdot)$ in this model, different basic degradation models can be obtained. For example, as the author did in the paper, if $c(u) = u, h(u) = 1$ and $D(u)$ is a gamma process, then the gamma degradation model can be obtained. In addition, Park and Padgett [24] also proposed the hyper-cuboidal volume approach to solve the problem that conventional acceleration functions can only include one parameter.

For the gamma process, see Lawless and Crowder [25]. They point out that the gamma process

has two important properties, which are mentioned in introduction part. The pdf of gamma distribution in the gamma process equals to equation (1.1).

These two properties are the starting point for the study of gamma processes. Lawless and Crowder [25] used a gamma process with covariates and random effects to model a degradation process in accelerated environments, or varying degradation rates in a single environment factor. This can be realized by introducing covariables into the function of shape parameters, that is, replacing $\alpha(t)$ with $\alpha(te^{\beta \mathbf{x}})$. By introducing random variables, z, into the scale parameters, which is replacing $\beta(t)$ with $z\beta(t)$, heterogeneity of different degradation paths can be reflected. Figure 5 shows the gamma process and expected degradation path with a scale parameter of 2 and a shape parameter of 3.
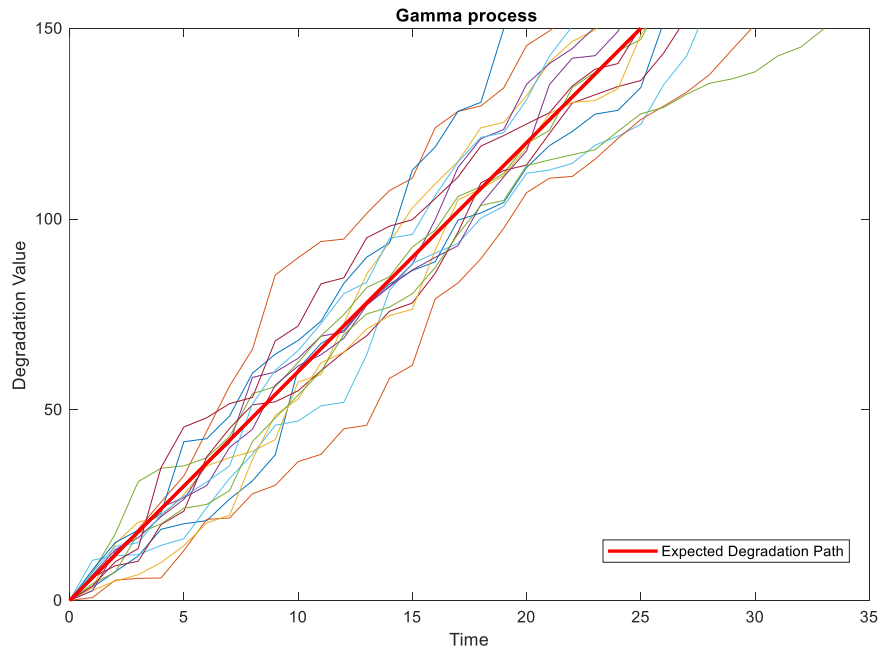
Figure 5 Gamma degradation process and expected degradation path

Examples of practical applications of gamma degradation processes can be found in the study of Cholette and Yu [26]. Combining the gamma degradation process with the actual physical meaning, a semi-physical model is proposed to study the degradation process of boiler heat exchanger. The model analyzes and calculates the degradation of the heat exchanger (downtime

due to explosion and cogeneration loss) and helps to optimize the update of the heat exchanger. The authors introduce the physical model expression into the shape parameter of the gamma process so that the shape parameter becomes a function of flue temperature and the mass of vapor flow. The obtained gamma process is applied to predict the thickness of the flue wall. The gamma process presented in this research work is an example of an application of a degradation process.

This thesis considers establishing an accelerated test model of reinforcement corrosion with concrete surface cracks. There have also been many studies on accelerated test degradation models. Ling and Tsui [27] described a gamma process-based accelerated degradation model under different pressures and gave its likelihood function. They used a logarithmic transformation to convert a random degradation variable from 0 to 1 into a random variable subject to a gamma distribution, with a shape parameter $\alpha_{ij} = \lambda_i(t_j^c - t_{j1}^c)$ and a scale parameter of β_i, λ_i is a parameter in the shape parameter. Then, they considered the accelerating effect of pressure grade x_i on the degradation process and introduced it into shape parameters and scale parameters, to obtain the following expressions:

$$\lambda_i = e^{a+b\log x_i} \tag{2.5}$$

$$\beta_i = e^{u+v\log x_i} \tag{2.6}$$

The gamma degradation model is an accelerated test model considering pressure levels. The acceleration factor in this model is the pressure level x_i, but sometimes the acceleration function has more than one variable. For this situation, Park and Padgett [24] proposed a hyper-cuboidal volume approach to solve it. For example, suppose for the situation where failure is dependent on the size of the specimen under test that there are two accelerating variables denoted by L & A. Then considering the two-dimensional size of a specimen as $L \times A$. Thus, it is reasonable to use $V = L \times A$ as an accelerating volume or cuboidal measure.

Just as the corrosion model of Tuutti et al [27], the corrosion of steel reinforcement can be divided into two stages. Therefore, it is necessary to establish a two-stage degradation model for

the rebar degradation process. There have been two-stage degradation modeling research with the same function form [28,29] or different functions for each stage has been investigated [30,31]. The degradation stage switching point can be set to be the alarm threshold [28] and the first hitting time (FHT) regards the alarm threshold will be the time point to separate two stages.

Dong and Cui [33] described an example of a two-stage degradation model, where the degradation process can be divided into two parts by a single change point, and then they established the Wiener-gamma and gamma-gamma processes. Figure 6 shows the time-degradation quantity image of the two-stage degradation process.
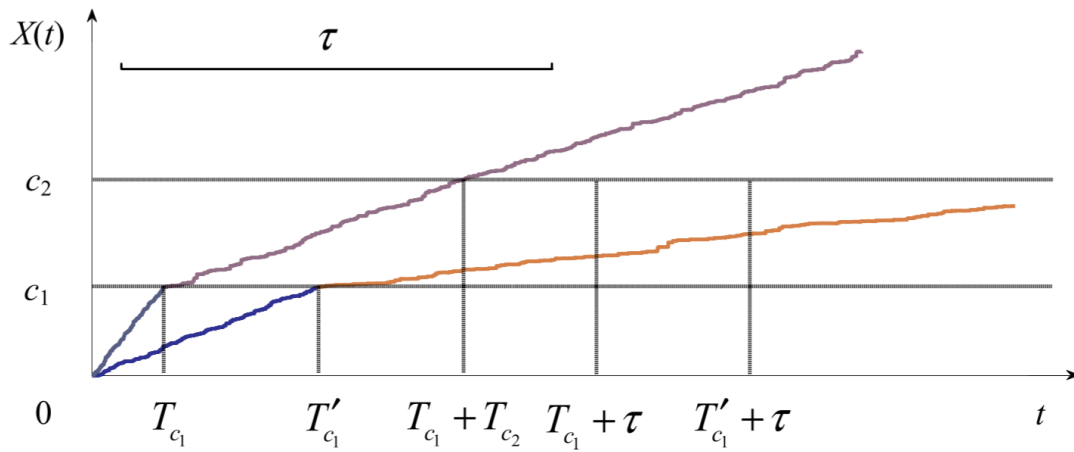
Figure 6 Two sample paths for the 2-stage degradation process [33]

In Figure 6, c_1 is the alarm line. Dong and Cui [33] pointed out that many systems have two thresholds, the alarm line and the failure threshold. The alarm line corresponding to the variable point is given by the manufacturer of the part, which indicates the value that the part should work safely under normal working conditions (such as corrosion margin, warning water level, etc.). Therefore, the system should be in a safe or acceptable working stage before the change point. However, when the degradation value is greater than the alarm line, external factors will increase their influence on the system, which will lead the system degradation to another stage. Similarly, Chen and Tsui [34], developed a two-stage degradation model for a system to monitor the rotational bearings. In their model, the degradation model follows a linear path with a random error added in. There is a switch point γ_i, which is a specific time point, the degradation rate before

and after γ_i are different. This makes the entire degradation model matches the actual bearing degradation path. These research efforts develop two-stage degradation models based on the linear regression. The stage change points are based on degradation level and time, respectively. However, their models are all based on linear regression model. For bridge rebar degradation, many stochastic process-based degradations models are used to measure the degradation level [35,36].

Wang and Guo [37] proposed a two-phase degradation model motivated by the degradation of LCD monitors. In their model, a specific change value *D* is introduced to determine whether the degradation is at phase 1 or phase 2. They assumed when the LCD's degradation level hits the change value *D*, the degradation process changes to phase 2, where the degradation rate is lower than the first phase. They assumed the degradation in the first phase can be governed by a gamma process and the second degradation stage is a Wiener process. For example, LCD monitor degradation data were used to verify their model. Wang and Guo [37] proposed is a good example to demonstrate how a 2-stage degradation model is combined with the stochastic process-based degradation models. However, for many conditions, the degradation process is a one-direction process. Wiener process applied in Wang and Guo [37] is a non-monotonic stochastic process, which is inappropriate to measure the monotonic degradation process such as bridge rebar degradation.

Current research have made a detailed review on the corrosion and degradation models of steel reinforcement in concrete, fully explaining the various physical and chemical reactions in the corrosion process of steel reinforcement [40,41], as well as the influencing factors in the corrosion process [42]. The research about the degradation process shows the gamma degradation process, the accelerated test degradation process, competing failure process [44], the acceleration function affected by multiple environmental factors [39], and a two-stage degradation model. There are also corresponding practical examples for the application of a gamma degradation process [43]. However, the above studies did not conduct a proper model for the corrosion of rebars embedded in concrete with pre-crack and chloride effected. The accelerated experimental model and the two-

stage degradation model are not combined with the actual physics of concrete corrosion.

3. Influence of environmental factors and initial degradation model

The degradation process of rebar is affected by the crack width, crack depth and chlorine concentration, and should worsen with the increase of these factors. The degradation level presents a monotone increasing degradation process. At the same time, the level of degradation is random, and the same degradation results may not be obtained under the same external conditions. In this section, three bridge rebar degradation models are proposed, and a linear regression is applied to decide which factor effects degradation the most. All these degradation models are based on a linear gamma degradation process, where the shape parameter is $\alpha(t) = \alpha_0 t$. In equation (1.1), since observations of the rebar degradation process are made monthly, the Δt in the shape parameter function of the degradation process is always equal to 1.

General rebar degradation model considers four influencing factors of the degradation process, among which "crack width", "crack depth", and "chloride percentage" only affects the scale parameter β while "type of rebar" varies with the shape parameter function $\alpha(t)$.

Accelerated test degradation model is based on the following assumption: the experimental condition "0.5-inch crack width" and "1-inch crack width" are used to simulate the different aged rebar degradation process. In this case, the parameter "accelerated ratio (A)" is introduced in the scale parameter function to measure the effects of the impact factors crack width and "crack depth" on the degradation rate. In this model, crack width and depth on the concrete affect the parameter A in shape parameter, while the scale parameter in the degradation process is only affected by chloride percentage.

$$g(x; A\alpha_0(t) - A\alpha_0(s), \beta) = \frac{x^{A\alpha_0(t) - A\alpha_0(s) - 1} e^{\frac{-x}{\beta}}}{\beta^{A\alpha_0(t) - A\alpha_0(s)} \Gamma(A\alpha_0(t) - A\alpha_0(s))}$$

(3.1)

$$A = \left(\frac{u_2 u_3}{d_0 w_0} \right)^k$$

The actual corrosion is not always at a constant rate for the four types of rebar tested, black steel (BS), epoxy coated steel (EC), stainless steel (SS), and corrosion resistant alloy steel (MMFX). During about the first year of the experiment, the chloride ions would penetrate through the concrete and erode the outer coating of the remaining three types of reinforcement. This time period is called degradation latency, which varies with the type of rebar. During this period, the corrosion rate of steel bars is relatively slow, especially for some corrosion resistant rebars. As the chloride ions pass through the protective coating, they would start to erode the reinforcement. Based on this theory, a two-stage degradation model is proposed.

Following are rebars relative to this proposal, as shown in Figures 7 and 8

i.   Black steel (conventional steel rebars)

ii. Epoxy Coated steel rebars

iii. Duplex 2205 (318) Stainless steel rebars

v.   Chrome X 9000 MMFX rebars, Martensitic Microcomposite Formable Steel (MMFX).
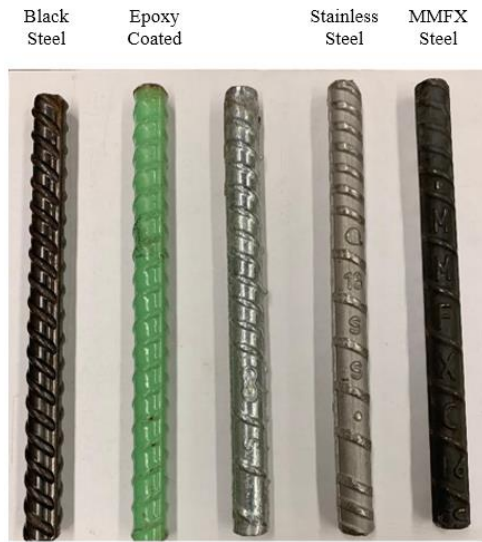
Figure 7 Different types of corroded rebar

Figure 8 Different Types of Corroded Rebar

3.1. Data analysis

The proposed rebar degradation models are based on the data supplied from civil engineering

laboratory. The data points, which measure the corrosion potentials of the rebars in test samples, are obtained by measuring the voltage between the rebars in the experiment corrosion samples. In the experiment samples, different types of rebars are buried in concrete blocks where artificial cracks are made. Above each concrete block, there is a dam with different concentration of sodium chloride solution. The corrosion potential is treated as rebar degradation in this proposal.

There are four types of rebar, Black Steel (BS), Epoxy Coated Steel (EC), Stainless Steel (SS), and MMFX. Three factors affect the rebar corrosion, crack width, crack depth, and chloride percentage in the solution. The experiment measured the corrosion of four types of rebars at 3% and 15% chlorine concentration under the condition of different artificial crack size (uncracked, 0.011×0.5, 0.011×1, 0.035×0.5 and 0.035×1). The entire experiment lasted for 33 months, thus there are 330 data points for each rebar in this dataset.

The plots of the original data points changing over time are shown in Figure 9 to 17:
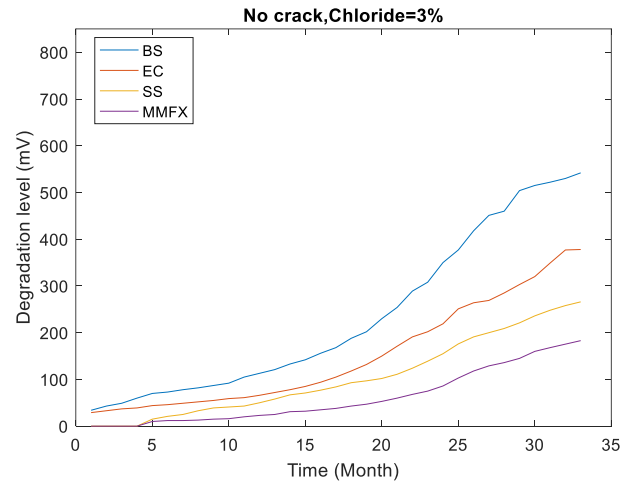
Figure 9 Rebars Degradation Level of Cracked Concrete Class A (no crack) Exposing to 3% Concentration of Sodium Chloride
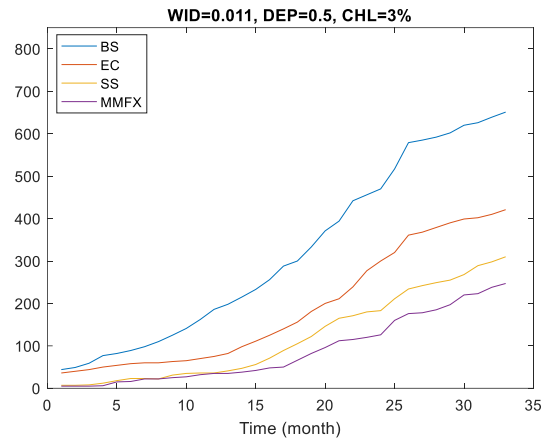
Figure 10 Rebars Degradation Level of Cracked Concrete Class A (Crack Width=.011", Crack Depth=.5")

Exposing to 3% Concentration of Sodium Chloride
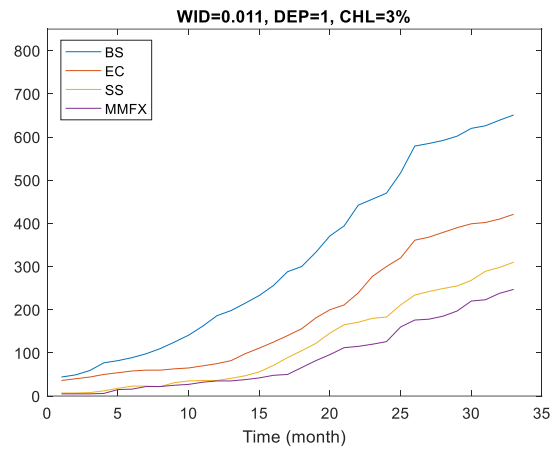
Figure 11 Rebars Degradation Level of Cracked Concrete Class A (Crack Width=.011", Crack Depth=1")

Exposing to 3% Concentration of Sodium Chloride
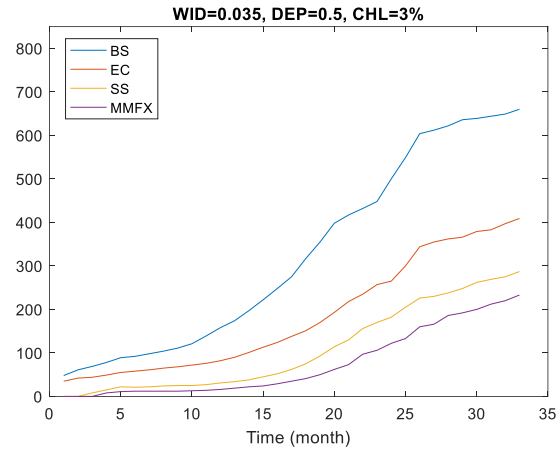
Figure 12 Rebars Degradation Level of Cracked Concrete Class A (Crack Width=.035", Crack Depth=.5")

Exposing to 3% Concentration of Sodium Chloride
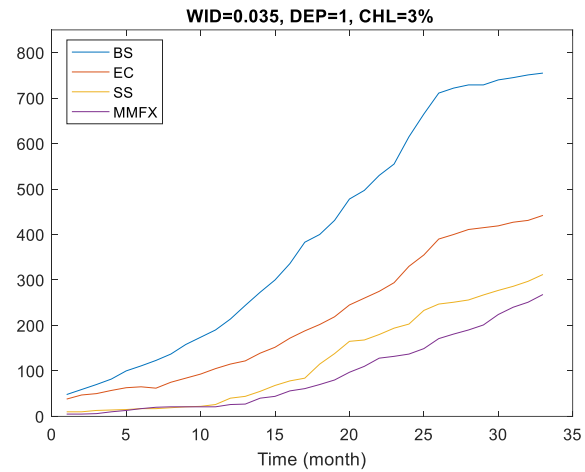
Figure 13 Rebars Degradation Level of Cracked Concrete Class A (Crack Width=.035", Crack Depth=1")

Exposing to 3% Concentration of Sodium Chloride
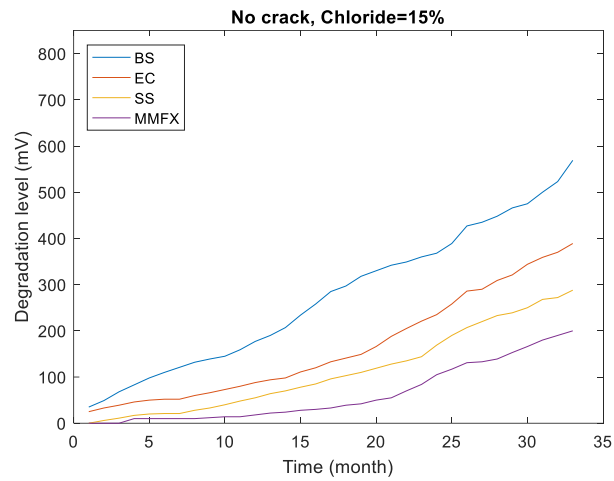
Figure 14 Rebars Degradation Level of Cracked Concrete Class A (no crack) Exposing to 15%

Concentration of Sodium Chloride
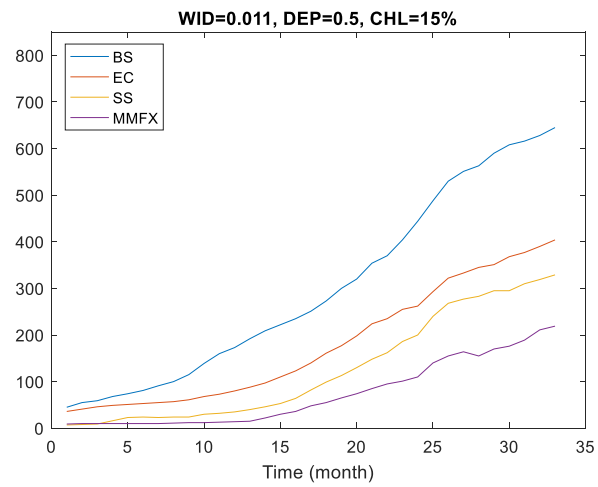
Figure 15 Rebars Degradation Level of Cracked Concrete Class A (Crack Width=.011", Crack Depth=.5")

Exposing to 15% Concentration of Sodium Chloride
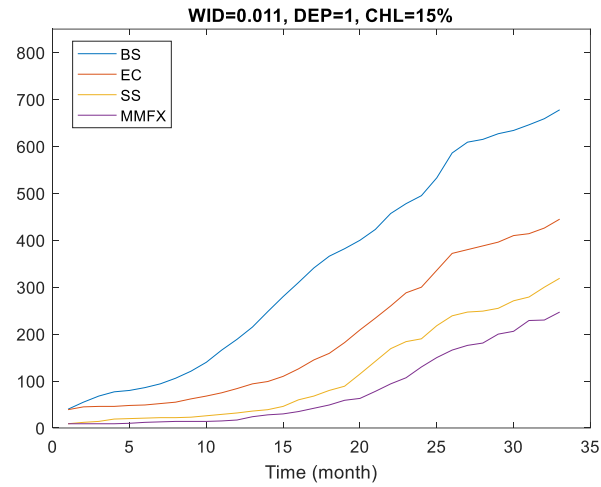
Figure 16 Rebars Degradation Level of Cracked Concrete Class A (Crack Width=.011", Crack Depth=1")

Exposing to 15% Concentration of Sodium Chloride
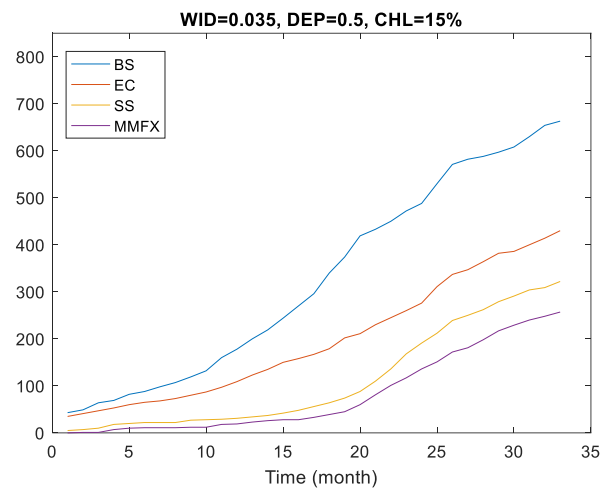
Figure 17 Rebars Degradation Level of Cracked Concrete Class A (Crack Width=.035", Crack Depth=.5")

Exposing to 15% Concentration of Sodium Chloride
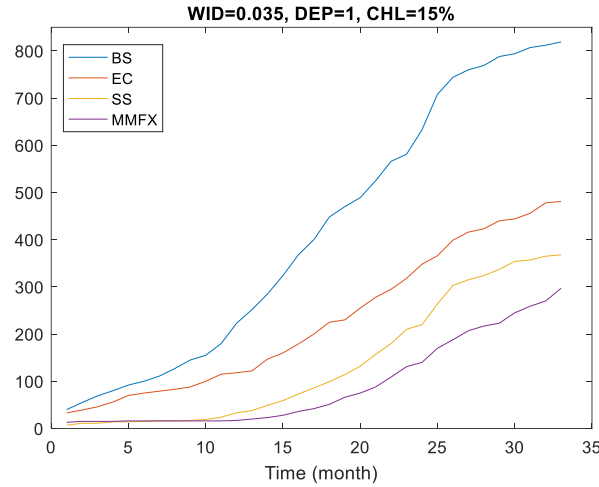
Figure 18 Rebars Degradation Level of Cracked Concrete Class A (Crack Width=.035", Crack Depth=1")

Exposing to 15% Concentration of Sodium Chloride

As is shown above, the order of corrosion resistance of rebars is $BS < EC < SS < MMFX$. The material MMFX is the most robust to resist corrosion. This conclusion is true for every case. There are differences in the initial degradation of different materials, as time goes on, the differences will gradually increase after about 14 months, but the differences will stabilize after 25 months. All the degradation paths are concave in the first 25 month, and then they will go to approximate parallel after about 25 months.

The incremental per unit time interval in gamma process is independent and follows gamma distribution with shape parameter $[\alpha(t_2) - \alpha(t_1)]$ and scale parameter β. Therefore, by subtracting the data of each month from the data of the previous month, the monthly degradation incremental data of rebars are obtained. Assuming the degradation process is a gamma process, so the incremental data between each two times follow gamma distribution. The time difference between each data point is always equal to 1, as well as the function of shape parameter $\alpha(t) = \alpha_0 t$, all the incremental data follows gamma distribution with shape parameter equals $\alpha_0 t$ and scale parameter β. The expected value for the gamma distribution is $(\alpha_0 t/\beta)$, which represents the degradation rate in this scenario.

Assuming that the degradation process is a gamma process, then the monthly increment in the

degradation process follows the gamma distribution. The parameters value of α_0 and β in the gamma distribution can be calculated using maximum likelihood estimation. Table 2 presents the parameter estimation of the four types of rebar degradation process, using the MATLAB built-in function "MLE" to calculate the parameter results. u_2, u_3, u_4 represent the crack width, crack depth, and chloride percentage.

Table 2: BS and EC Degradation Parameter Estimated by Function "MLE"

Variables			BS			EC		
u_2 (WID)	u_3 (DEP)	u_4 (CHL)	α_0	β	α_0 / β	α_0	β	α_0 / β
No Crack		3%	2.112	0.133	15.880	1.552	0.142	10.930
		15%	4.333	0.260	16.665	2.791	0.245	11.392
0.011	0.5	3%	3.174	0.185	17.157	1.709	0.155	11.063
0.011	0.5	15%	3.379	0.180	18.772	1.975	0.172	11.500
0.011	1	3%	2.452	0.129	19.008	1.530	0.127	12.031
0.011	1	15%	3.145	0.158	19.905	1.357	0.107	12.688
0.035	0.5	3%	1.816	0.095	19.116	1.856	0.159	11.688
0.035	0.5	15%	2.917	0.153	19.418	3.515	0.285	12.344
0.035	1	3%	2.168	0.098	22.122	2.402	0.190	12.625
0.035	1	15%	2.397	0.098	24.459	2.226	0.159	14.000

Table 3: SS and MMFX Degradation Parameter Estimated by Function "MLE"

Variables			SS			MMFX		
u_2 (WID)	u_3 (DEP)	u_4 (CHL)	α_0	β	α_0 / β	α_0	β	α_0 / β
No Crack		3%	3.322	0.400	8.305	1.613	0.282	5.720
		15%	3.300	0.333	9.009	1.063	0.170	6.253
0.011	0.5	3%	2.068	0.234	8.844	1.495	0.250	5.969
0.011	0.5	15%	0.826	0.082	10.063	0.673	0.103	6.563
0.011	1	3%	1.337	0.141	9.469	0.969	0.128	7.562

0.011	1	15%	1.055	0.109	9.687	0.717	0.096	7.438
0.035	0.5	3%	0.872	0.097	8.969	0.951	0.131	7.281
0.035	0.5	15%	1.208	0.122	9.906	0.997	0.124	8.031
0.035	1	3%	1.148	0.122	9.438	1.172	0.143	8.219
0.035	1	15%	0.928	0.082	11.281	0.560	0.063	8.875

The degradation rate α_0/β increases with the growing of crack width, crack depth, and chloride solution concentration. MMFX has the lowest degradation rate α_0/β, then it is SS, EC, BS decreasingly. This is consistent with the previous result observed from the original degradation path.

The expected degradation path can be plotted based on the degradation rate (α_0/β) above. Using this as the slope can plot the expected degradation path. When expected degradation path is plotted into a same figure window with the real rebar degradation path, there can be some deviation at the middle of degradation. This is because the maximum likelihood estimates always fits well with the tail part.

The expected degradation path and the real rebar corrosion data are plotted as in Figure 19 to 22, where the red straight line represents the expected degradation path $E[X(t)]$ and the yellow, green, blue line represents the rebar degradation under the condition when crack depth equals "no crack", "0.5-inch depth crack", and "1-inch depth crack" respectively.
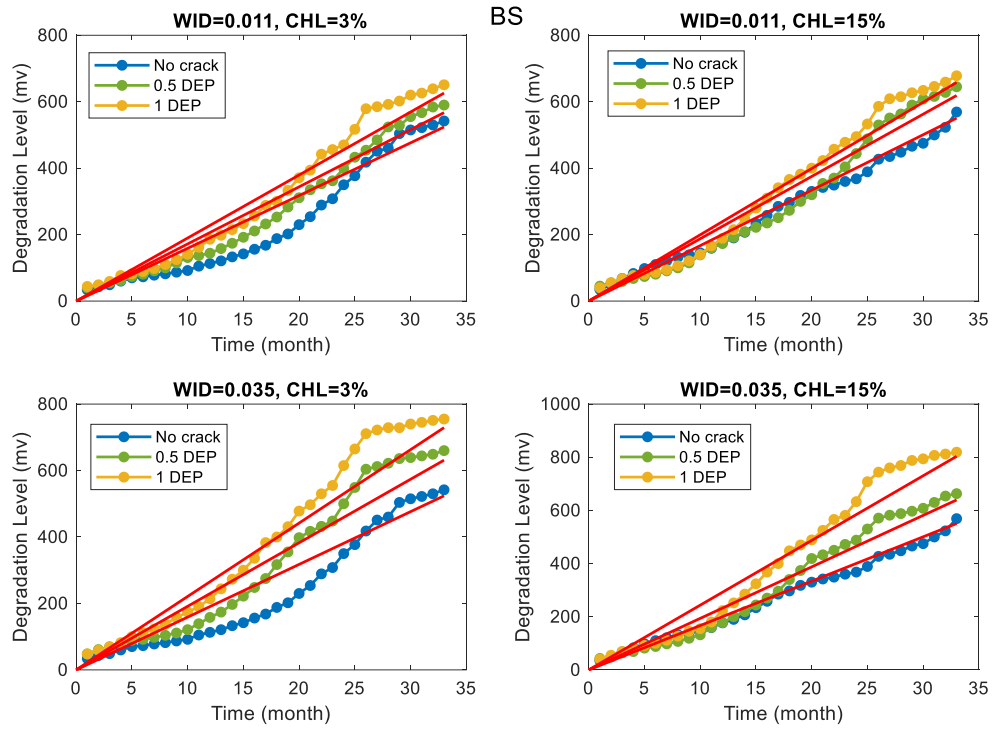
Figure 19: BS Expected and Real Degradation Level under Cracked Concrete Class A
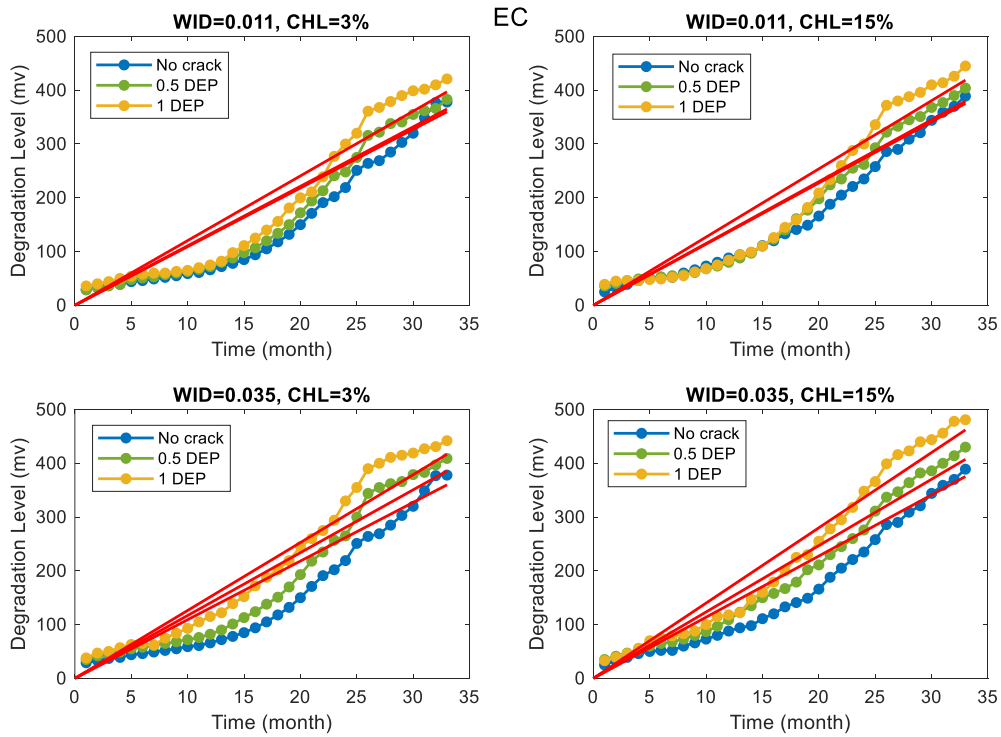
Figure 20: EC Expected and Real Degradation Level under Cracked Concrete Class A
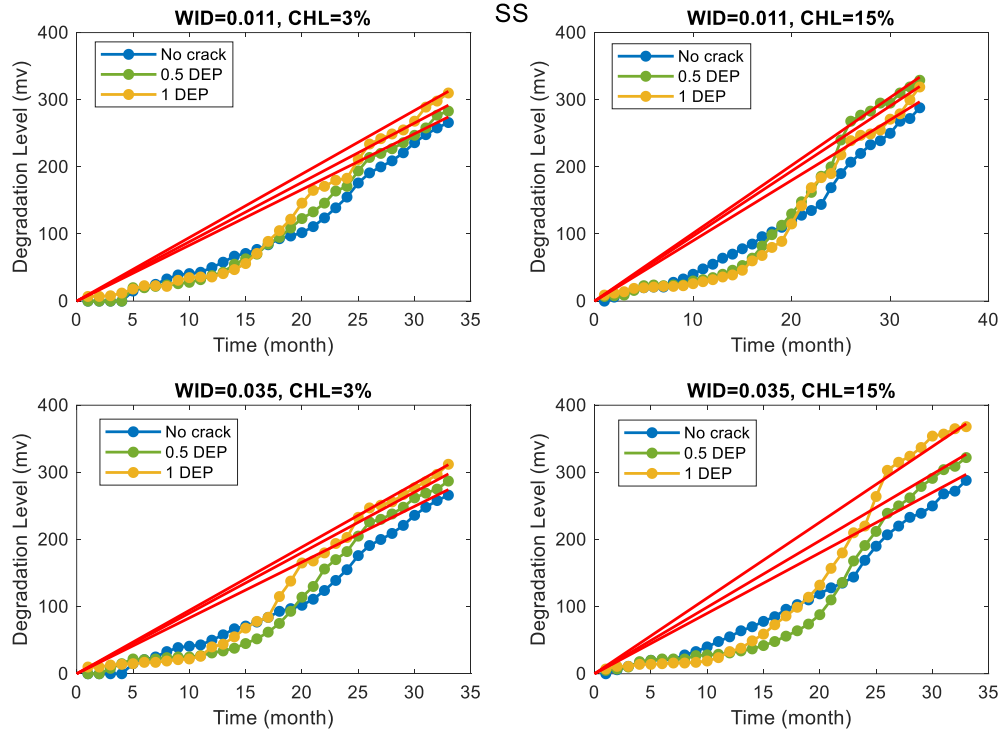
Figure 21: SS Expected and Real Degradation Level under Cracked Concrete Class A
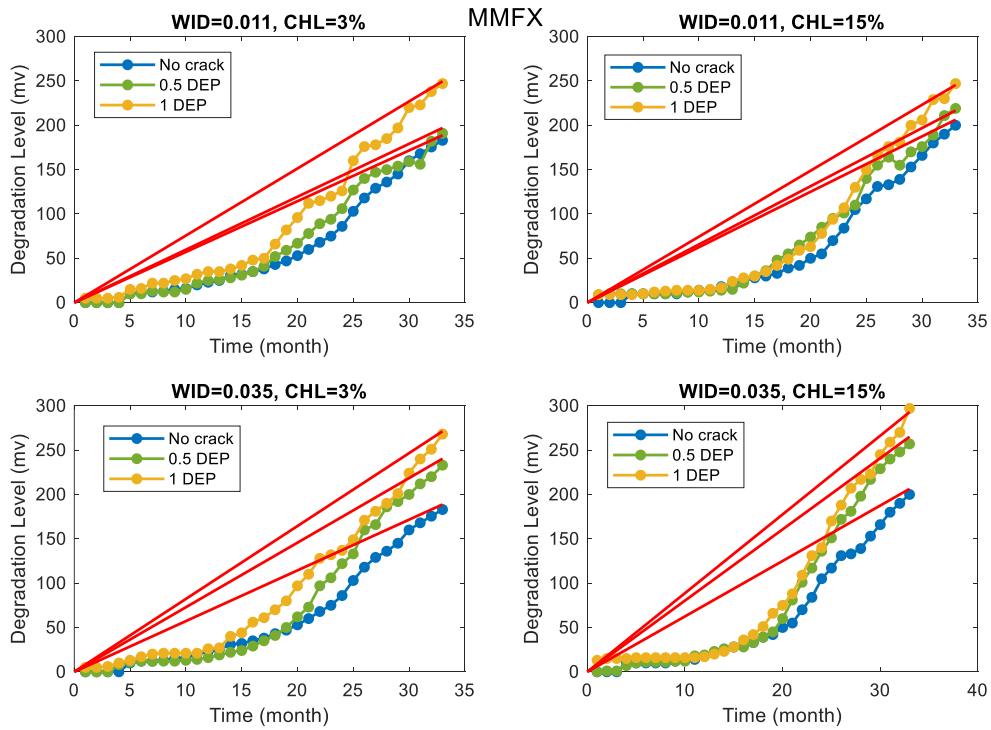
Figure 22: MMFX Expected and Real Degradation Level under Cracked Concrete Class A

WID, DEP, CHL represent crack width, crack depth, and chloride percentage, respectively. The x-axis is time, while y-axis is degradation level measured by millivolt. According to the original data, most of the materials have little difference in the initial stage of corrosion. When EC is under 0.011 crack width, the depth has little effect on corrosion. When MMFX is under concentration of 15%, crack depth had little effect on corrosion.

Figure 21 and Figure 22 show a problem: for SS rebars and MMFX rebars with WID = 0.035 and CHL = 3%, in the early stage of the experiment, the non-crack test condition is more likely to have the rebar corroded when compared the cracked test condition. This may be due to measurement reasons.

In most figures, the expected degradation path deviates from the actual degradation in the middle part due to the concave shape of the real degradation path. The degradation curves of BS and EC are linear and fit well with the expected curves. SS and MMFX degradation curve show obvious bending and poor fit with the expected curve.

Although there is a deviation between expected degradation and real path at the middle time range, the expected degradation path gets close to the real data at the end in most conditions. This is because the expected degradation curve is estimated by calculating the expected monthly increment, which is calculated from the parameters obtained by the maximum likelihood estimate. The real monthly increments are somewhat uniformized by this method while the real monthly incremental is small at beginning and large at the end, which leads the degradation path to be a convex curve.

Multiple linear regression was used to look at the effects of WID, DEP, and CHL on $\alpha, \beta,$ and α/β, and the results shown in Tables 4 and 5 The null hypothesis that the p-value test for each variable is the coefficient equal to zero (no effect). Therefore, a lower p-value indicates that the predictive variable is a meaningful complement to the model, which means it has significant impact to the response.

Table 4: Multiple Linear Regression for α, β

	α			β		
BS	DEP	WID	CHL	DEP	WID	CHL
Coefficients	-0.27	-24.70	7.51	-0.05	-1.89	0.35
t-value	-0.51	-1.83	2.78	-1.35	-2.22	2.05
p-value	0.63	0.12	0.03	0.23	0.07	0.09
EC	DEP	WID	CHL	DEP	WID	CHL
Coefficients	-1.01	32.40	4.69	-0.10	2.28	0.32
t-value	-1.95	2.48	1.79	-2.38	2.09	1.48
p-value	0.10	0.05	0.12	0.06	0.08	0.19
SS	DEP	WID	CHL	DEP	WID	CHL
Coefficients	-1.36	-27.10	-2.88	-0.17	-3.30	-0.44
t-value	-2.25	-1.78	-0.94	-2.44	-1.86	-1.25
p-value	0.07	0.13	0.38	0.05	0.11	0.26
MMFX	DEP	WID	CHL	DEP	WID	CHL
Coefficients	-0.44	-3.10	-3.65	-0.10	-1.35	-0.63
t-value	-2.09	-0.58	-3.40	-2.66	-1.45	-3.37
p-value	0.08	0.58	0.01	0.04	0.20	0.02

Table 5: Multiple Linear Regression for α/β, ln(α/β)

	α / β			ln (α / β)		
BS	DEP	WID	CHL	DEP	WID	CHL
Coefficients	4.02	85.3	9.69	0.21	4.34	0.492
t-value	3.71	3.12	1.77	4.64	3.8	2.14
p-value	0.01	0.021	0.128	0.004	0.009	0.076
EC	DEP	WID	CHL	DEP	WID	CHL
Coefficients	1.534	23.5	5.98	0.128	1.937	0.487
t-value	3.46	2.1	2.66	3.88	2.33	2.92
p-value	0.013	0.081	0.037	0.008	0.059	0.027
SS	DEP	WID	CHL	DEP	WID	CHL
Coefficients	1.073	16.3	8.2	0.114	1.66	0.849
t-value	2.47	1.49	3.72	2.74	1.57	4.03
p-value	0.049	0.188	0.01	0.034	0.167	0.007
MMFX	DEP	WID	CHL	DEP	WID	CHL
Coefficients	1.469	41.67	4.01	0.211	5.77	0.57
t-value	3.93	4.42	2.12	4.18	4.52	2.23
p-value	0.008	0.004	0.078	0.006	0.004	0.068

These conclusions can be drawn from the Table 4 and 5： 1) crack depth has a significant impact on the corrosion rate of rebar; 2) the crack width has a significant influence on the corrosion rate of BS and MMFX, but it cannot be proved that the crack width also has a significant influence on the corrosion rate of EC and SS; 3) chloride percentage has a significant effect on the corrosion rate of EC and SS, but it cannot be proved that chloride percentage also has a significant effect on the corrosion rate of the other two kinds of rebar.

Through the analysis and plotting of the original data, it can be seen that: 1) the corrosion resistance of the four kinds of rebar is significantly different. 2) the degradation curve of the rebar

presents a concave shape. 3) the crack size of the concrete surface and chloride ion concentration have an impact on the corrosion rate of the rebar. 4) the corrosion difference of reinforcement under different conditions will begin to increase after a period of time.

In consideration of these situations, this research proposed the one-stage-degradation model and preliminarily 2-stage degradation model in the following part.

3.2 One-stage gamma models

3.2.1 General rebar degradation model

For general rebar degradation model, concrete width, concrete depth, and chloride solution percentage impact the scale parameter beta β and shape parameter α varies with rebar materials. Each degradation incremental in these gamma process models follows gamma distribution which shape parameter equals $\alpha(t_2) - \alpha(t_1)$. Considering the general rebar degradation model is a linear model where $\alpha(t) = \alpha_0 t$, and the data is collected monthly, the shape parameter for each incremental in this model is $\alpha_0 t_2 - \alpha_0 t_1 = \alpha_0$.

Thus, for each independent degradation incremental, there is:

$$X(t_2) - X(t_1) \sim g(x; \alpha(t_2)\text{-}\alpha(t_1), \beta)$$

$$g(x; \alpha, \beta) = \frac{x^{\alpha-1} e^{\frac{-x}{\beta}}}{\beta^\alpha \Gamma(\alpha)} \tag{3.2}$$

Where

$$\alpha(t) = \alpha_0 t \tag{3.3}$$

$$\beta = \beta(\mathbf{u}) \tag{3.4}$$

$\beta(u)$ defines as follows:

$$\beta(\mathbf{u}) = \beta_0 e^{b_1 u_1 + b_2 u_2 + b_3 u_3 + b_4 u_4} \tag{3.5}$$

$$\beta(\mathbf{u}) = \beta_0 e^{b_1 u_1 + b_3 u_3 + b_4 u_4 + b_5 u_2 u_3} \tag{3.6}$$

$$\beta(\mathbf{u}) = \beta_0 e^{b_3 u_3 + b_4 u_4 + b_5 u_2 u_3} \tag{3.7}$$

Equations (3.5), (3.6), (3.7) are $\beta(\mathbf{u})$ in three different models. u_1 is a binary variable to determine if the concrete has an initial crack. If there is crack $u_1 = 0$, otherwise $u_1 = 1$. Parameters u_2, u_3, u_4 represent crack width, crack depth, and chloride percentage, respectively. When there is no crack on the concrete, set $u_2 = 0.1, u_3 = 0.0022$. In the real scenario, the crack width and crack depth have large scale difference, and they also have some degree of correlation. Thus, the item $u_2\,u_3$ is added to balance the scale difference in model (2). In order to avoid u_1 over-interfering with model results when the crack size is very tiny, at that time u_2 and u_3 goes for a very small number, $b_1\,u_1$ is eliminated in model (3). Another type of parameter $b_i, (i = 1,2,3,4,5)$ here are the coefficients of u_i.

By writing $\beta_0 = e^{b_0}$, the $\beta(\mathbf{u})$ in above model can be written as:

$$\beta(\mathbf{u}) = e^{b_0 + b_1 u_1 + b_2 u_2 + b_3 u_3 + b_4 u_4} \tag{3.8}$$

$$\beta(\mathbf{u}) = e^{b_0 + b_1 u_1 + b_3 u_3 + b_4 u_4 + b_5 u_2 u_3} \tag{3.9}$$

$$\beta(\mathbf{u}) = e^{b_0 + b_3 u_3 + b_4 u_4 + b_5 u_2 u_3} \tag{3.10}$$

Using maximum likelihood estimation to estimate those unknown parameters $\alpha_{0,} b_i$ $(i = 1,2,3,4,5)$, the maximum likelihood functions for each degradation model is:

$$L(\alpha_0, b_0, b_1, b_2, b_3, b_4) = \prod_{i=1}^{n} P(x_i; \alpha_0, b_0, b_1, b_2, b_3, b_4) \tag{3.11}$$

$$L(\alpha_0, b_0, b_1, b_3, b_4, b_5) = \prod_{i=1}^{n} P(x_i; \alpha_0, b_0, b_1, b_3, b_4, b_5) \tag{3.12}$$

$$L(\alpha_0, b_0, b_3, b_4, b_5) = \prod_{i=1}^{n} P(x_i; \alpha_0, b_0, b_3, b_4, b_5) \tag{3.13}$$

Where:

$$P(x_i) = \frac{\beta(\mathbf{u})^{\alpha(t_2)-\alpha(t_1)} \, x_i^{\alpha(t_2)-\alpha(t_1)-1} e^{-\beta(\mathbf{u})x_i}}{\Gamma(\alpha(t_2)-\alpha(t_1))} \tag{3.14}$$

Because $\alpha(t) = \alpha_0 t$; $t_2 - t_1 = 1$

$$P(x_i) = \frac{\beta(\mathbf{u})^{\alpha_0} \, x_i^{\alpha_0-1} e^{-\beta(\mathbf{u})x_i}}{\Gamma(\alpha_0)} \tag{3.15}$$

For the convenience to the calculation, logarithm is taken to the likelihood functions to derivative log-likelihood function as follows:

$$lnL(\alpha_0,b_0,b_1,b_2,b_3,b_4) = \sum_{i=1}^{n} \ln\left(P(x_i;\alpha_0,b_0,b_1,b_2,b_3,b_4)\right) \tag{3.16}$$

$$lnL(\alpha_0,b_0,b_1,b_3,b_4,b_5) = \sum_{i=1}^{n} \ln\left(P(x_i;\alpha_0,b_0,b_1,b_3,b_4,b_5)\right) \tag{3.17}$$

$$lnL(\alpha_0,b_0,b_3,b_4,b_5) = \sum_{i=1}^{n} \ln\left(P(x_i;\alpha_0,b_0,b_3,b_4,b_5)\right) \tag{3.18}$$

Maximizing L is equivalent to maximizing $\ln(L)$. To solve the optimum problem, two approaches are used here. 1) Let the partial derivative expression of the unknown parameter in the log-likelihood function be equal to 0 and solve the roots of the system. 2) Use non-linear optimization method.

Table 6: Values of Parameters in Accelerated Gamma Process Models

Model	Material	α_0	b_0	b_1	b_2	b_3	b_4	b_5	L-function value
Model (3.8)	BS	2.614	-1.666	-0.118	-5.130	-0.266	-0.500	--	-1199.400
	EC	1.924	-1.594	-0.118	-2.841	-0.193	-0.487	--	-1081.377
	SS	1.242	-1.862	-0.002	-1.532	-0.107	-0.855	--	-1035.034
	MMFX	0.914	-1.669	-0.158	-6.864	-0.292	-0.567	--	-947.484
Model (3.9)	BS	2.617	-1.783	0.000	--	-0.104	-0.496	-7.041	-1199.149
	EC	1.924	-1.660	-0.052	--	-0.112	-0.486	-3.499	-1081.392
	SS	1.242	-1.898	0.033	--	-0.050	-0.852	-2.466	-1035.000
	MMFX	0.913	-1.830	0.003	--	-0.114	-0.566	-7.641	-947.662
Model (3.10)	BS	2.617	-1.783	--	--	-0.104	-0.496	-7.041	-1199.149
	EC	1.923	-1.698	--	--	-0.068	-0.487	-3.491	-1081.440
	SS	1.242	-1.874	--	--	-0.079	-0.852	-2.459	-1035.013
	MMFX	0.913	-1.829	--	--	-0.116	-0.566	-7.643	-947.662

Results for different models are shown in the following Table 6. In model (3.8), b_2, b_3, b_4, are all negative, which means as crack width, crack depth, and chloride percentage goes up, the degradation incremental also goes up. Similar results apply to model (3.9). Since b_1 in model (3.9) is almost 0 for all materials, remove b_1 and get model (3.10). By comparing the likelihood function values, L-function value, it can be seen that there is no significant difference between model (3.9) and model (3.10).

Since all the incremental follow gamma distribution. The expected value of incremental can be derivative from: $\frac{d}{dt}E[X(t)] = \alpha(t)/\beta = \alpha_0/\beta(\mathbf{u})$. For the actual scenario, the physical meaning of the expected value is the rate at which the rebar degrades and corrodes. The degradation rate $\frac{d}{dt}E[X(t)]$ obtained as shown in Table 7:

Table 7: Degradation Rate Calculated from General Rebar Degradation Models

| | | CHL=3% | | | | | CHL=15% | | | |
| | | NO crack | WID=0.011 | | WID=0.035 | | NO crack | WID=0.011 | | WID=0.035 | |
			DEP=0.5	DEP=1	DEP=0.5	DEP=1		DEP=0.5	DEP=1	DEP=0.5	DEP=1
Model (3.8)	BS	15.795	16.972	19.388	19.196	21.928	16.772	18.021	20.586	20.382	23.283
	EC	10.818	10.926	12.032	11.697	12.881	11.469	11.583	12.755	12.400	13.656
	SS	8.218	8.797	9.281	9.127	9.628	9.105	9.747	10.283	10.113	10.668
	MMFX	5.779	6.160	7.128	7.263	8.405	6.186	6.593	7.630	7.774	8.997
Model (3.9)	BS	15.799	17.302	18.946	18.827	22.434	16.768	18.362	20.107	19.981	23.809
	EC	10.818	11.071	11.937	11.545	12.983	11.468	11.736	12.655	12.239	13.764
	SS	8.219	8.830	9.178	9.095	9.737	9.103	9.780	10.165	10.074	10.785
	MMFX	5.779	6.398	7.064	7.012	8.468	6.185	6.847	7.560	7.505	9.082
Model (3.10)	BS	15.800	17.302	18.946	18.827	22.435	16.768	18.362	20.107	19.981	23.810
	EC	10.659	11.238	11.850	11.719	12.885	11.300	11.915	12.563	12.425	13.661
	SS	8.297	8.747	9.222	9.009	9.782	9.191	9.689	10.215	9.979	10.836
	MMFX	5.783	6.393	7.066	7.007	8.489	6.190	6.842	7.563	7.499	9.086

The model shows that the corrosion resistance of different materials ranges from large to small: BS, EC, SS and MMFX. As the crack size and chlorine concentration increase, the corrosion rate will also increase. This is consistent with the actual situation.

Since the values of crack width, crack depth and chlorine concentration are too small, the above model can be supplemented after logarithmic processing of u_2 ($width$), u_3 ($depth$) as possible model forms:

$$\beta = e^{b_0 + b_1 u_1 + b_2 \ln u_2 + b_3 \ln u_3 + b_4 u_4} \tag{3.19}$$

$$\beta = e^{b_0 \quad + b_2 \ln u_2 + b_3 \ln u_3 + b_4 u_4} \tag{3.20}$$

$$\beta = e^{b_0 + b_1 u_1 + b_2 \ln u_2 + b_3 \ln u_3 + b_4 u_4 + b_5 \ln u_2 \ln u_3} \tag{3.21}$$

$$\beta = e^{b_0 \quad + b_2 \ln u_2 + b_3 \ln u_3 + b_4 u_4 + b_5 \ln u_2 \ln u_3} \tag{3.22}$$

$$\beta = e^{b_0 + b_1 u_1 \quad + b_3 \ln u_3 + b_4 u_4 + b_5 \ln u_2 \ln u_3} \tag{3.23}$$

$$\beta = e^{b_0 \quad + b_3 \ln u_3 + b_4 u_4 + b_5 \ln u_2 \ln u_3} \tag{3.24}$$

The results for the estimated parameters are presented in table 8.

Table 8: The Parametric Results of The Supplementary Model Part 1

	Material	α_0	b_0	b_1(INIT)	b_2(WID)	b_3(DEP)	b_4(CHL)	b_5(DEP*WID)	L-function value
Model (3.19)	BS	2.631	-2.447	-0.626	-0.103	-0.198	-0.526	--	-1199.383
	EC	1.933	-1.911	-0.262	-0.020	-0.113	-0.544	--	-1081.531
	SS	1.319	-2.070	-0.180	-0.032	-0.075	-0.854	--	-1032.517
	MMFX	0.923	-2.427	-0.709	-0.086	-0.237	-0.695	--	-947.715
Model (3.20)	BS	2.593	-2.201	--	-0.047	-0.038	-0.502	--	-1200.826
	EC	1.918	-1.884	--	-0.016	-0.028	-0.493	--	-1081.930
	SS	1.314	-1.993	--	-0.015	-0.031	-0.860	--	-1032.581
	MMFX	0.912	-2.334	--	-0.067	-0.026	-0.542	--	-948.210
Model (3.21)	BS	2.448	-2.735	2.253	-0.214	-1.611	-2.874	-0.365	-1208.327
	EC	1.927	-2.029	-0.017	-0.045	-0.319	-0.500	-0.045	-1081.459
	SS	1.337	-2.525	1.229	-0.148	-0.923	-0.792	-0.209	-1032.690
	MMFX	0.915	-2.538	-0.200	-0.122	-0.030	-0.676	-0.001	-947.996
Model (3.22)	BS	2.000	-2.860	--	-0.138	-0.526	-0.496	-0.084	-1205.185
	EC	1.924	-2.151	--	-0.076	-0.354	-0.486	-0.056	-1081.394
	SS	1.393	-2.065	--	-0.044	-0.185	-0.852	-0.027	-1029.944
	MMFX	0.914	-2.759	--	-0.164	-0.532	-0.564	-0.087	-947.601
Model (3.23)	BS	2.000	-3.322	-0.319	--	-0.197	-0.497	0.000	-1206.309
	EC	1.921	-1.855	-0.276	--	-0.139	-0.491	0.000	-1081.663
	SS	1.392	-1.890	-0.073	--	-0.079	-0.857	-0.001	-1030.034
	MMFX	0.911	-2.124	-0.325	--	-0.207	-0.580	0.000	-948.275
	BS	2.000	-2.315	--	--	-0.286	-0.496	-0.029	-1206.448
	EC	1.920	-1.849	--	--	-0.215	-0.491	-0.025	-1081.766
	SS	1.392	-1.890	--	--	-0.108	-0.857	-0.009	-1030.035

	MMFX	0.910	-2.108	--	--	-0.227	-0.577	-0.019	-948.412
Model (3.24)									

In table 8, these models differ in log-likelihood function value, *L*-function values, but not by much. Therefore, it can be said that the results obtained by maximum likelihood estimation are reasonable.

Supplementary models after taking logarithm of $u_2(width), u_3(depth), u_4(chloride)$

$$\beta = e^{b_0 + b_1 u_1 + b_2 \ln u_2 + b_3 \ln u_3 + b_4 \ln u_4} \tag{3.25}$$

$$\beta = e^{b_0 \quad + b_2 \ln u_2 + b_3 \ln u_3 + b_4 \ln u_4} \tag{3.26}$$

$$\beta = e^{b_0 + b_1 u_1 + b_2 \ln u_2 + b_3 \ln u_3 + b_4 \ln u_4 + b_5 \ln u_2 \ln u_3} \tag{3.27}$$

$$\beta = e^{b_0 \quad + b_2 \ln u_2 + b_3 \ln u_3 + b_4 \ln u_4 + b_5 \ln u_2 \ln u_3} \tag{3.28}$$

$$\beta = e^{b_0 + b_1 u_1 \quad + b_3 \ln u_3 + b_4 \ln u_4 + b_5 \ln u_2 \ln u_3} \tag{3.29}$$

$$\beta = e^{b_0 \quad + b_3 \ln u_3 + b_4 \ln u_4 + b_5 \ln u_2 \ln u_3} \tag{3.30}$$

The results for estimated parameters can be found in table 9.

Table 9: The Parametric Results of The Supplementary Model Part 2

	Material	α_0	b_0	$b_1(INIT)$	$b_2(WID)$	$b_3(DEP)$	$b_4(CHL)$	$b_5(DEP*WID)$	L-function value
Model (3.25)	BS	2.621	-2.570	-0.479	-0.099	-0.149	-0.038	--	-1199.458
	EC	1.916	-2.210	-0.372	-0.051	-0.121	-0.042	--	-1081.401
	SS	1.316	-2.320	-0.182	-0.032	-0.078	-0.064	--	-1032.516
	MMFX	0.918	-2.911	-0.838	-0.158	-0.226	-0.043	--	-947.499
Model (3.26)	BS	2.593	-2.347	--	-0.048	-0.038	-0.037	--	-1200.826
	EC	1.917	-2.032	--	-0.016	-0.027	-0.037	--	-1081.930
	SS	1.317	-2.238	--	-0.014	-0.031	-0.064	--	-1032.580
	MMFX	0.911	-2.503	--	-0.069	-0.024	-0.041	--	-948.210
Model (3.27)	BS	2.000	-3.061	0.396	-0.152	-0.713	-0.037	-0.132	-1205.159
	EC	1.924	-2.244	-0.344	-0.064	-0.192	-0.036	-0.013	-1081.375
	SS	1.393	-2.390	0.543	-0.064	-0.441	-0.063	-0.094	-1029.910
	MMFX	0.914	-2.844	-0.749	-0.142	-0.211	-0.042	0.000	-947.484
Model (3.28)	BS	2.000	-3.005	--	-0.138	-0.526	-0.037	-0.084	-1205.185
	EC	1.924	-2.293	--	-0.076	-0.354	-0.036	-0.056	-1081.394
	SS	1.393	-2.314	--	-0.044	-0.185	-0.064	-0.027	-1029.944
	MMFX	0.914	-2.923	--	-0.164	-0.532	-0.042	-0.087	-947.601
Model (3.29)	BS	2.000	-2.467	-0.319	--	-0.197	-0.037	0.000	-1206.309
	EC	1.921	-1.997	-0.276	--	-0.139	-0.037	0.000	-1081.663
	SS	1.392	-2.140	-0.075	--	-0.078	-0.064	-0.001	-1030.034
	MMFX	0.911	-2.293	-0.325	--	-0.207	-0.043	0.000	-948.275
	BS	2.000	-2.459	--	--	-0.286	-0.037	-0.029	-1206.448
	EC	1.920	-1.992	--	--	-0.215	-0.037	-0.025	-1081.766
	SS	1.392	-2.140	--	--	-0.108	-0.064	-0.009	-1030.035

| | MMFX | 0.910 | -2.277 | -- | -- | -0.227 | -0.043 | -0.019 | -948.412 |
| Model (3.30) | | | | | | | | | |

In table 9, the logarithm of the crack size and chlorine concentration was taken, but the size of α_0 and the final *L*-function value in the model were not affected. The model still retains its previous properties and is consistent with the actual situation.

The results of the models (3.19), (3.20), (3.25) and (3.26) are obtained by using the nonlinear optimization method, which is calculated by using the built-in function "fmincon" of MatLab. The algorithm is interior point, and the starting point is [1, 0, 0, 0, 0, 0]. The rest of the models adopt the improved particles swarm optimization (PSO), which starts from multiple random starting points for nonlinear optimization, thus avoiding the influence of artificially assigned starting points on the results. The constraint for both approaches applied here is that b_2, b_3, b_4, and b_5 are all negative values.

"*L*-function value" refers to the value of the log-likelihood function when the likelihood function obtains the optimal solution shown in the row. Considering that if the likelihood function is directly used, the value of the likelihood function will be very close to 0 in the optimal value, and it may be impossible to calculate, the logarithmic likelihood function is used. The larger the logarithmic likelihood function value is, the larger the likelihood function value is, the more accurate the estimated parameters are. In this way, the advantages and disadvantages of different models can be compared. All the models presented in this section have similar accuracy.

3.2.2   Accelerated test degradation model

This reinforcement degradation experiment considers the following situation: the experiment under the conditions with cracks is an accelerated test for the experiment under conditions without cracks. Even under different conditions, the corrosion process of the same kind of rebar should be

similar, and only the degradation time changes with the experimental conditions. In this case, it is assumed that for the same kind of rebar, the corrosion velocity under non-crack experimental conditions is $\frac{d}{dt}E[X_0]$, then the corrosion velocity under other crack experimental conditions should be $A \times \frac{d}{dt}E[X_0]$, where A is greater than 1, referring to the ratio of the corrosion velocity under such conditions to the corrosion velocity under non-crack conditions.

Based on the above assumptions, the accelerated test degradation model is established as follows:

Let the crack width and crack depth under "no crack" condition be 0.1 inch and 0.0022 inch to facilitate subsequent calculations.

For each independent degradation incremental, there is equation (3.31). In addition, for the scale parameter β, there is:

$$\beta = \beta_0 e^{b_4 u_4} \tag{3.31}$$

$$d_0 = 0.1; w_0 = 0.0022;$$

Parameters u_2, u_3, u_4 here represent "crack width", "crack depth", and "chloride percentage", respectively. A is the degradation speed ratio, which can be obtained by the slope ratio of the expected degradation curve with and without cracks. Parameters d_0 and w_0 indicates the benchmark crack size, which makes the value of degradation ratio A equal to 1 for uncrack condition degradation path.

Figure 23 shows how to calculate the parameter A for material BS when $u_2 = 0.035$ and $u_4 = 3\%$:
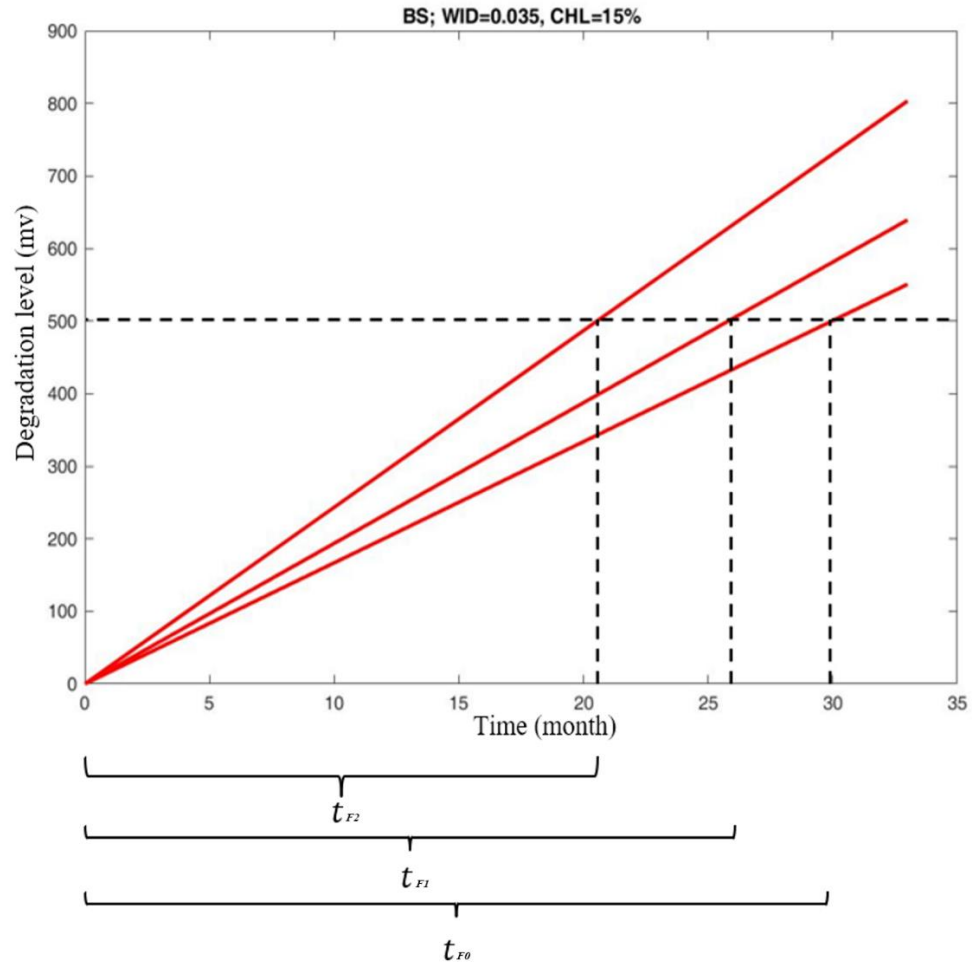
Figure 23: Expect Degradation Path for BS Rebars Degradation level of Cracked Concrete Class A (Crack

Width=.035") Exposing to 15% Concentration of Sodium Chloride

Those red lines in Figure 23 are expected degradation process. Using MATLAB built-in function "MLE" the shape parameter α and scale parameter β can be calculated for BS when crack width is 0.035 and chloride percentage is 15%. Using the degradation rate α / β as the slope can obtain the expected degradation process in the figure. The order of the lines in the figure is depth=1", depth=0.5", and uncrack in order of slope.

When $u_2 = 0.035, u_3 = 0.5, u_4 = 15\%$,

$$A = \frac{\frac{500}{t_{F1}}}{\frac{500}{t_{F0}}} = \frac{t_{F0}}{t_{F1}} \tag{3.35}$$

When $u_2 = 0.035, u_3 = 1, u_4 = 15\%$,

$$A = \frac{\frac{500}{t_{F2}}}{\frac{500}{t_{F0}}} = \frac{t_{F0}}{t_{F2}} \tag{3.36}$$

For k

$$k = \log_{\frac{u_2 u_3}{d_0 w_0}} A \tag{3.37}$$

Table 10 shows the values of A and k in different situations. The result is consistent with the conclusion of Data Analysis. That is, the increase of crack width, crack depth and chlorine concentration will accelerate the corrosion rate.

Table 10: The Parametric Results of A and k for Different Conditions

u_2(WID), u_4(CHL)		A		k	
		u_3(DEP)=0.5	u_3(DEP)=1	u_3(DEP)=0.5	u_3(DEP)=1
0.011,3%	BS	1.083	1.195	0.049	0.077
0.011,15%		1.124	1.195	0.072	0.077
0.035,3%		1.205	1.392	0.116	0.144
0.035,15%		1.161	1.459	0.093	0.164
0.011,3%	EC	1.014	1.103	0.009	0.043
0.011,15%		1.011	1.115	0.007	0.047
0.035,3%		1.072	1.158	0.043	0.064
0.035,15%		1.085	1.231	0.051	0.09
0.011,3%	SS	1.064	1.139	0.038	0.057
0.011,15%		1.118	1.076	0.069	0.032
0.035,3%		1.079	1.135	0.047	0.055
0.035,15%		1.101	1.254	0.06	0.098
0.011,3%	MMFX	1.044	1.322	0.027	0.121
0.011,15%		1.05	1.19	0.03	0.076
0.035,3%		1.273	1.437	0.15	0.158
0.035,15%		1.285	1.42	0.156	0.152

The parameter k calculated here can be used to derive the parameters α_0 and β in the accelerated test degradation model using maximum likelihood estimation. For each increment in the degradation process, using the accelerated test degradation model:

Shape parameter:

$$\alpha(t) = \alpha_0 (\tfrac{u_2 u_3}{d_0 w_0})^k t \tag{3.38}$$

Scale parameter:

$$\beta = \beta_0 e^{b_4 u_4} = e^{b_0 + b_4 u_4} \tag{3.39}$$

Where $d_0 = 0.1$, $w_0 = 0.0022$

When estimating parameters for a specific condition, only data that meets that condition is used. Since the corresponding parameter $A=1$ for the condition of no crack, the parameter α_0 and β in the accelerated test degradation model under the condition of no crack yields the same results as those obtained directly from "mle" built-in function. Table 11 shows the results.

Table 11: Parameters α_0, b_0, and b_4 in The Accelerated Test Degradation Model Derived From

Parameter A Using MLE

WID, CHL		α_0	b_0	b_4
0.011,3%		2.17	-1.854	-1.122
0.011,15%	BS	2.491	-1.624	-1.061
0.035,3%		1.066	-2.329	-0.253
0.035,15%		1.34	-2.018	-0.885
0.011,3%		1.453	-1.594	-0.602
0.011,15%	EC	1.42	-1.979	-0.376
0.035,3%		1.627	-1.741	-0.386
0.035,15%		1.863	-1.431	-1.192
0.011,3%		1.346	-1.686	-1.915
0.011,15%	SS	0.772	-2.056	-2.122
0.035,3%		0.78	-2.148	-2.569
0.035,15%		0.701	-2.038	-1.941
0.011,3%		0.834	-1.758	-1.225
0.011,15%	MMFX	0.569	-2.176	-0.873
0.035,3%		0.509	-1.96	-1.071
0.035,15%		0.34	-1.903	-0.388

In table 11, the obtained parameters α_0 and β can be used to calculate the shape parameters α and scale parameters β of the entire degradation process, as well as the degradation velocity α/β. They are shown in Tables 12 and 13.

Table 12: Parameters α and β in the Accelerated Test Degradation Model Derived from Parameter *A* Using MLE

u_2(WID), u_4(CHL)		α		β	α/β	
		u_3(DEP)=0.5	u_3(DEP)=1		u_3(DEP)=0.5	u_3(DEP)=1
0.011,3%	BS	2.544	2.936	0.151	16.848	19.444
0.011,15%		3.144	3.37	0.168	18.714	20.06
0.035,3%		1.768	2.207	0.097	18.227	22.753
0.035,15%		2.011	3.078	0.116	17.336	26.534
0.011,3%	EC	1.495	1.717	0.199	7.513	8.628
0.011,15%		1.452	1.71	0.131	11.084	13.053
0.035,3%		1.964	2.246	0.173	11.353	12.983
0.035,15%		2.327	2.943	0.2	11.635	14.715
0.011,3%	SS	1.523	1.679	0.175	8.703	9.594
0.011,15%		0.965	0.875	0.093	10.376	9.409
0.035,3%		0.96	1.032	0.108	8.889	9.556
0.035,15%		0.91	1.153	0.097	9.381	11.887
0.011,3%	MMFX	0.908	1.34	0.166	5.47	8.072
0.011,15%		0.628	0.765	0.1	6.28	7.65
0.035,3%		0.981	1.13	0.136	7.213	8.309
0.035,15%		0.672	0.736	0.141	4.766	5.22

Table 13: Parameters α and β under Uncracked Condition Derived from Parameter A Using MLE

	Material	$u_4(CHL)$	α	β	α/β
Uncracked	BS	3%	2.112	0.133	15.880
		15%	4.333	0.260	16.665
	EC	3%	1.552	0.142	10.930
		15%	2.791	0.245	11.392
	SS	3%	3.322	0.400	8.305
		15%	3.000	0.333	9.009
	MMFX	3%	1.613	0.282	5.720
		15%	1.063	0.170	6.253

It can be seen from the results of Tables 12 and 13 that the accelerated test degradation model basically conforms to the actual physical laws, that is, increasing the crack width (u_2), crack depth (u_3) and chlorine concentration (u_4) will increase the corrosion rate (α/β) of the rebar. Only when EC is under u_2=0.011, u_3=0.5, u_4=15%, and MMFX is under u_2=0.011, u_3=1, u_4=15%, and u_2=0.035, the results of the model are inconsistent with the physical situation, which may be caused by the randomness of the original data.

3.3 Initial 2-stage degradation models

It can be found from the figures of the rebar degradation paths that all the degradation paths show two distinctive degradation stages, which leads to the deviation between the actual degradation process and the expected degradation process of the one-stage model in the middle of the degradation. Therefore, in this case, using a two-stage linear degradation model can make the expected degradation process closer to the actual degradation process.

The two-stage degradation process has the following physical significance: during the first stage of corrosion, most chloride ions remain on the surface of the concrete and do not penetrate the concrete and the coat of rebars. At this time, the steel bars corrode slowly at a low rate, which is called rebar degradation latency. After enough chloride ions pass through the concrete and the coat of the rebar is penetrated by chloride ions, the reinforcement enters the second stage of corrosion, at which time the rebar corrodes at a faster rate.

The primary two-stage degradation model still assumes that the rebar degradation follows a linear gamma degradation process. There is a specific degradation level, known as alarm threshold for each material, denoted as x_0. Before and after the degradation level hitting that threshold, the degradation has different parameter values. The time of the first degradation stage is called degradation latency, noted as T_1 here. The values of the specific thresholds for different materials in the model are obtained by observing the figures. In the preliminarily research, the values of switch point for BS, EC, SS, and MMFX are 160mv, 110mv, 60mv, and 50mv, respectively.

For each degradation stage, the degradation increments $X(t_2) - X(t_1)$ follow a gamma distribution is as equation (3.2) shows, and $\beta(\mathbf{u})$ defined as follows:

$$\beta(\mathbf{u}) = e^{b_0 + b_2 u_2 + b_3 u_3 + b_4 u_4} \tag{3.40}$$

When the artificial environmental condition is uncracked, an assumption is applied as crack width (u_2) is 0.0011 inch, crack depth (u_3) is 0.05 inch. Based on this assumption, using maximum

likelihood estimation, the parameter for each material in both degradation stages can be obtained. The function "fmincon" is applied to maximum the likelihood function. Out of the consistency between model and actual physical scenario, the constraints for the optimization are: b_2, b_3, b_4 are non-positive numbers. These constraints guaranteed that as crack size or chloride percentage goes up, the degradation rate would also go up.

Following in Table 14 is the result for parameters in the initial 2-stage degradation model, $fval$ is the log-likelihood function value corresponding to the parameters value.

Table 14: Parameters in initial2-stage degradation model

Material	Stage	α	b_0	$b_2(WID)$	$b_3(DEP)$	$b_4(CHL)$	$fval$
BS	1	5.580	-0.432	0.000	-0.215	-1.335	-297.057104
	2	2.850	-1.970	-1.682	-0.159	0.000	-811.126824
EC	1	3.400	-0.326	0.000	-0.122	-1.003	-308.380335
	2	3.167	-1.617	-0.260	-0.047	0.000	-643.059965
SS	1	1.730	-0.780	0.000	0.000	0.000	-308.480375
	2	3.676	-1.084	-9.218	-0.128	0.000	-570.393767
MMFC	1	1.053	-0.876	0.000	0.000	0.000	-323.782581
	2	3.628	-0.953	0.000	-0.227	-1.484	-453.503291

When a parameter value is zero, it means the effect from variables corresponding to the parameter is very small or zero based on the experiment datasets. In this initial 2-stage degradation model, for BS and EC, crack width has no effect to the degradation in stage 1, and chloride percentage has no effect in stage 2; for SS, crack width, crack depth, or chloride percentage has no impact in stage 1 while chloride percentage has no impact in stage 2; for MMFX, crack width, crack depth, or chloride percentage has no impact in stage 1 while crack width has no impact in stage 2.

The shape parameter α, scale parameter β, and degradation rate α/β in the degradation

process can be derived based on the parameter values in Table 14.The detailed results are presented in Tables 15 and 16:

Table 15: Parameters α, β, and α/β Under 3% Chloride Concentration for Different Materials

Material			$u_4(CHL)=3\%$				
			uncracked	$u_2(WID)=0.011$		$u_2(WID)=0.035$	
				$u_3(DEP)=0.5$	$u_3(DEP)=1$	$u_3(DEP)=0.5$	$u_3(DEP)=1$
BS	α	Stage 1	5.632				
		Stage 2	2.870				
	β	Stage 1	0.617	0.560	0.503	0.560	0.503
		Stage 2	0.138	0.126	0.117	0.121	0.112
	α/β	Stage 1	9.127	10.054	11.195	10.054	11.195
		Stage 2	20.780	22.696	24.574	23.631	25.586
EC	α	Stage 1	3.503				
		Stage 2	3.168				
	β	Stage 1	0.696	0.659	0.620	0.659	0.620
		Stage 2	0.198	0.193	0.189	0.192	0.188
	α/β	Stage 1	5.033	5.317	5.651	5.317	5.651
		Stage 2	16.002	16.386	16.776	16.489	16.881
SS	α	Stage 1	1.772				
		Stage 2	3.665				
	β	Stage 1	0.458	0.458	0.458	0.458	0.458
		Stage 2	0.333	0.287	0.269	0.230	0.216
	α/β	Stage 1	3.865	3.865	3.865	3.865	3.865
		Stage 2	11.015	12.783	13.628	15.949	17.003
MMFX	α	Stage 1	1.054				

		Stage 2	3.754				
	β	Stage 1	0.416	0.416	0.416	0.416	0.416
		Stage 2	0.365	0.329	0.294	0.329	0.294
	α/β	Stage 1	2.530	2.530	2.530	2.530	2.530
		Stage 2	10.295	11.402	12.773	11.402	12.773

Table 16: Parameters α, β, and α/β under 15% Chloride Concentration for Different Materials

Material			u_4(CHL)=15%				
			no crack	u_2(WID)=0.011		u_2(WID)=0.035	
				u_3(DEP)=0.5	u_3(DEP)=1	u_3(DEP)=0.5	u_3(DEP)=1
BS	α	Stage 1	5.632				
		Stage 2	2.870				
	β	Stage 1	0.526	0.477	0.429	0.477	0.429
		Stage 2	0.138	0.126	0.117	0.121	0.112
	α/β	Stage 1	10.712	11.800	13.140	11.800	13.140
		Stage 2	20.780	22.696	24.574	23.631	25.586
EC	α	Stage 1	3.503				
		Stage 2	3.168				
	β	Stage 1	0.617	0.584	0.550	0.584	0.550
		Stage 2	0.198	0.193	0.189	0.192	0.188
	α/β	Stage 1	5.676	5.997	6.374	5.997	6.374
		Stage 2	16.002	16.386	16.776	16.489	16.881
SS	α	Stage 1	1.772				
		Stage 2	3.665				

	β	Stage 1	0.458	0.458	0.458	0.458	0.458
		Stage 2	0.333	0.287	0.269	0.230	0.216
	α/β	Stage 1	3.865	3.865	3.865	3.865	3.865
		Stage 2	11.015	12.783	13.628	15.949	17.003
MMFX	α	Stage 1	1.054				
		Stage 2	3.754				
	β	Stage 1	0.416	0.416	0.416	0.416	0.416
		Stage 2	0.305	0.276	0.246	0.276	0.246
	α/β	Stage 1	2.530	2.530	2.530	2.530	2.530
		Stage 2	12.302	13.625	15.263	13.625	15.263

It can be known from these tables that: 1) According to the degradation rate, the order of corrosion resistance of the rebar should be BS<EC<SS or MMFX. SS is more corrosion-resistant than MMFX when the chloride percentage is 3%. 2) The degradation rate in stage 2 is significantly higher than it in stage 1. This result is consistent with the physical mechanism of 2-stage degradation.

The above data are presented in Figures 24 to 27 and compared with the original data as follows, where the red line represents the expected degradation curve, derived from initial 2-stage degradation model:

BS
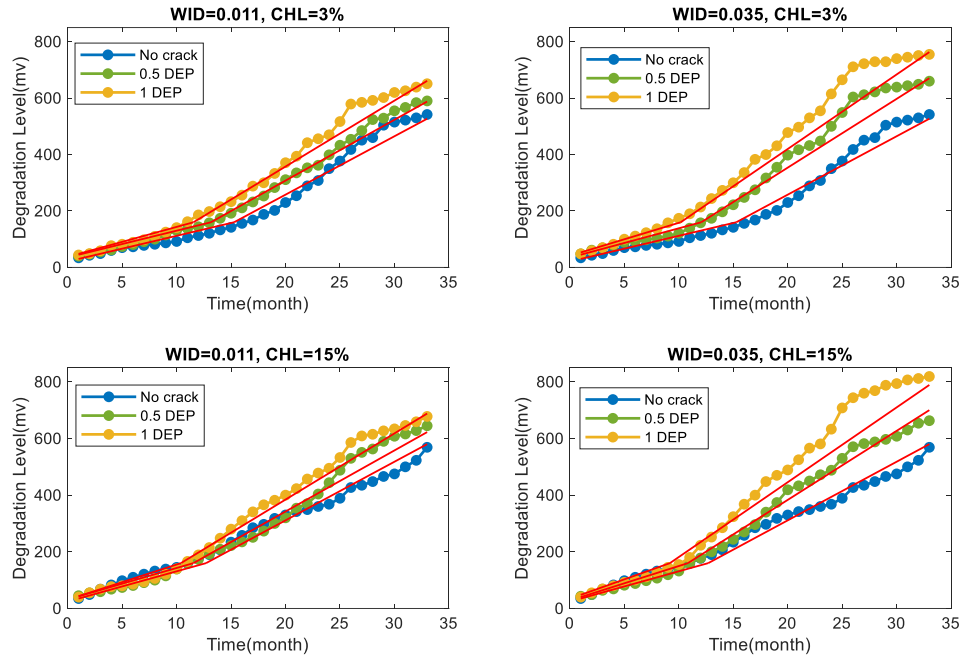
Figure 24: BS Expected and Real Degradation level for 2-stage gamma process model under Cracked

EC
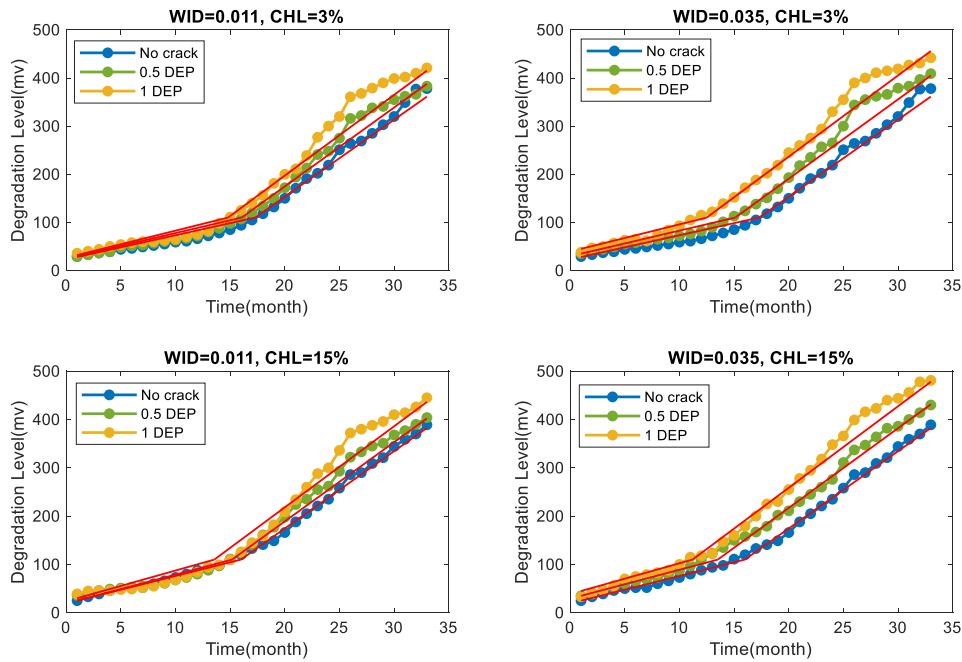
Figure 25: EC Expected and Real Degradation level for 2-stage gamma process model under Cracked

SS
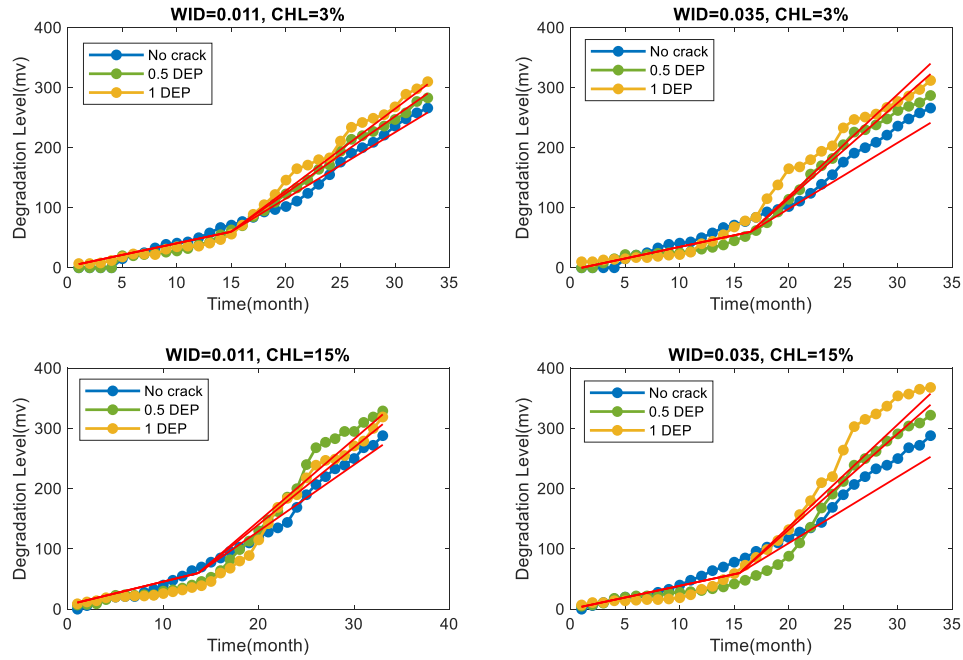
Figure 26: SS Expected and Real Degradation level for 2-stage gamma process model under Cracked

MMFX
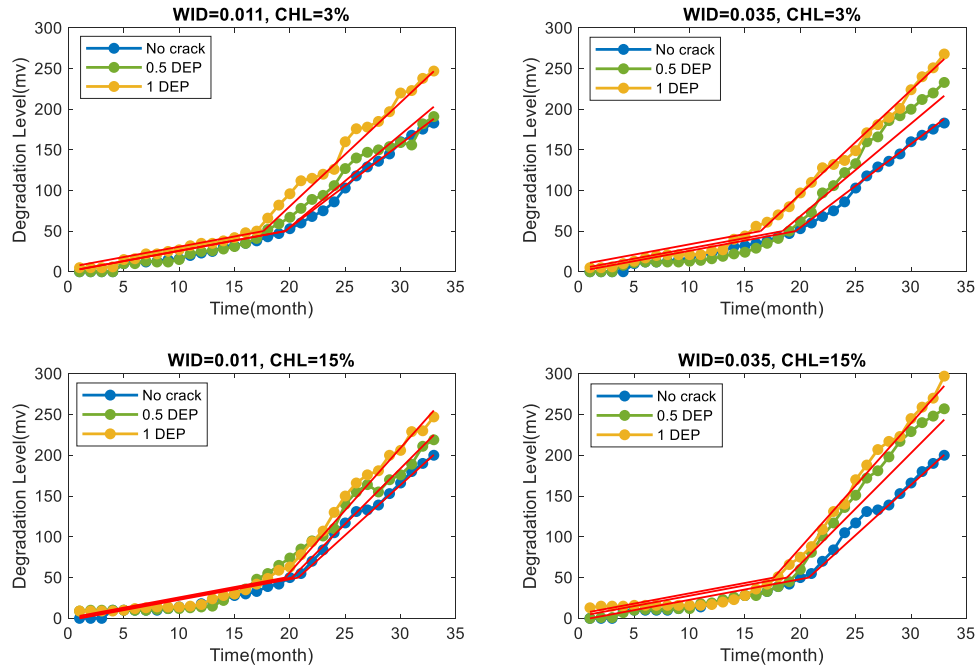
Figure 27: MMFX Expected and Real Degradation level for 2-stage gamma process model under Cracked

The two-stage degradation models fit the actual data well. In addition, the results show the expected second stage degradation path of the same rebar at the same chloride concentration seems to be parallel. This indicates that for the second stage of the corrosion process, the size of the crack may not have a significant effect on the rate of degradation.

The corresponding physical scenario is as follows: after the degradation initiation time, degradation latency, the concentration of chloride ions penetrating through concrete to the surface of rebar is limited by the concentration of the applied chloride solutions on the surface of concrete. At this point, even if the concrete crack size increases, it is unable to make the chlorine concentration at the surface of rebar increase significantly. Therefore, the corrosion rate in the second stage is not very sensitive to the crack size.

Table 17 presents the degradation of different rebar under various conditions:

Table 17: The Degradation Latency of Different Rebar under Various Conditions

Degradation Latency t_L (month)	$u_4(CHL)=3\%$				
	no crack	$u_2(WID)=0.011$		$u_2(WID)=0.035$	
		$u_3(DEP)=0.5$	$u_3(DEP)=1$	$u_3(DEP)=0.5$	$u_3(DEP)=1$
BS	16.33	13.13	10.90	12.13	9.13
EC	17.38	16.23	14.92	14.75	11.50
SS	13.22	14.63	15.27	16.80	14.38
MMFX	19.50	17.82	17.00	19.00	15.50
	$u_4(CHL)=15\%$				
BS	11.06	11.00	10.77	11.00	10.20
EC	14.92	15.00	15.00	12.07	10.67
SS	12.56	15.64	16.00	17.50	15.07
MMFX	20.00	17.29	18.10	19.33	17.89

As can be seen from the Table 17, 1) for BS and EC, the degradation latency increases with the increase of $u_2(WID), u_3(DEP)$. This corresponds to the physical meaning. As

$u_2(WID), u_3(DEP)$ increase, chlorine irons penetrate the concrete surface more quickly and the degradation delay decreases accordingly. 2). When chloride concentration is 3%, the difference between degradation latencies of BS under different crack sizes is larger than that of other rebar materials. This means in first stage when chloride concentration is 3%, the crack size has greater impacts on BS than that on other rebar materials 3). For BS and EC, when chloride percentage is 15%, the degradation latency varies less when compared with it when chloride percentage is 3%. This means crack size has more impact on BS and EC in stage 1 when chloride percentage is 3% compared with that when chloride concentration is 15%.

4. Advanced 2-stage degradation model

Based on the result obtained from the initial 2-stage degradation model, the advanced 2-stage degradation models are proposed. The models still consider the degradation process consists of two different stages, which are the corrosion initiation stage with relatively lower degradation rate and the corrosion propagation stage with a relatively higher degradation rate. x_0 denotes the alarm threshold in terms of degradation level, separating two degradation stages. x_0 is selected to be 160 mv, 130 mv, 60 mv, and 50 mV, respectively, for BS, EC, SS, and MMFX rebar materials. Latency is the time when corrosion level reaches the alarm threshold. *H* denotes the failure threshold.

The advanced 2-stage stochastic model is developed according to the actual degradation behaviors, where the degradation rate is affected by pre-cracking size *a* (*a* = DEP×WID) and chloride concentration *C* in stage 1, the corrosion initiation stage. In stage 2, the corrosion propagation stage, only chloride concentration mainly affects the degradation rate. The reason why the pre-cracking size is adopted as stress variable here instead of crack width or crack depth is that crack width and crack depth are correlated variables in practice. When the crack width gets larger, the crack depth goes deeper. It is more reasonable to adopt pre-cracking size instead of crack width

or crack depth, respectively, as the environmental stress variable. Pre-cracking size a are 0.0055, 0.011, 0.0175 and 0.035 inch^2, based on the considered pre-cracking widths and depths. Two sodium chloride concentrations (C), 3% and 15%, are adopted in the experimental program. As a result, we have datasets under 10 different stress level combinations in terms of a and C.

4.1. Gamma-gamma 2-stage degradation model

Similar to the previous initial 2-stage degradation model, the gamma-gamma 2-stage degradation model describes the 2-stage degradation paths divided by the alarm threshold x_0 interms of the degradation level. The degradation in each stage can be modeled by a gamma process with different stress-affected shape parameters. The pre-cracking size a ($a = \text{DEP} \times \text{WID}$) and chloride concentration C are the environmental stress variables here. Pre-cracking size a are 0.0055, 0.011, 0.0175 and 0.035 inch^2 based on the considered pre-cracking widths and depths. For the convenience of calculation and modeling, pre-cracking size is set to be 5.5×10^{-6} inch^2 when there is no crack over the test concrete specimen. Two sodium chloride concentrations (C), 3% and 15%, are adopted in the experimental program. As a result, There are 10 different stress level combinations in terms of a and C for the experimental data.

Both degradation process follows a gamma process, which means the degradation increment between any time interval follows gamma distribution, i.e., $X(t) - X(s) \sim \text{gamma}\big(\alpha(t) - \alpha(s), \beta(\mathbf{u})\big)$, $X(t)$ is the degradation level at time t. $\alpha(t) - \alpha(s)$ is the gamma distribution shape parameter. $\beta(\mathbf{u})$ is the scale parameter which is a function of $\mathbf{u}$. $\mathbf{u}$ denotes the vector that contains the stress variables which have impacts on degradation. Then the probability density function (PDF) of the degradation increment can be derived as Eq. (4.1),

$$f(x; \mathbf{u}) = \frac{\beta(\mathbf{u})^{\alpha(t)-\alpha(s)} x^{\alpha(t)-\alpha(s)-1} \exp\big(-\beta(\mathbf{u})x\big)}{\Gamma\big(\alpha(t) - \alpha(s)\big)}, \, x > 0 \tag{4.1}$$

The scale parameter $\beta(\mathbf{u})$ varies in different stages. In the first stage, considering the

physical enviorment effects, $\beta(\mathbf{u})$ is a function associate with a and C as $\beta(a,C)=\beta_{10}e^{b_1(a-a_0)+b_2(C-C_0)}$. In the second, $\beta(\mathbf{u})$ is assumed to be affected only by chloride concentration C in the second stage, where it can be expressed as $\beta(C)=\beta_{20}e^{b_3(C-C_0)}$ in the corrorsion propogation stage. This assumption is reasonable either from the prospect of physical corrosion process or from the previous data observation result. The shape parameters in two stages follow a linear assumption and can be expressed as $\alpha(t)=\alpha_{10}t$ and $\alpha(t)=\alpha_{20}t$ respectively. a_0 denotes the crack size for the concrete specimen under un-cracked condition, which is 5.5×10^{-6} inch^2. C_0 denotes the baseline of chloride concentration, and it is assumed to be 1% in this work. α_{10}, α_{20}, β_{10}, β_{20}, b_1, b_2, and b_3 are the model parameters here. It should be noted that the degradation level of concrete samples is collected every month, so the time interval for degradation increment is 1 month.

The degradation rate DR measures the change of degradation level each month. Theoretically, it should always be a non-negative value with unit of mV/month in this research. The degradation rate in the first and second stage, DR_1 and DR_2, can be derived as Eq (4.2) and Eq (4.3) as following:

$$DR_1 = \frac{d}{dt}E[X_1(t)-X_1(s);a,C]=\frac{\alpha_{10}}{\beta_{10}e^{b_1(a-a_0)+b_2(C-C_0)}} \tag{4.2}$$

$$DR_2 = \frac{d}{dt}E[X_2(t)-X_2(s);C]=\frac{\alpha_{20}}{\beta_{20}e^{b_3(C-C_0)}} \tag{4.3}$$

The model parameters can be estimated from the experimental dataset using MLE approach. In this study, the likelihood function of the parameters is maximized using interior point algorithm, a non-linear optimization approach. The results are listed in the Table 18. α_{10}, β_{10}, b_1, and b_2 are the model parameters in stage 1; α_{20}, β_{20}, and b_3 are the model parameters in stage 2. The results are shown in Table 18.

Table 18 The estimated model parameters for four rebar material with Class A concrete

Rebar with Class A	Stage 1: corrosion initiation				Stage 2: corrosion propagation		
	α_{10}	β_{10}	b_1	b_2	α_{20}	β_{20}	b_3
BS	5.651	0.633	-7.705	-1.327	2.814	0.120	--
EC	3.507	0.772	-9.326	-0.997	3.163	0.191	-0.001
SS	1.730	0.458	--	--	3.478	0.280	-1.434
MMFX	1.053	0.416	--	--	3.552	0.321	-1.477

According to the physical degradation mechanism, the larger the pre-cracking size a and chloride percentage C are, the higher DR will be. Thus, the parameters b_1, b_2, and b_3 should be non-positive values. When estimated, the value range of these parameters are set to be from negative infinity to zero while the rest parameters are set to be unlimited. Using results in Table 18 with Eq (4.2) and Eq (4.3), the DR for four materials under ten different enviormental stress can be obtained as Table 19.

Table 19 DR_1 and DR_2 for each rebar material under different a and C

Rebar	C	Stage 1 DR_1 (mV/month)					Stage 2 DR_2 (mV/month)
		Un-crack	Pre-cracking size a				
			0.0055	0.011	0.0175	0.035	
BS	3%	9.2	9.6	10.0	10.5	12.0	23.5
	15%	10.7	11.2	11.7	12.3	14.1	23.5
EC	3%	4.6	4.9	5.1	5.5	6.4	16.6
	15%	5.2	5.5	5.8	6.1	7.2	16.6
SS	3%	3.8	3.8	3.8	3.8	3.8	12.8
	15%	3.8	3.8	3.8	3.8	3.8	15.2
MMFX	3%	2.5	2.5	2.5	2.5	2.5	11.4
	15%	2.5	2.5	2.5	2.5	2.5	13.6

It can be seen from Table 19 that for all four materials, the degradation rate changes dramatically when the degradation goes into the second degradation stage. This result is consistent with the actual scenario where the corrosion speed is much faster in the corrosion propagation stage than it in the corrosion initiation stage. For BS and EC rebar, increase the pre-cracking size or chloride percentage can also increase the degradation rate in the first degradation stage. For SS and MMFX rebar, increasing the chloride percentage can also increase the degradation rate in the second degradation stage. This result is still consistent with the physical situation. However, consider the BS and EC in the second degradation stage and EC, MMFX in the first degradation stage. The degradation rate changes very small even the pre-cracking size a or the chloride concentration C is enlarged. This is because different corrosion resistance possessed by these four rebar materials account for the distinct sensitivity of corrosion initiation and propagation stages to pre-cracking size and chloride concentration.

Another notable thing here is, by increasing the pre-cracking size or the chloride concentration,

the degradation rate can also be increased to a different level. This means by increasing the environmental stress variables, an accelerated test can be applied here. Acceleration factor (A_F) determines how much the test is accelerated. A_F can be obtained by taking the ratio of mean time to failure at normal conditions ($MTTF_o$) to that predicted at accelerated conditions ($MTTF_s$) as Eq. (4.4),

$$A_F = \frac{MTTF_o}{MTTF_s} = \frac{E[T;\mathbf{u}_o]}{E[T;\mathbf{u}_s]} \tag{4.4}$$

where vector $\mathbf{u}_o$ denotes stress variables at normal conditions and vector $\mathbf{u}_s$ denotes the stress variables at stressed conditions. In the first degradation stage, the stress vector $\mathbf{u}$ contains pre-cracking size a and chloride concentration C while in the second degradation stage, the stress vector $\mathbf{u}$ is C only. Thus, the acceleration factor A_{F_1} and A_{F_2} for degradation stage 1 and stage 2 can be derived as Eq. (4.5) and Eq. (4.6).

$$A_{F_1} = \frac{E[T_1;a_0,C_0]}{E[T_1;a,C]} \tag{4.5}$$

$$A_{F_2} = \frac{E[T_2;C_0]}{E[T_2;C]} \tag{4.6}$$

Where T_1 and T_2 denotes the time period of stage 1 and stage 2. By combining Eq (4.5), Eq (4.6), with Eq (4.2) and Eq (4.3), the total acceleration factor A_F for entire degradation process and be obtained as Eq (4.7)

$$
\begin{aligned}
A_F &= \frac{E[T_1;a_0,C_0]+E[T_2;C_0]}{E[T_1;a,C]+E[T_2;C]}, \\
A_F &= \frac{E[T_1;a_0,C_0]}{E[T_1;a,C]+E[T_2;C]} + \frac{E[T_2;C_0]}{E[T_1;a,C]+E[T_2;C]} \\
&= \frac{E[T_1;a_0,C_0]}{E[T_1;a,C]}\frac{E[T_1;a,C]}{E[T_1;a,C]+E[T_2;C]} + \frac{E[T_2;C_0]}{E[T_2;C]}\frac{E[T_2;C]}{E[T_1;a,C]+E[T_2;C]} \\
&= A_{F_1}p_1 + A_{F_2}p_2 \\
\text{where } p_1 &= \frac{E[T_1;a,C]}{E[T_1;a,C]+E[T_2;C]}, \quad p_2 = \frac{E[T_2;C]}{E[T_1;a,C]+E[T_2;C]}
\end{aligned}
\tag{4.7}
$$

p_1 denotes the proportion of time that bridge rebar stays in stage 1. p_2 is the proportion of time that bridge rebar stays in stage 2. Further, the A_F for the whole degradation process can be obtained as Eq (4.8)

$$A_F = \frac{p_1}{e^{b_1(a-a_o)+b_2(C-C_o)}} + \frac{p_2}{e^{b_3(C-C_o)}}$$

$$= \frac{x_0\beta_{1o}}{x_0\beta_{1o}e^{b_1(a-a_o)+b_2(C-C_o)} + \dfrac{\alpha_{10}(H-x_0)\beta_{2o}e^{b_3(C-C_o)}}{\alpha_{20}}} + \frac{(H-x_0)\beta_{2o}}{\dfrac{\alpha_{20}x_0\beta_{1o}e^{b_1(a-a_o)+b_2(C-C_o)}}{\alpha_{10}} + \alpha_{10}(H-x_0)\beta_{2o}e^{b_3(C-C_o)}}$$

$$(4.8)$$

Where H denotes the failure threshold. It can be given from the demanding degradation level in terms of the designed life. From the Table 19, the acceleration factor in both stage, A_{F_1} and A_{F_2}, for all four material can be obtained. The results about A_{F_1} and A_{F_2} are shown in Table 20.

Table 20 A_{F_1} and A_{F_2} for the four bridge rebar with Class A concrete under different a and C

Rebar with Class A		Stage 1 A_{F_1}				Stage 2 A_{F_2}
		Pre-cracking size a				
	C	0.0055	0.011	0.0175	0.035	
BS	3%	1.07	1.12	1.17	1.34	1
	15%	1.26	1.31	1.38	1.58	1
EC	3%	1.07	1.13	1.20	1.41	1
	15%	1.21	1.27	1.35	1.59	1
SS	3%	1	1	1	1	1.03
	15%	1	1	1	1	1.22
MMFX	3%	1	1	1	1	1.03
	15%	1	1	1	1	1.23

In Table 20, for BS and EC material, the pre-cracking size and chloride concentration both can significantly impact the rebar corrosion in the corrosion initiation stage. As the increase of pre-

crack size and chloride concentration, the acceleration factor also increases. The impact from chloride concentration on acceleration factor of BS and EC in the first stage is similar. In the corrosion propagation stage, the influence from chloride percentage is very small. This may because the BS and EC material have poor corrosion resistance. Once the corrosion starts, it will spread at a high speed. For SS and MMFX, the pre-crack size or chloride percentage does not significantly accelerate the degradation in the corrosion initiation stage while the chloride concentration have impact on both materials in second degradation stage. This may be because both SS and MMFX material have good corrosion resistance. The chloride concentration can only have effect once the corrosion has started. The impact from chloride concentration on the acceleration factor of SS and MMFX in second degradation stage is similar.

The acceleration factor A_F indicates how much the experiment can be accelerated. Thus, based on the results in Table 20, the degree that how much the pre-cracking size and chloride concentration can reduce the corrosion initiation time can be calculated. Table 21 shows when compared with the corresponding materials under uncracked condition, the percentages of time reduce that the different pre-cracking size can contribute to.

Table 21 Percentage of corrosion initiation testing time reduced by inducing pre-cracking

Rebar	C	Pre-cracking size a			
		0.0055	0.011	0.0175	0.035
BS	3%	4.2%	8.0%	12.4%	23.3%
	15%	4.5%	8.5%	13.0%	24.1%
EC	3%	6.1%	9.8%	16.4%	28.1%
	15%	5.5%	10.3%	14.8%	27.8%

Similarly, the chloride concentraction can also be applied to accelerate the corrosion to reduce the experiment time. Table 22 shows when compared with the corresponding material under 3% chloride concentraction, how much percentages of time can be reduced by increasing chloride concentration to 15%

Table 22 Percentage of testing time of two stages reduced by raising chloride concentration

Rebar	C	Un-cracked	0.0055	0.011	0.0175	0.035	Rebar	C	Corrosion propagation
			Corrosion initiation (Pre-cracking size a)						
BS	15%	14.0%	14.3%	14.5%	14.6%	14.9%	SS	15%	15.8%
EC	15%	11.5%	10.9%	12.1%	9.8%	11.1%	MMFX	15%	16.2%

According to Tables 21 and 22, the accelerated testing plan can be conducted by introducing the pre-cracking and chloride concentration. The pre-cracking size can reduce the corrosion initiation time for EC more efficiently than for BS. However, when using chloride concentration as a stress variable, the corrosion initiation time for BS material will receive more impact than EC material.

Based on the parameters in Table 18 and degradation rate in Table 19, Figures 28, 29, 30, and 31 are presented to illustrate the actual degradation path and the expected degradation path. Each expected degradation path starts from the actual degradation level at the first month, and then goes to the alarm threshold x_0 with DR_1 in Table 19, and then goes to the failure threshold H with slope DR_2 in Table 19. Note that due to the H is usually much higher than the degradation level at the 33rd month, all the expected degradation path is cut at the 33rd month in the figure for the convenience of view.
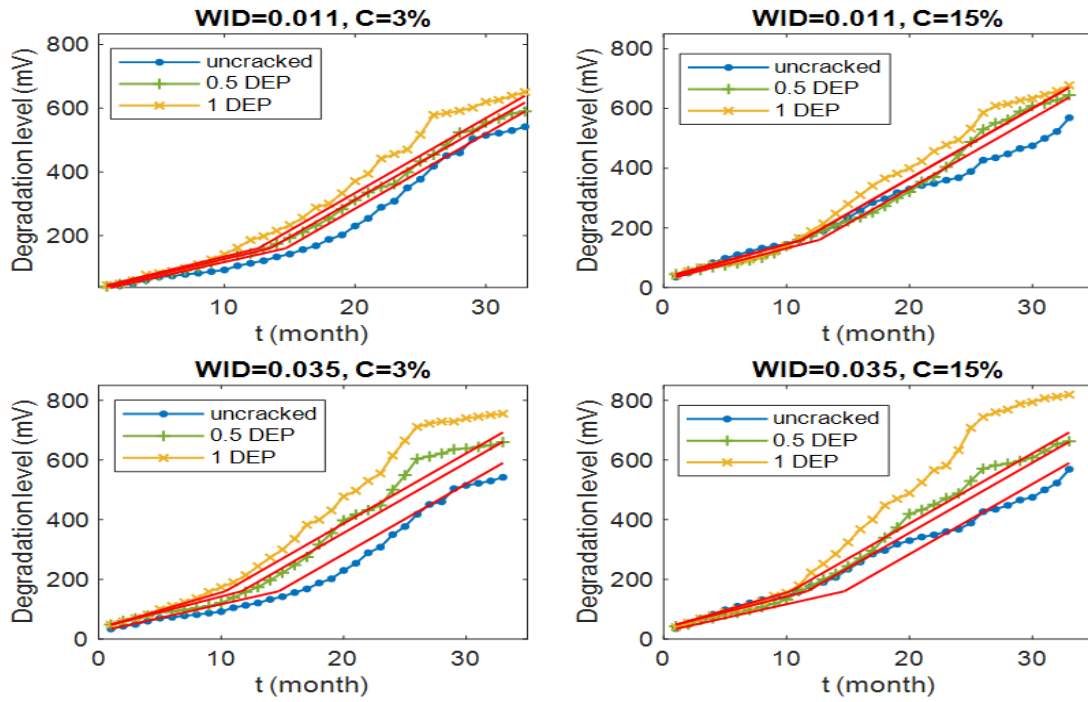
Figure 28 Actual corrosion and expected corrosion of BS rebar, G-G model
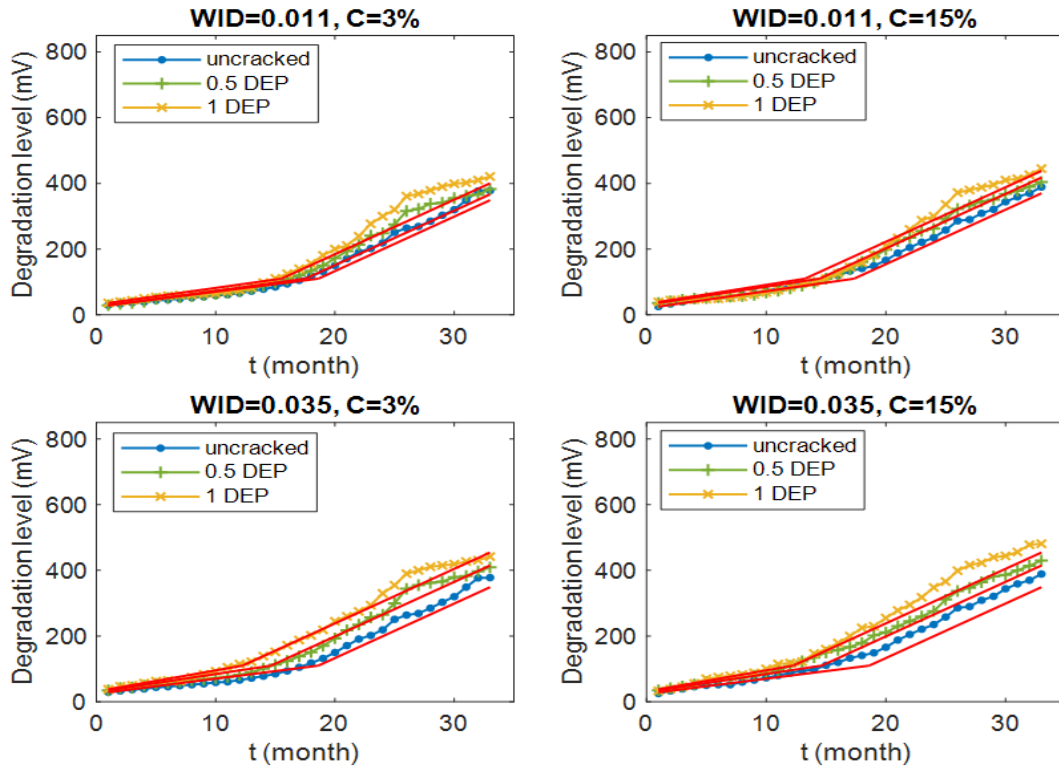
Figure 29 Actual corrosion and expected corrosion of EC rebar, G-G model

As can be seen from Figures 28 and 29, for different pre-crack sizes, the actual corrosion path of the first stage is almost always divergent, and the expected corrosion line is also divergent. The results show that the pre-crack size reduces the incubation period of reaching the alarm threshold x_0 in the first stage and effectively accelerates the initiation of corrosion. It is assumed that the level of chloride ions is dominant in the second corrosion stage, according to the model parameters, the corresponding expected corrosion lines are parallel (the chloride ion concentration C of each subgraph is the same), and most of the expected corrosion curves can approximate the actual corrosion direction of the second corrosion stage.

In order to illustrate the impact of chloride level on rebar corrosion, Figs. 30 and 31 show the corrosion paths of SS rebar and MMFX rebar with the same pre-cracking size in each subfigure while chloride concentration is different.
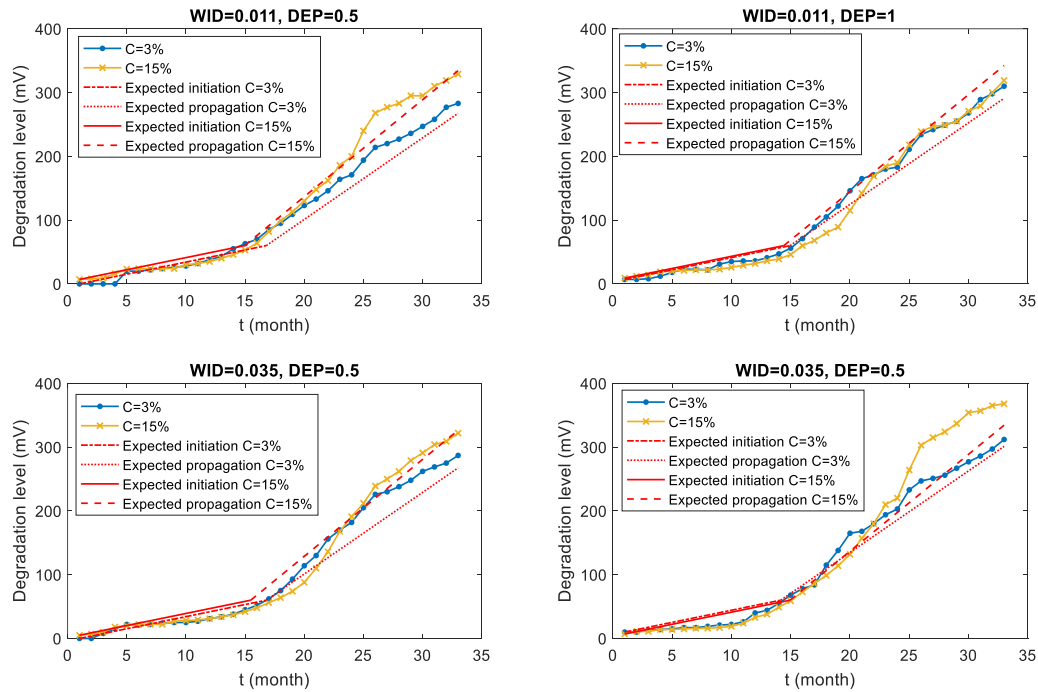
Figure 30 Actual corrosion and expected corrosion of SS rebar, G-G model
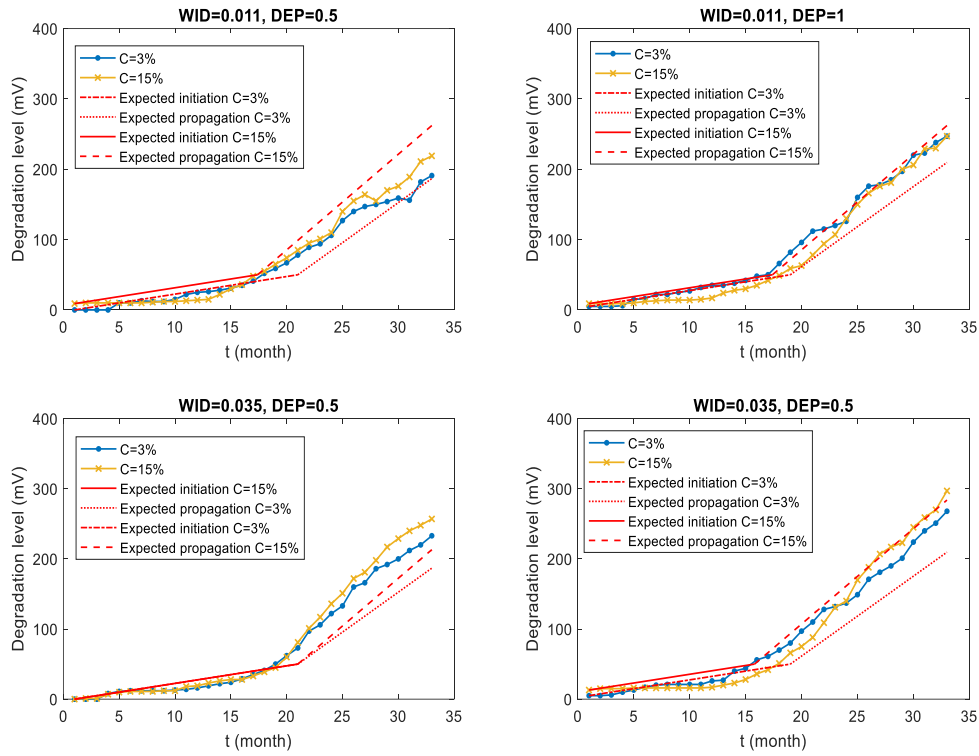
Figure 31 Actual corrosion and expected corrosion of MMFX rebar, G-G model

In Figures 30 and 31, according to the model parameters, the expected degradation paths in the first degradation stage are plotted parallel. These results are consistent with the actual degradation paths, which have no significant divergent in the first degradation stage. In the second stage, under the influence of chloride concentration, the expected degradation shows different degradation rate. Note that there might be some deviation in the figures, it is because the degradation has randomness inside. Especially, the variation of degradation level at the first month may significantly impact the observed effect for the expected path matching with the actual degradation. Besides the deviation caused by the randomness, the degradation tendency is well indicated by the gamma-gamma 2-stage degradation model.

4.2. Weibull-gamma 2-stage degradation model

In actual scene, the researchers usually do not pay attention to the degradation process in the

first degradation stage. Because the degradation process in the corrosion initiation stage is relatively small and the detection for the corrosion may have relatively larger error, researchers also using the time period to describe the first degradation stage. In the Weibull-gamma distribution, the second degradation stage is described using gamma process, like the second stage in gamma-gamma 2-stage degradation model. The first stage is evaluated to be a time-to-event model. As described before, the total degradation time $T = T_1 + T_2$, where T_1 is the degradation latency, the time that the rebar stays in the first degradation initiation stage until degradation level reaches the alarm threshold x_0. T_2 represents the time that the rebar stays in the second degradation stage, from x_0 until it reaches the failure threshold H. Considering the actual scene, it is reasonable to assume that $T_1 \sim \text{Weibull}\big(\eta(\mathbf{u_1}), \beta\big)$. Where $\eta(\mathbf{u_1})$ is the scale parameter, $\mathbf{u_1}$ denotes the vector contains the environmental stress variables. β is the shape parameter. The PDF and the reliability function $R(t; \mathbf{u_1})$ for this stage can be presented as Eq. (4.9) and Eq. (4.10),

$$f(t; \mathbf{u_1}) = \frac{\beta}{\eta(\mathbf{u_1})} \left(\frac{t}{\eta(\mathbf{u_1})} \right)^{\beta-1} e^{-\left(\frac{t}{\eta(\mathbf{u_1})} \right)^{\beta}} \tag{4.9}$$

$$R(t; \mathbf{u_1}) = e^{-\left(\frac{t}{\eta(\mathbf{u_1})} \right)^{\beta}} \tag{4.10}$$

The second stage in the Weibull-gamma 2-stage degradation model is a gamma process affected by the environmental stress variable $\mathbf{u_2}$. The degradation in the second degradation stage has statistically independent increments from arbitrarily time s to time t, $X(t) - X(s) \sim \text{gamma}(a(t) - a(s), \beta(\mathbf{u_2}))$, where the shape parameter of gamma process is assumed to be a linear to time t, $a(t) = at$. The scale parameter $\beta(\mathbf{u_2})$ is a function of environmental stress vector $\mathbf{u_2}$. $\beta(\mathbf{u_2})$ can include any number of environment stresses regarding scale parameter β as follows,

$$\beta(\mathbf{u_2}) = \beta_o e^{b_1(u_{21}-u_{21,o})+b_2(u_{22}-u_{22,o})+...+b_1(u_{2n_2}-u_{2n2,o})} = \eta_o e^{\sum_{i=1}^{n_2} b_i(u_{2i}-u_{2i,o})}$$

$$\beta(\mathbf{u_2}) = \beta_o \left(\frac{u_{21}}{u_{21,o}}\right)^{b_1}\left(\frac{u_{22}}{u_{22,o}}\right)^{b_2}...\left(\frac{u_{2n_2}}{u_{2n_2,o}}\right)^{b_{n_2}} = \eta_o \prod_{i=1}^{n_2}\left(\frac{u_{2i}}{u_{2i,o}}\right)^{b_i} \tag{4.11}$$

The PDF for the degradation increment in this stage can be derived as Eq (4.12).

$$f(x;\mathbf{u_2}) = \frac{\beta(\mathbf{u_2})^{a(t-s)} x^{a(t-s)-1}\exp(-\beta(\mathbf{u_2})x)}{\Gamma(a(t\text{-}s))}, x > 0 \tag{4.12}$$

$F_{X(T_2)}(H-x_0;\mathbf{u_2})$ is a gamma distribution CDF evaluated at $H-x_0$. Thus, the degradation process described above can be analyzed by combining the two degradation stages together. The reliability function of the rebar subjected to the entire degradation process can be presented as Eq. (4.13),

$$R(t;\mathbf{u_1},\mathbf{u_2}) = 1 - \int_0^t \left(1 - F_{X(t-v)}(H-x_0;\mathbf{u_2})\right)f_{T_1}(v,\mathbf{u_1})dv$$

$$= 1 - \int_0^t \left(1 - \int_0^{H-x_0}\frac{\beta(\mathbf{u_2})^{\alpha(t-v)}x^{\alpha(t-v)-1}e^{-\beta(\mathbf{u_2})x}}{\Gamma(\alpha(t-v))}dx\right)\frac{\beta}{\eta(\mathbf{u_1})}\left(\frac{v}{\eta(\mathbf{u_1})}\right)^{\beta-1}e^{-\left(\frac{v}{\eta(\mathbf{u_1})}\right)^{\beta}}dv \tag{4.13}$$

Assume there is only one environmental stress variable in the vector $\mathbf{u_1}$ and $\mathbf{u_2}$, for the first degradation stage, the scale parameter $\eta(\mathbf{u_1}) = \eta_0 u_{11}{}^{b_1}$. u_{11} is the only stress included in vector $\mathbf{u_1}$. For the second gamma distributed degradation stage, the scale parameter $\beta(\mathbf{u_2}) = \beta_0 e^{b_2 u_{21}}$. Vector $\mathbf{u_2}$ only contains a single stress u_{21}. η_0 and β_0 denote the baseline of the stress variables. b_1 and b_2 are model parameters. Fig. 32 illustrates how the expected two-stage degradation changes vs. time with stress $\mathbf{u_1} = (u_{11})$ and $\mathbf{u_2} = (u_{21})$ regarding each stage.
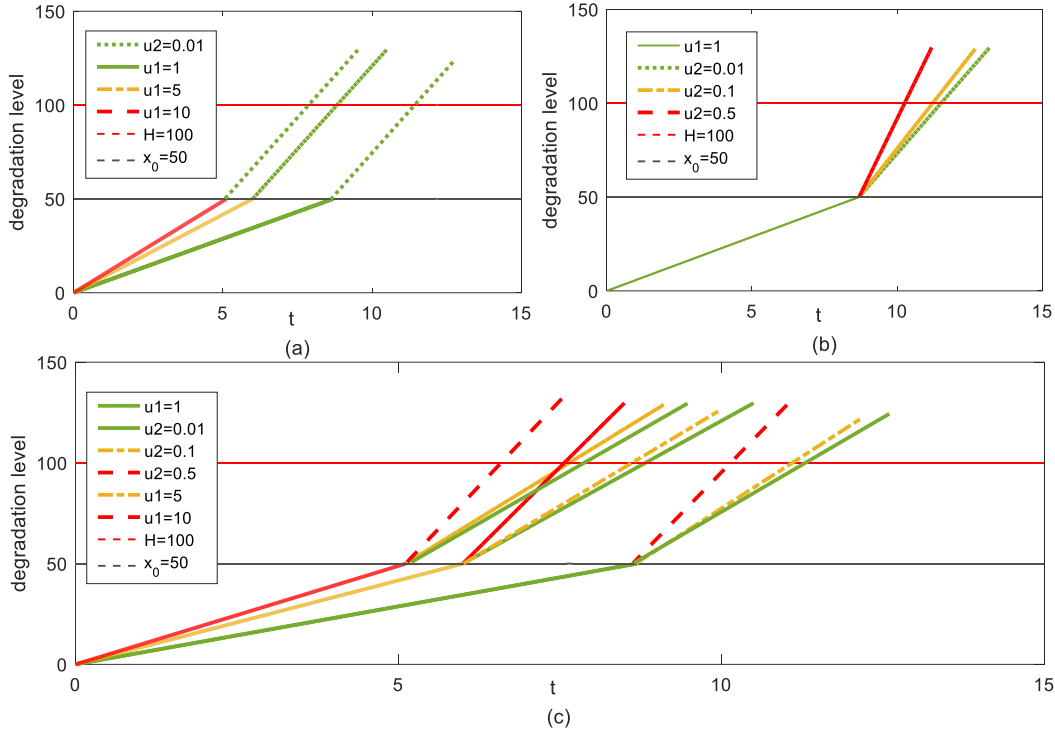
Figure 32 Expected two-stage degradation vs. time with stress variables u_1 and u_2; W-g model

Figure 32 clearly shows obvious 2-stage degradation. The first subplot (a) shows the increasing of $\mathbf{u}_1$ can significantly shorten the expected time for stage 1, which is T_1. On the other hand, as the degradation enters to the second stage at a specific degradation level, the increasing of $\mathbf{u}_1$ also significantly enlarges the degradation rate in the first stage degradation. The second subplot (b) shows the larger the environmental stress variable $\mathbf{u}_2$ is, the faster the degradation propagates in the second stage. This is consistent with the practical observation. The third subplot (c) gives a combination of subplot (a) and (b) to illustrate the influence from the stress variable to the degradation process. Figure 32 also shows the degradation can be applied to accelerated testing model with acceleration factor A_F, which can be calculated using Eq (4.4).

The scale parameter, $\eta(\mathbf{u_1}) = \eta_0 (a/a_0)^{b_1} (C/C_0)^{b_2}$, is a function of two stress variables which are initially artificial crack area a and chloride concentration C. a_0 is the baseline of crack area. $a_0 = DEP_0 \times WID_0$. DEP_0 and WID_0 are the baseline of crack depth and crack width. We assume

$DEP_0 = 0.05$, $WID_0 = 0.0011$, so $a_0 = 5.5 \times 10^{-5}$. C_0 denotes the baseline of chloride concentration, which is assumed to be 1% in this work. β denotes the shape parameter. Thus, model parameters are η_0, b_1, b_2 and β. Maximum likelihood estimation (MLE) method is applied to obtain these model parameters based on the degradation datasets from the first stage. As mentioned above, 10 different environmental stress (a and C) level are combined, so 10 different degradation latencies T_1 are collected for each bridge rebar. The likelihood function for the first stage is developed as Eq (4.14),

$$L(t_i; \beta, \eta_0, b_1, b_2) = \prod_{i=1}^{10} f(t_i; \beta, \eta_0, b_1, b_2)$$

$$\ell(t_i; \beta, \eta_0, b_1, b_2) = \ln L(t_i; \beta, \eta_0, b_1, b_2) = \sum_{i=1}^{10} \ln f(t_i; \beta, \eta_0, b_1, b_2)$$

(4.14)

where $f(t_i, \beta, \eta_0, b_1, b_2)$ is obtained by substituting $\eta(\mathbf{u_1}) = \eta_0 (a/a_0)^{b_1} (C/C_0)^{b_2}$ into Eq. (4.9).

When the time T_1 passes, the degradation level hits the alarm threshold x_0 and switch to the second degradation stage. The alarm threshold is obtained by observation of degradation datasets for each bridge rebar. For BS rebar, x_0 is set to be 160 mV; for EC rebar, x_0 is 110 mV; for SS rebar, x_0 is 60 mV and for MMFX rebar, x_0 is set to be 50 mV.

When applied to the rebar corrosion research, the environmental stress variable in the second stage is only chloride percentage C. For any degradation increment between time t to time s, $X(t) - X(s) \sim \text{gamma}(a(t) - a(s), \beta(C))$. The scale parameter $\beta(C) = \beta_0 e^{b_3 C}$. Thus, the CDF for the degradation increment can be derived as Eq (4.15)

$$\begin{aligned} F_{T_2}(t; C) &= \Pr\{T_2 < t; C\} \\ &= \Pr\{X(t) > H - x_0; C\} \quad \text{(gamma process)} \\ &= 1 - F_{X(T_2)}(H - x_0; C) \quad \text{(gamma process)} \end{aligned}$$

(4.15)

The reliability function $R(t)$ for the total degradation process can be derived as Eq (4.16)

$$R(t;a,C) = 1 - \Pr(T < t;a,C) = 1 - \Pr(T_1 + T_2 < t;a,C)$$

$$= 1 - \int_0^t \Pr(T_2 < t - v;C) f_{T_1}(v;a,C)dv$$

$$= 1 - \int_0^t \Pr\left(X(t-v) > H - x_0);C\right) f_{T_1}(v;a,C)dv \qquad (4.16)$$

$$= 1 - \int_0^t \left(1 - F_{X(t-v)}(H - x_0);C\right) f_{T_1}(v;a,C)dv$$

Based on Eq. (4.9) and Eq. (4.12) in, the detailed $R(t;a,C)$ can be derived as Eq (4.17) by bringing the corresponding CDF and PDF in,

$$R(t;a,C) = 1 - \int_0^t \left(1 - F_{X(t-v)}(H - x_0;C)\right) f_{T_1}(v,a,C)dv$$

$$= 1 - \int_0^t \left(1 - \int_0^{H-x_0} \frac{(\beta_0 e^{b_3 C})^{\alpha_0(t-v)} x^{\alpha_0(t-v)-1} e^{-\beta_0 e^{b_3 C} x}}{\Gamma(\alpha_0(t-v))} dx\right) \frac{\beta}{\eta_0 \left(\frac{a}{a_0}\right)^{b_1} \left(\frac{C}{C_0}\right)^{b_2}} \left(\frac{v}{\eta_0 \left(\frac{a}{a_0}\right)^{b_1} \left(\frac{C}{C_0}\right)^{b_2}}\right)^{\beta-1} e^{-\left(\frac{v}{\eta_0 \left(\frac{a}{a_0}\right)^{b_1} \left(\frac{C}{C_0}\right)^{b_2}}\right)^{\beta}} dv$$

$$(4.17)$$

The unknown parameters η_0, b_1, b_2, and β in the first degradation stage as well as b_3, β_0 in the second degradation stage can all be estimated via MLE approach. Again, the interior point approach. a non-linear optimization approach is applied to maximize the likelihood function. In order to ensure the model works with the actual physical scene, the constraint for parameters b_1, b_2, and b_3 are set to be from negative infinity to zero while the rest are set to be unlimited. The result for the parameters estimation is presented in Table 23.

Table 23 The estimated parameters in Weibull-gamma 2-stage degradation model

	Stage 1: Weibull distribution				Stage 2: gamma distribution		
	η_0	b_1	b_2	β	α_0	β_0	b_3
BS	17.18	-0.047	-0.081	15.330	2.814	0.120	--
EC	18.401	-0.030	-0.045	12.203	3.163	0.191	--
SS	15.753	--	--	11.926	3.478	0.284	-1.434

MMFX	19.685	-0.013	--	20.921	3.552	0.325	-1.477

For the BS and EC material, the degradation was affected by the crack size a and chloride percentage C in the first stage. For the SS and MMFX material, the degradation can be accelerated by chloride percentage in the second stage. However, the acceleration effect from C in second for BS and EC materials is too small. Similarly, the effects of a and C on SS, C on MMFX are also too small from the test data. Based on parameters in Table 23, the accelerator A_F with different a and C for MMFX material can be plotted in Figure 33.
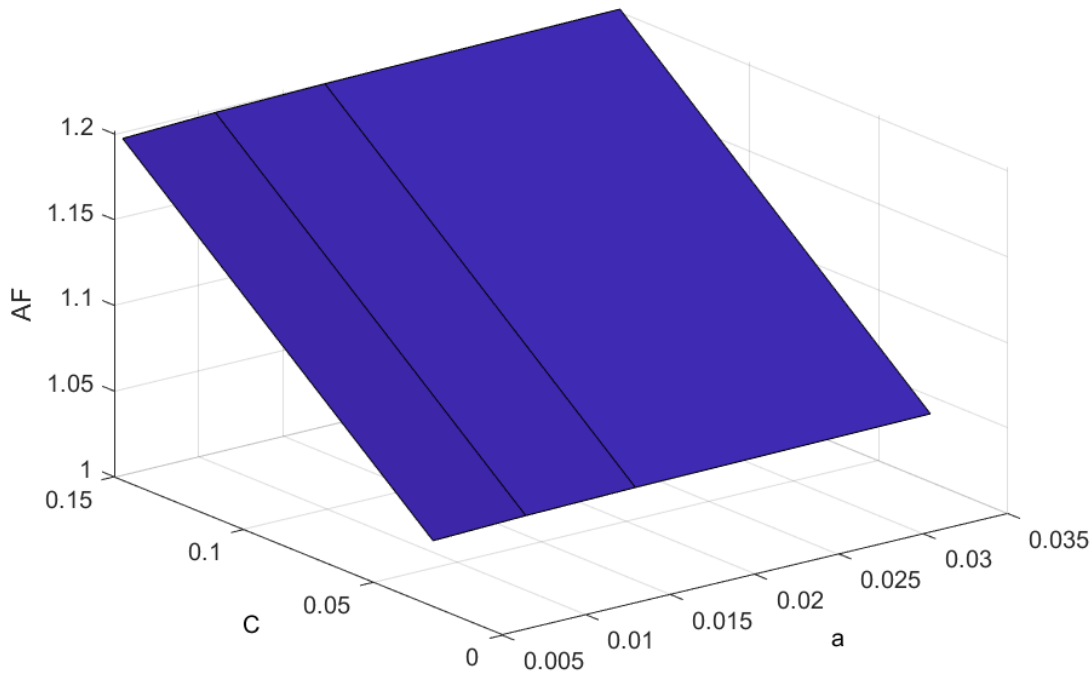
Figure 33 A_F values with different a and C for MMFX material

The acceleration factor increases with the pre-cracking size a and chloride percentage C. From Figure 23, A_F increases more on the C direction rather than a, which means the acceleration factor is more sensitive to the chloride percentage for MMFX when the total corrosion time is 33 months.

The degradation latency T_1 and the degradation rate in the second stage for all four material under ten different environmental stress can also be calculated based on the Table 21. The result is presented in Tedable 24

Table 24 T_1 and DR_2 for each rebar material under different a and C

Rebar		T_1; time for stage 1 (month)					Stage 2 *DR* (mV/month)
		Un-cracked	Pre-cracking size a				
	C		0.0055	0.011	0.0175	0.035	
BS	3%	15.2	12.2	11.8	11.6	11.2	23.5
	15%	13.3	10.7	10.4	10.2	9.8	23.5
EC	3%	16.8	14.6	14.3	14.1	13.8	16.6
	15%	15.6	13.6	13.3	13.1	12.9	16.6
SS	3%	15.1	15.1	15.1	15.1	15.1	12.8
	15%	15.1	15.1	15.1	15.1	15.1	15.2
MMFX	3%	19.2	18.1	17.9	17.8	17.6	11.4
	15%	19.2	18.1	17.9	17.8	17.6	13.6

For BS, EC, and MMFX rebar, the difference between T_1 under the mildest stress (a=0.0055, C=3%) and T_1 under the most aggressive stress ((a=0.035, C=15%) are 5.4 month, 3.9 month, and 1.6 month. This indicates the influence from environmental stress to the degradation latency reduces by BS, EC, MMFX. This incident confirms another fact, which is the order of corrosion resistance in the first stage is BS<EC<MMFX. This also confirms the Weibull-gamma 2-stage degradation model works properly using the Weibull-distributed T_1 assumption.

Using the result in Table 23, the reliability function can be calculated when given a specific H value. For demonstration purpose, H is assumed to be 1171 mV. This number is obtained by the Weibull-gamma 2-stage degradation model estimation for BS 5th year's degradation level under a=5.5×10^{-6} inch², C=1% condition. Figure 34 and 35 illustrate the reliability of MMFX and BS under different stress levels.
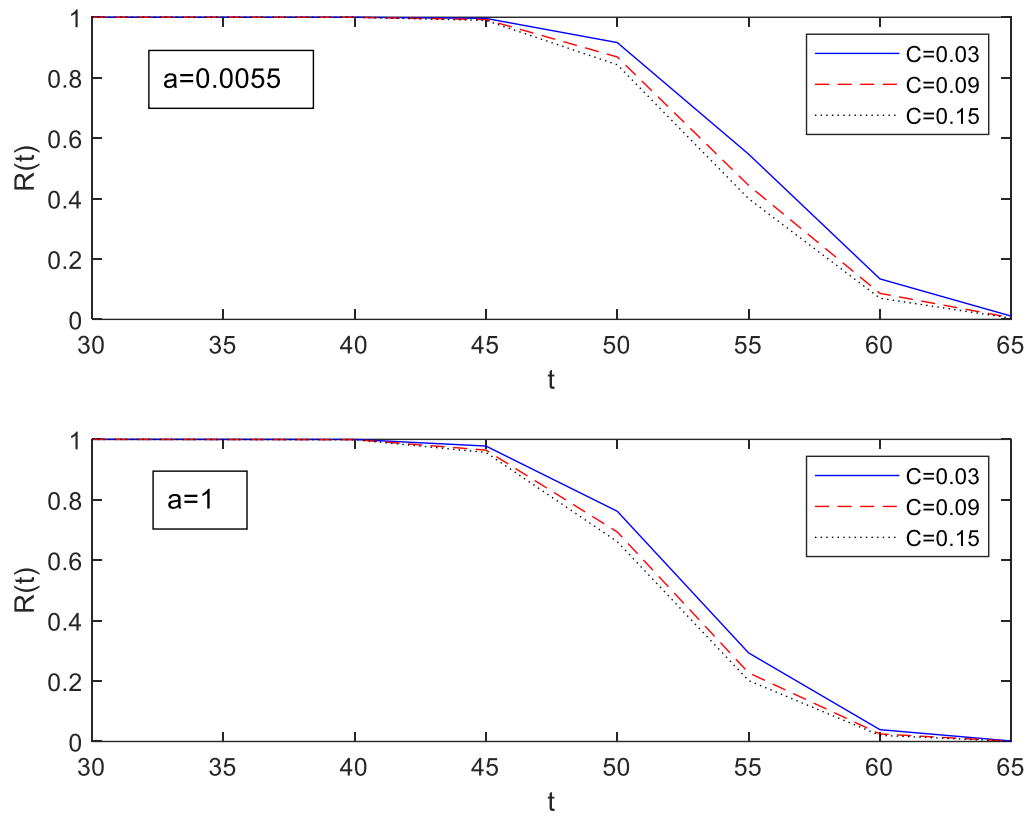
Figure 34 Reliability of BS under different stress levels
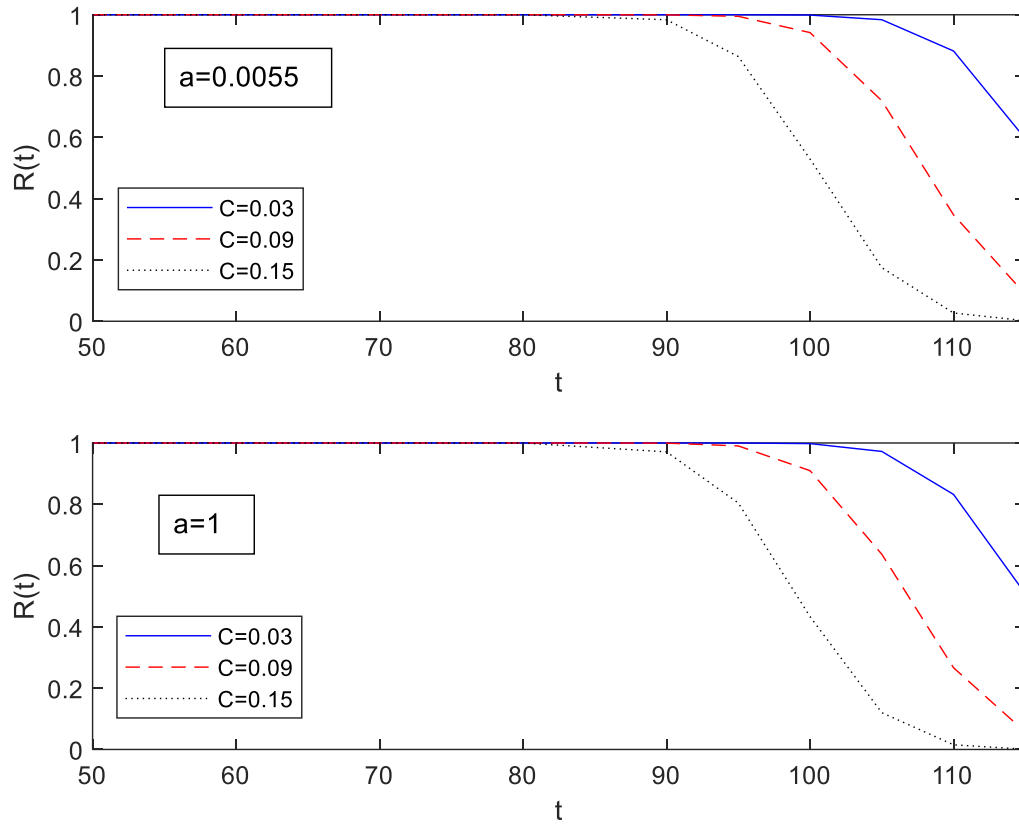
Figure 35 Reliability of MMFX under different stress levels

In Figures 34 and 35, the reliability of both materials reduces by increasing *a* and *C*. For MMFX material, the impact of *C* is small until the time goes to 110th month. By that time, the reliability reduces to almost zero when *C*=0.15 while the reliability remains about 50% when *C*=0.03. material. Similar phenomenon can be observed on the BS material though not as obvious as it on MMFX. In Figure 34, the reliability of BS starts to reduce at around 45th month when *a*=0.0055, while it starts to decrease at around 42nd month when the *a*=1. Similar phenomenon can also be observed on MMFX material but very small. All these above shows that: 1) Chloride percentage *C* has more impact on reliability than pre-cracking size *a*, when the failure threshold *H* is very large. This is because *a* exerts its influence at the early stage while *C* mainly contributes to the divergences of *R(t)* at the late stage. 2) Pre-cracking size has more impact on BS than on MMFX. This is because the MMFX material has better corrosion resistance. The impact from *a* in

the first stage is weakened.

5.   Machine learning based degradation forecasting

Machine learning is the ability of computer algorithms to autonomously learn from data and information and improve existing algorithms. Nowadays, machine learning is developing at an unprecedented speed. Machine learning is based on the concept of learning from past data and predicting the outcome of unknown/new situations, just as humans learning. But the advantage of computers is that they can handle a much larger range of data and are much more complex than humans can.

In this section, two basic machine learning approaches are applied to build up the degradation model and give forecasting to the degradation data, Linear regression, which can be seen as the simplest ANN model, as well as a traditional back propagation ANN network, are applied to predict the degradation level. Although all the previous models can give the data tendency in terms of time, it can only give a general expected degradation path. For a long-term degradation forecasting, either the gamma-gamma or the Weibull-gamma can work well. However, when the more accurate but short-term forecast is required, the machine learning will give a better performance. Besides, ANN approach can capture the relation or pattern in the data points that the researchers failed to notice. These features make the machine learning approach a good complementary to the general degradation model.

In this section, the environmental stress data (pre-cracking width, pre-cracking depth, chloride percentage) and the measured degradation level data are used to build up the train dataset. The size of the training dataset depends on the size of input delay. The latest three or five month degradation level are used to build up the dataset used for comparing with the forecasting results. All the machine learning models will give one output data each time, which means, these are all one-step-head forecasting model. The predicted data will be taken as the known data, as used for the next prediction. By repeating several times, more predicted data will be generated one by one. In this

section, several intersection options are test in the linear regression part, including no intersection and partial intersection, to examine the difference of the prediction. In the BP network part, different configurations and input delays are tested to find the better input delay and configuration.

Usually, the mean squared error (MSE) between the forecasted data and true values is adopted to measure the performance of a network. However, due to the scale difference, the root mean square error (RMSE) divided by the mean of true value is adopted in this study to measure the deviation between the forecasted data and true value. For example, the true degradation data for the BS, under uncracked condition and 3% chloride concentration, from 30th to 33rd month, are 522 mV, 530 mV, and 542 mV. For MMFX under same condition, the last 3-month degradation data are 168 mV, 176 mV, and 183 mV. The forecasted results for BS are 503 mV, 515 mV, and 527 mV, while the results for MMFX are 149 mV, 161 mV, and 168 mV. Although these two results has the same MSE values, the foresting result for BS actually is better than the results for MMFX. However, the "RMSE/mean" for these two predicted results are 3% and 9% respectively, which clearly shows the prediction for BS are better. Bi-LSTM RNN are also introduced to give forecast for the degradation data. For there might be long-term dependent relation in the degradation data, RNN network can give better performance.

5.1. Data preparation

There are three environmental stress variables to the rebar corrosion in this study, that is, pre-cracking size, pre-cracking width, and chloride concentration. Thus, for each material, there are 10 different environmental stress variables combinations. The entire project has lasted for 33 month and the degradation level was recorded monthly, which means there were 33 data points for each material under each stress level. 330 data points about degradation level for each material are collected. The last three or five-month's data are reserved to evaluate the forecast. The input delay is set to be 3 or 5, i.e., for situation where input delay is 3, there are three continuous corrosion data used for one-step ahead corrosion prediction. Since three stress conditions are considered

during the experiment, pre-cracking width (W), pre-cracking depth (D) and chloride concentration (C), these three stress variables are also included in the data sample. The general data sample format in this work is shown in Tables 23 and 24. W_i, D_i, and C_i means the stress values under condition i.   There are 10 different environmental conditions in this study.

Table 25 Data sample under stress condition i when input delay is 3, last 5 data reserved

	W	D	C	$\mathbf{X}_1$	$\mathbf{X}_2$	$\mathbf{X}_3$	Y
No.1	W_i	D_i	C_i	x_1	x_2	x_3	x'_4
No.2	W_i	D_i	C_i	x_2	x_3	x_4	x'_5
…	W_i	D_i	C_i	…	…	…	…
No.27	W_i	D_i	C_i	x_{27}	x_{28}	x_{29}	x'_{30}
No.28	W_i	D_i	C_i	x_{28}	x_{29}	x'_{30}	x'_{31}
No.29	W_i	D_i	C_i	x_{29}	x'_{30}	x'_{31}	x'_{32}
No.30	W_i	D_i	C_i	x'_{30}	x'_{31}	x'_{32}	x'_{33}

In Table 25, the variables W, D, C, $\mathbf{X}_1$, $\mathbf{X}_2$, $\mathbf{X}_3$ are combined to be the input part, which can also be thought as the independent variables. The variable Y is the target, which is the dependent variable. x_i means the actual corrosion data collected at the ith month, while x'_i denotes the corrosion prediction at the ith month.

Table 26 Data sample under stress condition i when input delay is 5, last 3 data reserved

	W	D	C	$\mathbf{X}_1$	$\mathbf{X}_2$	$\mathbf{X}_3$	$\mathbf{X}_4$	$\mathbf{X}_5$	Y
No.1	W_i	D_i	C_i	x_1	x_2	x_3	x_4	x_5	x'_6
No.2	W_i	D_i	C_i	x_2	x_3	x_4	x_5	x_6	x'_7
…	W_i	D_i	C_i	…	…	…	…	…	
No.25	W_i	D_i	C_i	x_{25}	x_{26}	x_{27}	x_{28}	x_{29}	x'_{30}
No.26	W_i	D_i	C_i	x_{26}	x_{27}	x_{28}	x_{29}	x_{30}	x'_{31}
No.27	W_i	D_i	C_i	x_{27}	x_{28}	x_{29}	x_{30}	x'_{31}	x'_{32}

No.28	W_i	D_i	C_i	x_{28}	x_{29}	x_{30}	x'_{31}	x'_{32}	x'_{33}

In Table 26, the variables *W, D, C,* $\mathbf{X}_1, \mathbf{X}_2, \mathbf{X}_3, \mathbf{X}_4, \mathbf{X}_5$ are combined to be the input part, which can also be thought as the independent variables. When the input delay is 3 and 5 last month's data are reserved for the testing set, as shown in Table 25, 30 data samples will be created since 33 monthly corrosion data are collected for each rebar material under each condition. The 1st to 27th data will be used as the training set since the data input part (*W, D, C,* $\mathbf{X}_1, \mathbf{X}_2, \mathbf{X}_3$) are all from real experimental data. The 28th to 30th data will be used as the testing set to exam the forecasting model performance. When the input delay is set to be 5, and there are 3 last month's data reserved as the test data set, as shown in Table 26, the total dataset will reduce to 28. Similarly, the 1st to 25th data will be used as training set and the 26th to 30th will be used as the testing set.

5.2. Linear regression model

The linear regression model uses the training and testing dataset as chapter 5.1 indicates. Multiple linear regression can be regarded as a simplest ANN model without hidden layers, and the relation between the input layers and the output layers is linear. The regression analysis usually based on the predictor variables, also known as independent variables or regressor, to give forecast to the response variables. It can also be used to evaluate the impact of the predictor variables to the response variables. Multiple linear regression has the following format shown in Eq. (4.18)

$$\mathbf{Y} = \beta_0 + \beta_1 x_1 + \beta_2 x_2 + ... + \beta_{p-1} x_{p-1} + e \tag{4.18}$$

Where x_i indicates the predictor variables which have the relation to the response variable vector $\mathbf{Y}$. $\mathbf{B}=[\beta_0, \beta_1, ..., \beta_{p-1}]$ is the vector of parameter coefficients. e is the random error, which usually be assumed $e \sim (\sigma^2, 1)$. Assuming there are *n* samples, each sample follows the Eq. (4.18), thus the Eq. (4.19) can be derived

$$\begin{pmatrix} \mathbf{Y}_1 \\ \mathbf{Y}_2 \\ \vdots \\ \mathbf{Y}_n \end{pmatrix} = \begin{pmatrix} 1 & x_{11} & \cdots & x_{1(p-1)} \\ 1 & x_{21} & \cdots & x_{2(p-1)} \\ \vdots & \vdots & \vdots & \vdots \\ 1 & x_{n1} & \cdots & x_{n(p-1)} \end{pmatrix} \mathbf{B} + \begin{pmatrix} e_1 \\ e_2 \\ \vdots \\ e_n \end{pmatrix} \Leftrightarrow \mathbf{Y}_n = \mathbf{X}_{n \times p} \mathbf{B} + \mathbf{e} \qquad (4.19)$$

The coefficients matrix **B** can be found in two approaches. The analytical solution of **B** can be obtained by formula derivation, shown in Eq (4.20)

$$\hat{\mathbf{B}} = \left(\mathbf{X}^T \mathbf{X} \right)^{-1} \mathbf{X}^T \mathbf{Y} \qquad (4.20)$$

If the inverse of the matrix does not exist, reducing the prediction variables or using regularization methods could help. Another way to calculate the coefficient matrix **B** is using optimization approach, for example, gradient descent approach. By minimizing the MSE between the regression response and the observed true value, the coefficient matrix **B** can be identified. Using the data generated in chapter 5.1, the input variables matrix and the response matrix can be defined. Thus, the linear regression approach can be applied to BS, EC, SS and MMFX materials to give forecast of the degradation level in last 5 month. The Tables 27 and 28 show the summary for the regression result for BS material under different input delays.

Table 27 Regression summary for BS when input delay is 3, no intersection

	Coefficient	SE	p-value
INTERCEPTION	7.266	1.929	0
W	69.752	57.098	0.223
D	3.031	2.213	0.172
C	-3.963	11.34	0.727
$\mathbf{X}_1$	0.217	0.082	0.009
$\mathbf{X}_2$	-0.609	0.112	0
$\mathbf{X}_3$	1.419	0.067	0

Form Table 27, the independent variables $\mathbf{X}_1$, $\mathbf{X}_2$, $\mathbf{X}_3$ have significant impact to the linear regression because their p-value are all smaller than 0.05. However, the variables W and D are not

strictly independent. Usually, as W goes larger, D will have more impact on the corrosion process. Meanwhile, as W goes larger, D will be likely getting larger. Thus, it is reasonable to combine the independent variables W and D together as variable a, $a=W\times D$, which represents the pre-cracking area. The summary for the regression on BS corrosion data, considering a, is presented in Table 28.

Table 28 Regression summary for BS when input delay is 3, crack area considered

	Coefficient	SE	p-value
INTERCEPTION	8.408	1.761	0
a	144.681	59.461	0.016
C	-3.952	11.322	0.727
$\mathbf{X}_1$	0.216	0.082	0.009
$\mathbf{X}_2$	-0.609	0.111	0
$\mathbf{X}_3$	1.420	0.067	0

From Table 28, the independent variables $\mathbf{X}_1$, $\mathbf{X}_2$, $\mathbf{X}_3$, and a all have significant impact on the BS rebar corrosion. The results show the impact from chloride percentage are failed to prove. This may because the number of experimental data is too small. All the results shown in the table are consist with the results from previous 2-stage degradation models, which also validated the previous 2-stage degradation models.

The training MSE for the regression model without interaction item is 114.96 and the testing MSE is 5461.87. The training MSE for model with pre-cracking area is 114.58, the testing MSE is 5416.43. The regression model considering pre-cracking size a instead of W and D separately has better performance, but the difference between these two models are small. For the convenience of processing, in the machine learning part, the model considering pre-cracking size a is adopted. When the input delay is enlarged to be 5, the model summary for BS is shown in the Table 29.

Table 29 Regression summary for BS when input delay is 5, crack area considered

	Coefficient	SE	p-value
INTERCEPTION	8.357	1.998	0.000
a	143.796	66.291	0.031
C	-2.518	12.148	0.836
$\mathbf{X}_1$	-0.179	0.093	0.056
$\mathbf{X}_2$	0.221	0.143	0.124
$\mathbf{X}_3$	0.163	0.138	0.238
$\mathbf{X}_4$	-0.596	0.119	0.000
$\mathbf{X}_5$	1.410	0.070	0.000

In Table 29, pre-cracking size a, as well as $\mathbf{X}_4$, $\mathbf{X}_5$, which are the most recent two data point to the predicted data, all have the p-value smaller than 0.05. These variables have the significant impact on the regression. The model training MSE is 120.93, the testing MSE is 4864.856. Comparing the regression model with 3 input delay, the 5-input delay model have better performance. However, the performance improvement is not huge. Although the 5-input delay has more input variables than the 3 input delay model, the two more variables are from same dataset, and can be used as the target data to be predicted. These data have small power to impact the regression result, and the improvement from these are limited. In order to save the calculation cost. The linear regression model for rest materials are set to be 3 input delay model.

Figure 36 shows the result for the linear regression response plot for BS material. The blue dots are the data points in the training set. The yellow dots are the response, the regression results based on the model trained. The red bar is the error represents the deviation between the true value and the regression result. The x-axis represents the record number, which corresponds to the number of the data in part 5.1. The input delay is set to be five in the linear regression model. Thus, for each material, there will be 250 data points in total in the training set.
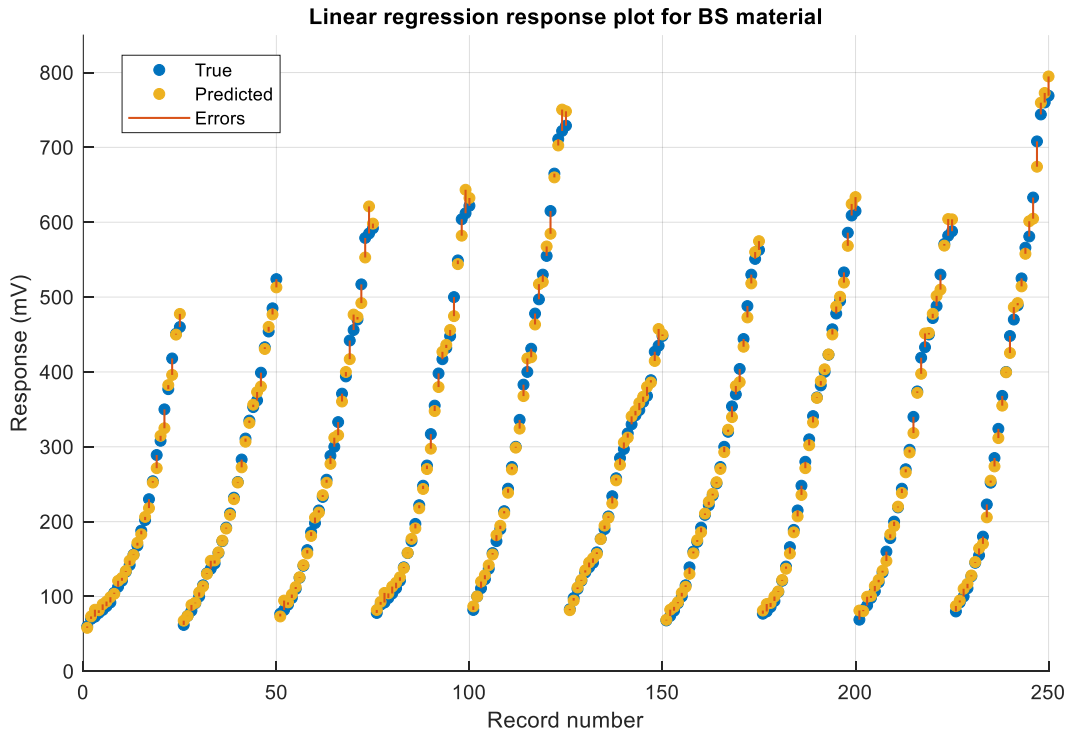
Figure 36 Linear regression response plot for BS material

In Figure 36, the response points fit the true value well when the true value is relatively low, or in the first half of the degradation process. As the degradation developing, the larger deviations start to appear. In the second half of the degradation process, but the few data points at the end, the regression results tend to underestimate the degradation level. By using the obtained regression model into forecasting the degradation level in 28th to 33rd month, which is the data reserved for the testing set as Table 25 shows, the result in Figure 37 and Table 30 can be obtained.
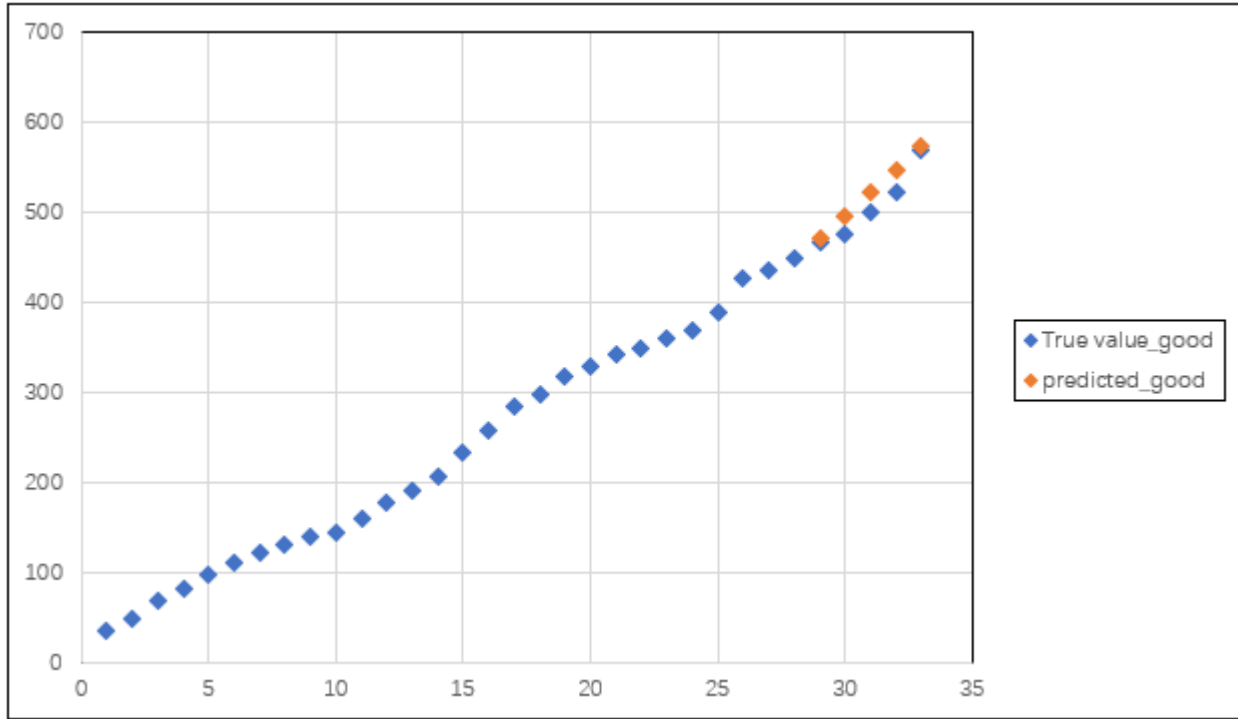
Figure 37 Predicted result and true value for BS material (W=0.0011, D=0.05, C=15%)

Figure 37 shows a good forecasting result for BS material obtained by the linear regression model. The orange squares are the predicted degradation level in 29th to 33rd month and they fitted the true degradation level well. In order to examine the forecast performance on BS material, the MSE of the forecasted data are calculated and presented in Table 30.

Table 30 Linear regression model forecast performance under different environment for BS

C	3%				
a	5.5×10^{-6}	0.0055	0.011	0.0175	0.035
Mean	531.79	614.59	690.33	727.27	853.09
MSE	786.04	2940.50	5061.61	8703.48	14934.41
RMSE	28.04	54.23	71.14	93.29	122.21
RMSE/Mean	0.05	0.09	0.10	0.13	0.14
C	15%				
a	5.5×10^{-6}	0.0055	0.011	0.0175	0.035
Mean	524.98	650.77	708.79	685.99	894.55
MSE	420.28	1850.23	4636.33	3755.36	11076.07
RMSE	20.50	43.01	68.09	61.28	105.24
RMSE/Mean	0.04	0.07	0.10	0.09	0.12

"Mean" in Table 30 represents the mean of the true degradation level in 29th to 33rd month under the corresponding environment. MSE and RMSE measures the deviation between the forecasted data and the true degradation level. Due to the scale difference between the degradation level under different environment, the RMSE divided by mean is adopted to measure the forecast performance under different environments. In Table 28, the best forecast performance is generated under un-cracked condition while the chloride percentage is 15% ($a=5.5\times10^{-6}$, $C=15\%$). The RMSE is 20.50 mV and the RMSE/mean is 0.04. Generally, for BS material, the performance of the linear regression model decreases as the pre-cracking area goes up, and it performs better in 3% chloride concentration than 15% chloride concentration.

Similarly, linear regression approach can also be applied on EC, SS, and MMFX materials to give forecasts of the degradation level in 29th to 33rd month. For EC, SS, and MMFX material, the input delay in the models is selected to be 3. The last five months' data are reserved to be the target value in the testing set. The 1st to 28th months' data is adopted as the response value in the training

set. The model summary is shown in Tables 31, 32, and 33.

Table 31 Regression summary for EC when input delay is 3, crack area considered

	Coefficient	SE	*p*-value
INTERCEPT	3.958	1.120	0.000
a	7.947	37.968	0.834
C	-3.330	7.501	0.657
X_1	0.230	0.094	0.015
X_2	-0.406	0.108	0.000
X_3	1.239	0.068	0.000

Table 32 Regression summary for SS when input delay is 3, crack area considered

	Coefficient	SE	*p*-value
INTERCEPT	2.478	0.996	0.014
a	23.256	34.498	0.501
C	5.043	6.937	0.468
X_1	0.004	0.084	0.966
X_2	-0.461	0.115	0.000
X_3	1.482	0.066	0.000

Table 33 Regression summary for MMFX when input delay is 3, crack area considered

	Coefficient	SE	*p*-value
INTERCEPT	1.679	0.775	0.031
a	24.627	27.523	0.372
C	0.802	5.516	0.885
X_1	-0.152	0.090	0.092
X_2	-0.165	0.116	0.154
X_3	1.349	0.069	0.000

In Tables 31, 32, and 33, the *p*-value of coefficient *a* and *C* are all greater than 0.05, which

indicates the significance of variable *a* and *C* are failed to be proved based on the training dataset. SE is the standard error of the coefficient, which measures the accuracy of the coefficient estimation. The smaller the standard error, the more accurate the estimation is. The corresponding *t*-value can be obtained by dividing the coefficient by its standard error. If the *p*-value associated with this *t* statistic value is less than the significant level, the coefficient can be determined to be significantly different from zero.

As introduced before, the degradation process can be divided into two different stage, the impact of variable *a* or *C* are different in each stage. Thus, it may be difficult for the multiple linear regression model to identify a steady effect and a coefficient in two different stages. Usually, the variables which are failed to be proved have significant impact should be eliminated and the linear regression parameters should be re-estimate only with the rest variables. However, in this research, the variables *a* and *C* both have corresponding physical meaning. Although the significances of variables *a* and *C* are not proved using the existed dataset, these variables will still be kept in order to making the model have physical sense. Using the obtained linear regression model, the 29th to 33rd months' data for EC, SS, and MMFX materials can be estimated. By comparing the forecast data with the true degradation level in the testing set, the model performance under different environments can be obtained and compared. Tables 34, 35, and 36 shows the model performance under different environment for EC, SS, and MMFX material, respectively.

Table 34 Linear regression model performance under different environment for EC

C	3%				
a	5.5×10^{-6}	0.0055	0.011	0.0175	0.035
Mean	357.11	421.26	470.88	449.41	509.53
MSE	227.25	4325.44	5640.71	4769.84	8409.10
RMSE	15.07	65.77	75.10	69.06	91.70
RMSE/Mean	0.04	0.16	0.16	0.15	0.18
C	15%				
a	5.5×10^{-6}	0.0055	0.011	0.0175	0.035
Mean	385.11	427.11	480.20	450.70	520.92
MSE	1011.40	2931.51	4728.25	2970.14	4863.71
RMSE	31.80	54.14	68.76	54.50	69.74
RMSE/Mean	0.08	0.13	0.14	0.12	0.13

For the forecast result of EC material, the best forecast result is made when there is no pre-crack while the chloride concentration is 3%, where the RMSE/mean is 0.04. The forecast performance varies much with the change of environmental stress. Similar like the forecast result for BS material, the regression generally performs better when the pre-cracking area is small. Although the RMSE/mean is smaller when the pre-cracking size a is 0.0175, the difference is small when compared with the RMSE/mean under condition where a is 0.011 or 0.0055. Apart from the performance when $a=5.5\times10^{-6}$ inch^2, the forecast result fits the true degradation level better when the chloride concentration is 15% rather than 3%.

Table 35 Linear regression model performance under different environment for SS

C	3%				
a	5.5×10^{-6}	0.0055	0.011	0.0175	0.035
Mean	249.92	268.98	293.93	283.16	302.69
MSE	52.46	106.79	127.42	350.63	322.50
RMSE	7.24	10.33	11.29	18.73	17.96
RMSE/Mean	0.03	0.04	0.04	0.07	0.06
C	15%				
a	5.5×10^{-6}	0.0055	0.011	0.0175	0.035
Mean	282.12	332.99	292.89	315.34	383.67
MSE	420.52	754.10	77.81	375.26	1244.36
RMSE	20.51	27.46	8.82	19.37	35.28
RMSE/Mean	0.07	0.08	0.03	0.06	0.09

For the SS material, the best forecast result is generated under conditions with 5.5×10^{-6} inch^2 pre-cracking area, 3% chloride percentage and 0.011 inch^2 pre-cracking area, 15% chloride percentage. When the pre-cracking size is 5.5×10^{-6}, 0.0055, or 0.035 inch^2, the forecast result is closer to the real degradation level in 3% chloride concentration than is in 15% chloride concentration. When the pre-cracking size is 0.011 or 0.0175 inch^2, the forecast result is closer to the real degradation level in 15% chloride concentration than is in 3% chloride concentration. All the RMSE/Mean is smaller than 0.1, which means the forecast for SS degradation in 29th to 33rd month made by linear regression model is relatively well.

Table 36 Linear regression model performance under different environment for MMFX

C	3%				
a	5.5×10^{-6}	0.0055	0.011	0.0175	0.035
Mean	168.54	181.28	222.99	234.57	234.42
MSE	26.17	209.42	39.27	628.29	19.29
RMSE	5.12	14.47	6.27	25.07	4.39
RMSE/Mean	0.03	0.08	0.03	0.11	0.02
C	15%				
a	5.5×10^{-6}	0.0055	0.011	0.0175	0.035
Mean	169.50	179.69	219.43	247.25	268.22
MSE	73.31	199.66	41.29	198.04	104.42
RMSE	8.56	14.13	6.43	14.07	10.22
RMSE/Mean	0.05	0.08	0.03	0.06	0.04

For MMFX material, the best prediction is made when a is 0.035 inch^2 and C is 3%. The forecast performance also varies much with the environmental stress, but most results fits the actual degradation level well. When the pre-cracking size is 5.5×10^{-6}, 0.0055, or 0.011 inch^2, the forecast result in 3% chloride concentration have the similar goodness of fit to the real degradation level with the result forecasted in 15% chloride concentration. For BS, EC, SS, and MMFX four material, in most conditions, the forecast result made by linear regression model fits the actual data better when the degradation level is relatively low. The regression respond data is closer to the real data in the first half of degradation process, while the forecasted results also perform better when the chloride percentage is 3% or the pre-cracking size is smaller in most cases. The MMFX and SS has the best forecast result, then it is result for BS, and then is the result for EC.

5.3. Back-propagated ANN

BP neural network is a multi-layer feedforward neural network. Its main characteristic is the signal has forward-direction propagation, and the error has backward-direction propagation. Specifically, for the following neural network model with only one hidden layer in Figure 38.
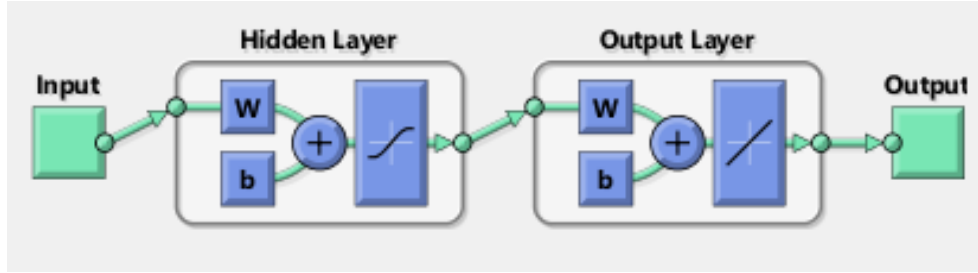
Figure 38 The structure of BP network with one hidden layer

The process of BP neural network is mainly divided into two stages. The first stage is the forward propagation of the signal, which passes through the hidden layer from the input layer to the output layer. The second stage is the back propagation of errors, from the output layer to the hidden layer, and finally to the input layer, and then adjust the weight and bias of the hidden layer to the output layer as well as the input layer to hidden layer.

A BP network can be built with the following steps. First, initialize the network. Suppose the number of nodes in the input layer is n, the number of nodes in the hidden layer is l, and the number of nodes in the output layer is m. The weight from the input layer to the hidden layer is ω_{ij}, the weight from the hidden layer to the output layer is ω_{jk}, the bias from the input layer to the hidden layer is a_j, and the bias from the hidden layer to the output layer is b_k. The learning rate is η, and the excitation function is $g(x)$. The excitation function is the Sigmoid function. In the form of Eq. (4.20)

$$g(x) = \frac{1}{1+e^{-x}} \tag{4.20}$$

Then, the output H_j of the hidden layer and the output O_k of the output layer can be derived as the Eq. (4.21) and Eq. (4.22)

$$H_j = g\left(\sum_{i=1}^{n} \omega_{ij} x_i + a_j\right) \tag{4.21}$$

$$O_k = \sum_{j=1}^{l} H_j \omega_{jk} + b_k \tag{4.22}$$

The error can be expressed as Eq. (4.23)

$$E = \frac{1}{2}\sum_{k=1}^{m} e_k^2 \tag{4.23}$$

Where $e_k = Y_k - O_k$, Y_k is the expected output result. The update of the weight follows the Eq. (4.24), which can be derived by minimum the error function by gradient descent approach.

$$\begin{cases} \omega_{ij} = \omega_{ij} + \eta H_j (1 - H_j) x_i \sum_{k=1}^{m} \omega_{jk} e_k \\ \omega_{jk} = \omega_{jk} + \eta H_j e_k \end{cases} \tag{4.24}$$

Eq. (4.24) is the back-propagation process for error. Similarly, the update of bias can be derived as the Eq. (4.25) shows

$$\begin{cases} a_j = a_j + \eta H_j \left(1 - H_j\right) \sum_{k=1}^{m} \omega_{jk} e_k \\ b_k = b_k + \eta e_k \end{cases} \tag{4.25}$$

There are many approaches to determine if the iteration should stop or not. The usual approach is to specify the number of the iteration or determine whether the difference between adjacent errors is less than a specified value. In this project, the maximum iteration is set to be 50,000 while MSE for the stop criteria varies with different materials. The network structure adopted in this thesis is shown in Figure 39.
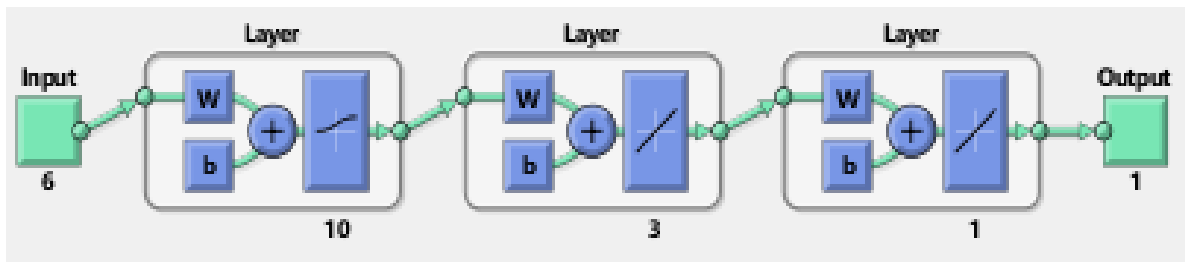

Figure 39 The structure of BP network with two hidden layers

There are 3 layers in the network, the first two are hidden layers, the last one is the output layer. The excitation function between the input layer to the first hidden layer is the Sigmoid function, and it is pure linear function between the first hidden layer to the second layer. The second hidden layer is connected by another pure linear function to the output layer. In this project, the output is set to be a number each time.

Like the linear regression model in chapter 5.2, the last three- or five-months' data are selected to be the dataset to evaluate the forecast performance. 85% of the first 28- or 30-months' data are selected to be the training dataset while the rest 15% are selected to consist the testing dataset. When giving predictions, the former predicted degradation level will be used as the known input data to generate the next month's forecast. By repeating this, the forecast can be made month by month. Two different input delays, 3 or 5, are tested here to determine under which does the network performs better. Two different network configurations, the number of neurons in the second hidden layer, are also tested to determine the number of the neurons in the hidden layers. Considering the degradation path has a small turn at around 26th month, the training dataset is also been enlarged by reducing the number of data reserved for forecast result evaluation from 5 to 3.

The performances before and after the training dataset enlargement are also compared. Due to the randomness in the ANN, each time the trained network is different. Thus, for each configuration, there are ten networks trained. The one with the best individual performance and the average performance of all ten networks under the same configuration are picked to evaluate which configuration is better.

For BS material, when there are 5 months' data reserved as the dataset for forecast evaluation, the average and best network performance under two input delay and two second hidden layers are presented in table 37.

Table 37 Performance for 10 networks under different input delay and neuron numbers for BS; 5 months'

data reserved

	3 neurons in the second hidden layer					
	Input delay is 3			Input delay is 5		
	Training MSE	Testing MSE	Forecasting MSE	Training MSE	Testing MSE	Forecasting MSE
Best performance	31.99	55.34	1010.29	19.10	96.68	1011.11
Average performance	34.29	104.20	1711.73	25.05	150.48	4024.97
	5 neurons in the second hidden layer					
	Input delay is 3			Input delay is 5		
	Training MSE	Testing MSE	Forecasting MSE	Training MSE	Testing MSE	Forecasting MSE
Best performance	25.26	108.32	1266.78	21.02	102.81	2849.06
Average performance	33.28	128.96	2258.54	24.74	137.17	3378.10

In Table 37, when judging from the best performance of all trained models, the network performs best when there are 3 neurons in the second layer and the input delay is set to be 3. The total training MSE under that condition is 31.99, testing MSE is 55.34, and the forecasting MSE is 654.74. Although the total training MSE is not the smallest, the testing MSE and forecasting MSE are both smallest, which indicates the result fits the actual degradation well and can give good prediction in the future 5 months.

When judging from average performance of all ten generated networks, still the network generated when there are 3 neurons in the second hidden layer and the input delay is 3 has the best testing and forecast performance. It also can be seen that, for BS material, when the input delay is 3, the trained model performs better than the model trained with 5 input delay. Besides, for the number of hidden neurons in the second layer, 3 performs better than 5. When there are 5 neurons in the second hidden layer, the ANNs have smaller training MSE but greater testing MSE and forecasting MSE, which indicates there may be over fitting in the models. Based on results in Table 35, the BP network in this chapter all have 3 neurons in the second hidden neuron. Using the best trained model with two different input delays, the forecast result about degradation level for last five month can be estimated. Figure 40 shows the responses plot when training the ANN model. Figure 41 shows the forecast result for BS material when the crack width is 0.035 inch, crack depth is 0.5 inch, chloride percentage is 3%.
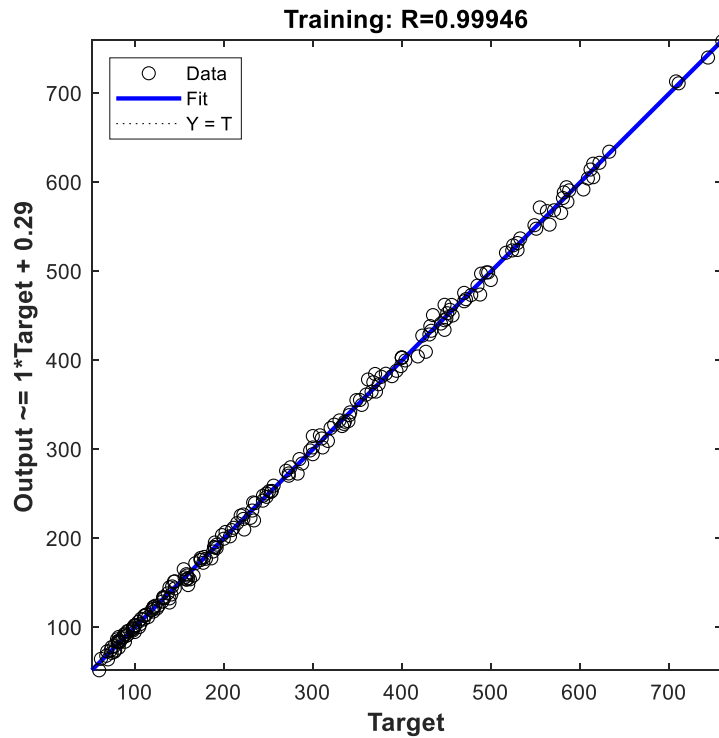
Figure 40 The training state plot for BS material

Forecast result and true value for BS; W=0.035, D=0.5, C=3%
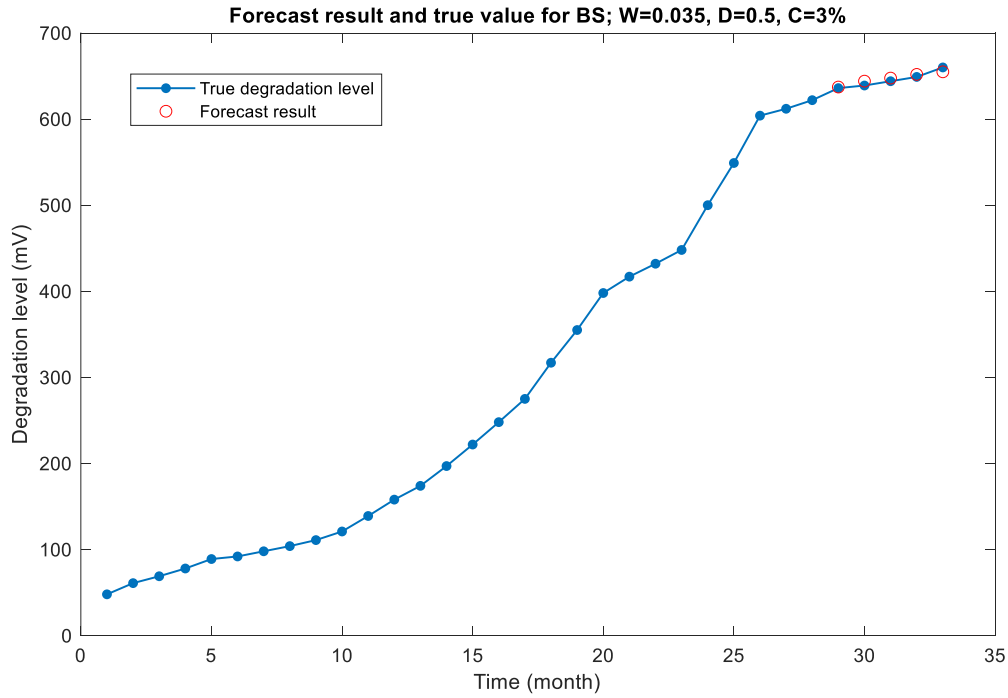
Figure 41 Forecast result and true value for BS; W=0.035, D=0.5, C=3%, input delay is 3

Figure 40 shows the output result and the target value in the training set when the training iterations stopped. The output result basically lines on the fitted line, which shows the output fits the target value very well in the training dataset. Figure 40 illustrates the predicted results and the true value for BS material with input delay is set to be 3. The forecast result fit the true degradation very well. This indicates the BP-ANN is capable to give prediction in the future 5 month for BS material. In order to examine the forecast performance on BS material, the MSE between the forecasted data and the true value under different environments are calculated and presented in Table 38.

Table 38 ANN model forecast performance under different environment for BS

W	0.0011	0.011	0.011	0.035	0.035
D	0.05	0.5	1	0.5	1
C=3%					
Mean	502.85	567.38	624.64	647.15	740.31
MSE	411.14	234.18	202.13	14.99	46.12
RMSE	20.28	15.30	14.22	3.87	6.79
RMSE/Mean	0.04	0.03	0.02	0.01	0.01
C=15%					
Mean	462.38	560.97	682.99	609.33	780.49
MSE	2994.48	3543.23	1214.93	765.06	670.94
RMSE	54.72	59.52	34.86	27.66	25.90
RMSE/Mean	0.12	0.11	0.05	0.05	0.03

Table 38 shows the best forecast performance for BS material is when the pre-cracking width is 0.035 inch, crack depth is 0.5 inch, and chloride percentage is 3%. The corresponding RMSE/Mean is 0.01, Compared with Table 28, the forecast result generated by linear regression model, the ANN model generally performs better especially when the pre-cracking size is relatively large. The ANN model forecast works better under 3% chloride percentage rather than 15% chloride. As the pre-cracking size goes larger, the forecast result goes better, which is the opposite to the linear regression result.

The ANN forecast can also be applied to the EC, SS, and MMFX materials. Table 37 shows the model performance summary for all four materials. For each material, the ANN is trained for ten individual times. The best performance and the average performance are found and shown in Table 39. Tables 40, 41, and 42 shows the ANN model performance under different environment for EC, SS, and MMFX material, respectively.

Table 39 ANN performance for different materials

Best performed model				
	BS	EC	SS	MMFX
Training MSE	31.99	9.66	11.07	7.48
Testing MSE	55.34	40.61	63.74	29.42
Forecast MSE	1010.29	429.57	573.37	710.52
Average performance				
Training MSE	34.29	10.70	10.51	7.47
Testing MSE	104.20	43.08	38.46	32.70
Forecast MSE	1711.73	832.70	892.57	1356.98

In table 39, the MSE between the different materials varies significantly. Because of the difference of corrosion resistance, there are scale difference between the different materials' degradation level. For BS material, which has the greatest measured number for the degradation level, the forecast MSE is larger than the rest material. However, this does not indicate that the forecast for the degradation is poor. By taking RMSE/Mean, the scale difference can be reduced. The RMSE/Mean for EC, SS, and MMFX in shown in Tables 40, 41, and 42, respectively.

Table 40 ANN model forecast performance under different environment for EC

W	0.0011	0.011	0.011	0.035	0.035
D	0.05	0.5	1	0.5	1
C=3%					
Mean	313.48	366.20	394.31	383.41	425.40
MSE	1372.97	76.06	137.22	104.68	62.10
RMSE	37.05	8.72	11.71	10.23	7.88
RMSE/Mean	0.12	0.02	0.03	0.03	0.02
C=15%					
Mean	335.23	371.89	417.40	387.48	425.97
MSE	616.75	134.65	60.75	330.87	1399.67
RMSE	24.83	11.60	7.79	18.19	37.41
RMSE/Mean	0.07	0.03	0.02	0.05	0.09

Table 40 shows the forecast performance generated from the best performed ANN in 10 individual ANNs. The best result can be found when giving forecast to condition where crack width is 0.035 inch, crack depth is 1 inch, and the chloride percentage is 3%. When the chloride percentage is 3%, the forecast result fits the actual data well except the uncracked condition data. Figure 42 shows the output result and the target value when the training iterations stopped.
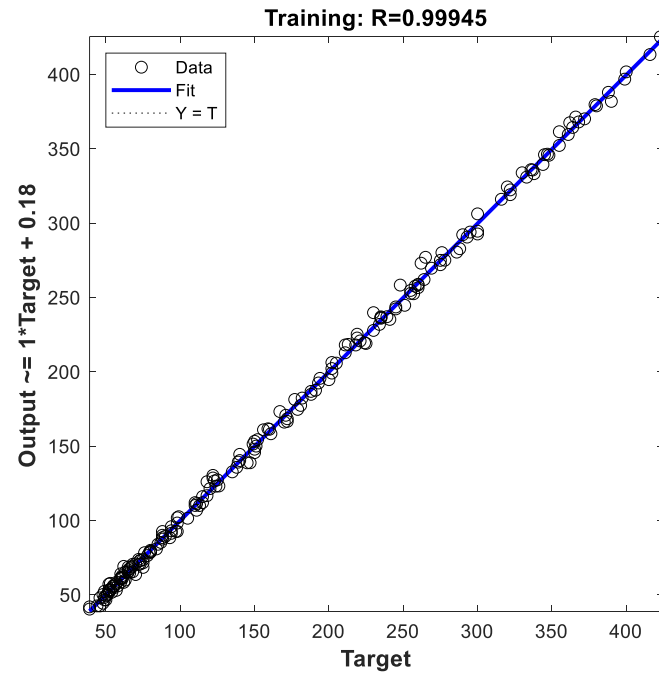
Figure 42 The training state plot for EC material

The ANN regression data fits true data very well. Figure 42 and Table 40 show that ANN model can give good regression results for EC material degradation under different condition. Compared with the result in Table 34, the ANN performs better than the linear regression model. Table 41 shows the forecast summary for SS rebar.

Table 41 ANN model forecast performance under different environment for SS

W	0.0011	0.011	0.011	0.035	0.035
D	0.05	0.5	1	0.5	1
C=3%					
Mean	238.69	268.53	271.27	247.04	257.72
MSE	65.92	132.55	221.74	569.64	1141.78
RMSE	8.12	11.51	14.89	23.87	33.79
RMSE/Mean	0.03	0.04	0.05	0.10	0.13
C=15%					
Mean	246.80	345.63	268.39	317.23	366.77
MSE	404.27	2112.88	491.29	357.56	236.11
RMSE	20.11	45.97	22.16	18.91	15.37
RMSE/Mean	0.08	0.13	0.08	0.06	0.04

In table 41, the forecast result for EC varied much with the environment changing. The best forecast result is made when there is no pre-crack on the concrete surface, and the chloride concentration is 3%. When the chloride percentage is 3%, the forecast performance degrades with the growing of pre-cracking area. However, when the chloride percentage is 15%, the forecast performance improves with the growing of the pre-cracking size. When compared with the result generated by the linear regression model, ANN performs better when the crack width is 0.035 inch, crack depth is 1 inch and the chloride percentage is 15%.
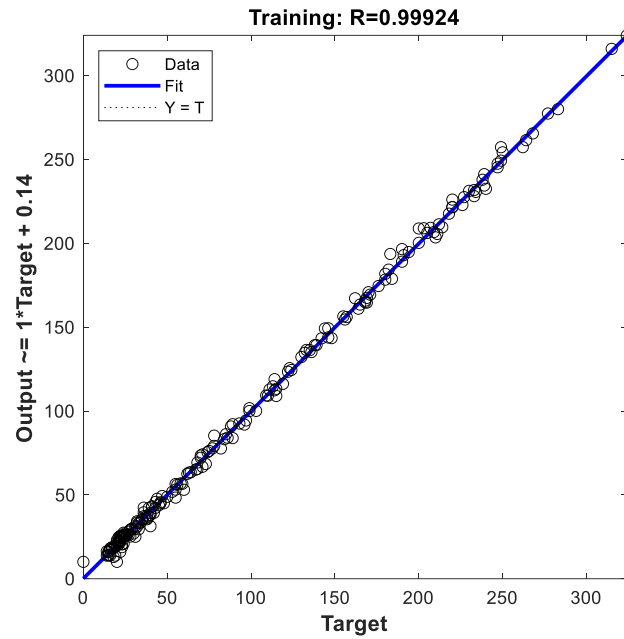
Figure 43 The training state plot for SS material

Figure 43 shows the output result and the target value when the training iterations stopped. The output result basically lines on the fitted line, which shows the ANN does good regression to the degradation process of SS rebar. Table 42 show the forecast summary for MMFX rebar.

Table 42 ANN model forecast performance under different environment for MMFX

W	0.0011	0.011	0.011	0.035	0.035
D	0.05	0.5	1	0.5	1
C=3%					
Mean	133.45	156.90	192.80	198.92	218.14
MSE	1250.58	368.52	1287.81	267.00	550.01
RMSE	35.36	19.20	35.89	16.34	23.45
RMSE/Mean	0.26	0.12	0.19	0.08	0.11
C=15%					
Mean	161.64	165.35	183.81	237.60	254.36
MSE	303.35	1051.93	1751.87	27.84	246.25
RMSE	17.42	32.43	41.86	5.28	15.69
RMSE/Mean	0.11	0.20	0.23	0.02	0.06

In table 43, for MMFX material, the RMSE/Mean for the forecast results are all greater than 0.1 when there is no crack or pre-cracking width is 0.011 inch. The best forecast result can be obtained when crack width is 0.035 inch, crack depth is 0.5 inch and the chloride percentage is 15%. When compared with the result in Table 34 generated from linear regression, the ANN gives better prediction under the condition where crack width is 0.035 inch, crack depth is 0.5 inch. Under the other eight conditions, the linear regression model can give better forecast result than the ANN gives. In total, the BP-ANN forecast for degradation level in 28th to 33rd month, with 3 input delay, performs best on BS and EC material, then is SS, the last one is MMFX material.

Figure 44 gives the relation between the regression result and the true data in the training process. The regression fitted line fits the true datapoints well. The ANN model can provide good regression result for degradation process of MMFX material.
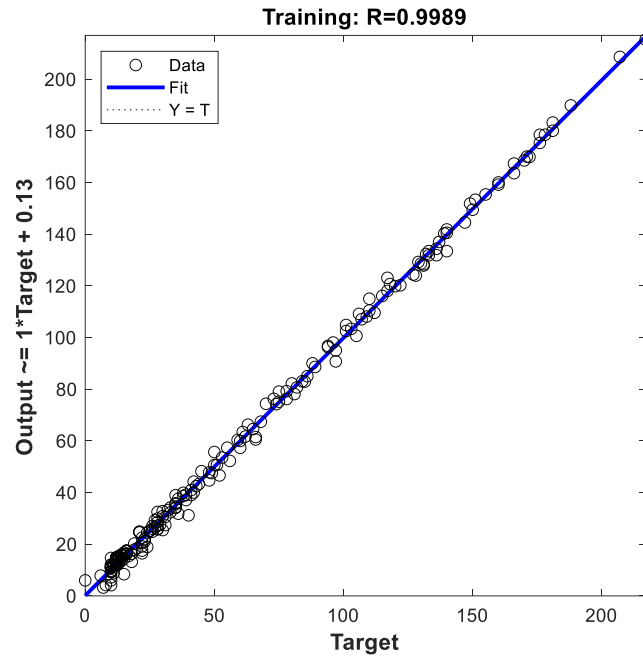
Figure 44 The training state plot for MMFX material

When the number of data reserved for forecast evaluation is reduced from 5 to 3, which means only last 3 months' data are reserved for forecast evaluation while 85% of data from 1st month to 30th month are adopted to be the training dataset, the training data will be enlarged and the period to be forecasted is shortened. Using the enlarged training set, the last 3-month degradation level are forecasted. The ANN still has 10 neurons in the first hidden layer, 3 neurons in the second hidden layer and the excitation function between the input layer and the first hidden layer is the sigmoid function. The connection between the second hidden layer to the output layer is a pure linear connection. Based on these conditions, the ANN with 3 data reserved for forecast is built and tested on BS material. Still, there are 10 ANNs created when input delay is set to be 3 and 5. Table 43 shows the average performance and the best performance of the training and forecasting.

Table 43 ANN performance for different materials using different input delay; last 3 months' data for

forecast

	Input delay is 3				Input delay is 5			
	BS	EC	SS	MMFX	BS	EC	SS	MMFX
	Best performance							
Training MSE	45.57	12.45	15.01	10.97	30.41	9.41	9.21	5.24
Testing MSE	125.82	32.45	17.98	22.71	98.27	34.90	23.48	24.98
Forecasting MSE	381.25	342.12	295.15	215.97	370.50	295.48	244.73	190.43
	Average performance							
Training MSE	37.023	14.827	12.285	11.096	32.31	9.87	8.85	6.57
Testing MSE	111.614	48.081	41.224	35.850	124.79	44.30	34.98	30.30
Forecasting MSE	832.900	462.509	410.333	610.510	689.74	438.84	369.79	303.17

In table 43, the forecasting MSE is significantly reduced when compared with the previous result. Besides, the ANN model performs better when the input delay is set to be 5 than it is set to be 3. This may because using more past data can help the ANN stay on the past tendency, which helps better performance in short time forecast. However, if a long-time forecast is needed, too much input delay may cause the ANN failed to capture the most recent changes, which leads to deviation after farther time. Besides, for BS material, enlarging the training set can improve the forecast result. The BP-ANN also performs better when given forecast for last 3-month degradation level than giving the forecast for degradation level in last five month.

5.4. Bi-directional long-short term memory neural network

The deep learning Bi-Long Short Memory (Bi-LSTM) Network is adopted to forecast the degradation level of rebars. Bi-LSTM network is a kind of RNN (Recurrent neural network), which is consisted of forward LSTM network and backward LSTM network. The structure of a bi-directional RNN is shown as Figure 45.
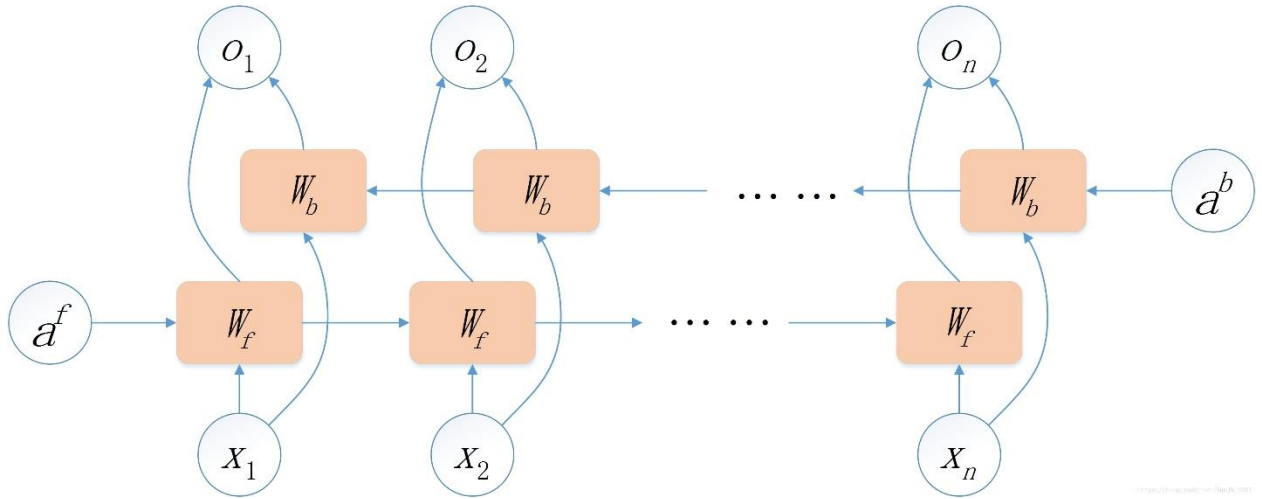
Figure 45 The structure of Bi-RNN

where a^f is the initial "output" of the forward RNN and the a^b is the initial "output" of the backward RNN. From Figure 45, compared with the general ANN, RNN can take the previous output into the account, which helps the network have memory in the previous results.

The Bi-RNN consists of two RNN with opposite calculation direction, this allows the Bi-RNN taking both the previous input data and the subsequent datapoints into account when giving the forecast. The structure of RNN allows it to consider the earlier input data. Unfortunately, RNN does not handle long sequences very well. One of the main reasons is that gradient explosion and gradient disappearance are easy to occur in RNN during training, which leads to the fact that the gradient cannot be transmitted all the way in a long sequence during training, so that RNN cannot capture the influence of long distance. Thus, the LSTM is introduced to avoid these problems.

The purpose of the Bi-LSTM is to look at a sequence both from front-to-back as well as from back-to-front. In this way, a bi-LSTM layer learns bidirectional long-term dependencies between

time steps of time series or sequence data. Compared with general ANN, Bi-LSTM can take the influence from the previous degradation record when giving forecast. Besides, Bi-LSTM also provides a good forecasting performance when the longer-time-ago record of degradation is important.

The trend for rebar degradation level under certain condition can be given using gamma-gamma two-stage degradation model. For predicted degradation levels, the value may be differing from the expected degradation level in short time. After a longer time, the tendency of the forecasted degradation level should be consistent with the tendency that gamma-gamma two-stage models shows. In this work, the differences between actual degradation level and expected degradation level from gamma-gamma two-stage model are applied to give forecast for the future degradation. The output of the Bi-LSTM plus the expected degradation level is the forecasted degradation level. The input delay is set to be 3, which means 3 previous consecutive data will be used to give one-step ahead prediction to the next data. The general data sample format in this work is shown in table 44. W_i, D_i and C_i means the stress values under condition i.

Table 44 The data sample for Bi-LSTM network

	W	D	C	$\mathbf{X}_1$	$\mathbf{X}_2$	$\mathbf{X}_3$	Y
No.1	W_i	D_i	C_i	x_1-E_1	x_2-E_2	x_3-E_3	x'_4-E_4
No.2	W_i	D_i	C_i	x_2-E_2	x_3-E_3	x_4-E_4	x'_5-E_5
…	W_i	D_i	C_i	…	…	…	…
No.27	W_i	D_i	C_i	x_{27}-E_{27}	x_{28}-E_{28}	x_{29}-E_{29}	x'_{30}-E_{30}
No.28	W_i	D_i	C_i	x_{28}-E_{28}	x_{29}-E_{29}	x'_{30}-E_{30}	x'_{31}-E_{31}
No.29	W_i	D_i	C_i	x_{29}-E_{29}	x'_{30}-E_{30}	x'_{31}-E_{31}	x'_{32}-E_{32}
No.30	W_i	D_i	C_i	x'_{30}-E_{30}	x'_{31}-E_{31}	x'_{32}-E_{32}	x'_{33}-E_{33}

In Table 44, the variables $W, D, C, \mathbf{X}_1, \mathbf{X}_2, \mathbf{X}_3$ are the input variables. The variable Y is the target, which is the dependent variable. x_i means the actual corrosion data collected at the ith month, while x'_i denotes the corrosion prediction at the ith month. E_i denotes the expected degradation

path at ith month based on gamma-gamma two stage degradation model. By giving forecast to the difference between the $x_i^{'}$ and E_i, the predicted degradation path can be find.

To get a better idea of the Bi-LSTM neural network's performance, the neural network for each reinforcement prediction is independently trained and tested ten times. The hyper-parameter setting is shown as follows, miniBatch Size = 32, Maximum number of training epoch is 600, two bidirectional LSTM (Bi-LSTM) layers are adopted, the number of hidden unites (the hidden size) in each layer is 250. Adam optimizer is used as the solver for training network. Table 45 shows the summary of the Bi-LSTM RNN performance working on forecasting degradation level for each rebar.

Table 45 Bi-LSTM performance for forecast of different materials

Best performed model				
	BS	EC	SS	MMFX
Training MSE	97.21	29.69	33.65	25.95
Testing MSE	163.05	49.69	40.61	22.90
Forecast MSE	540.02	169.59	70.59	43.66
Average performance				
Training MSE	106.53	36.36	32.15	25.02
Testing MSE	131.16	50.75	45.51	27.25
Forecast MSE	662.66	211.30	88.44	47.77
Fluctuation range				
Training MSE	97.21~112.60	29.69~41.65	28.21~39.19	22.64~26.20
Testing MSE	119.58~163.05	44.63~56.76	28.16~56.31	21.22~38.35
Forecast MSE	540.02~721.39	169.59~237.24	70.59~103.37	43.66~52.29

The fluctuation ranges in Table 45 come from 10 times independent training and forecasting result for each rebar. Compared with the performance of BP-ANN, the Bi-LSTM works better especially for SS and MMFX rebar. This is because in the real world, the degradation level in the

next month is associated with the degradation level in many previous months. For example, if the degradation level has been steadily accelerating in the last six months, it is likely that the degradation level will continue to increase in the following month, even if the increasing rate of degradation level has slowed in the previous month. Bi-LSTM networks can capture this trend of long-term dependence and thus have better performance than normal BP-ANN. Another reason is that the expected degradation level based on the gamma-gamma two-stage model is introduced as the baseline of the prediction in this forecast. This greatly reduces the uncertainty of the forecast and therefore has a better performance. Figures 46 and 47 shows the training process for BP-ANN and Bi-LSTM RNN using BS rebar degradation data, respectively.
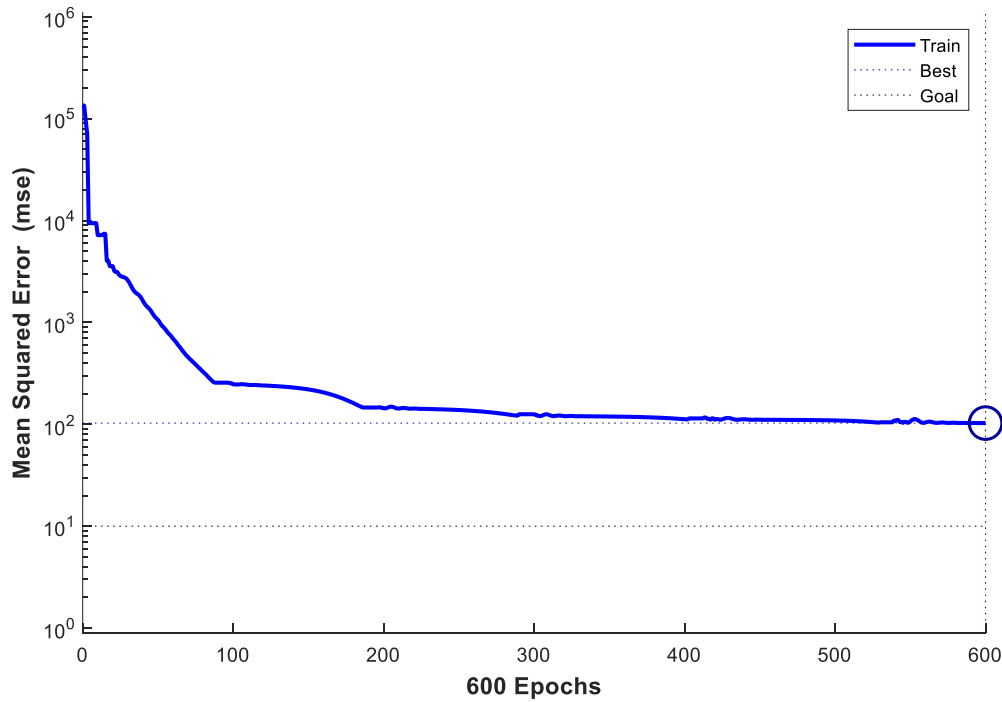
Figure 46 Training process for BP-ANN using BS degradation data
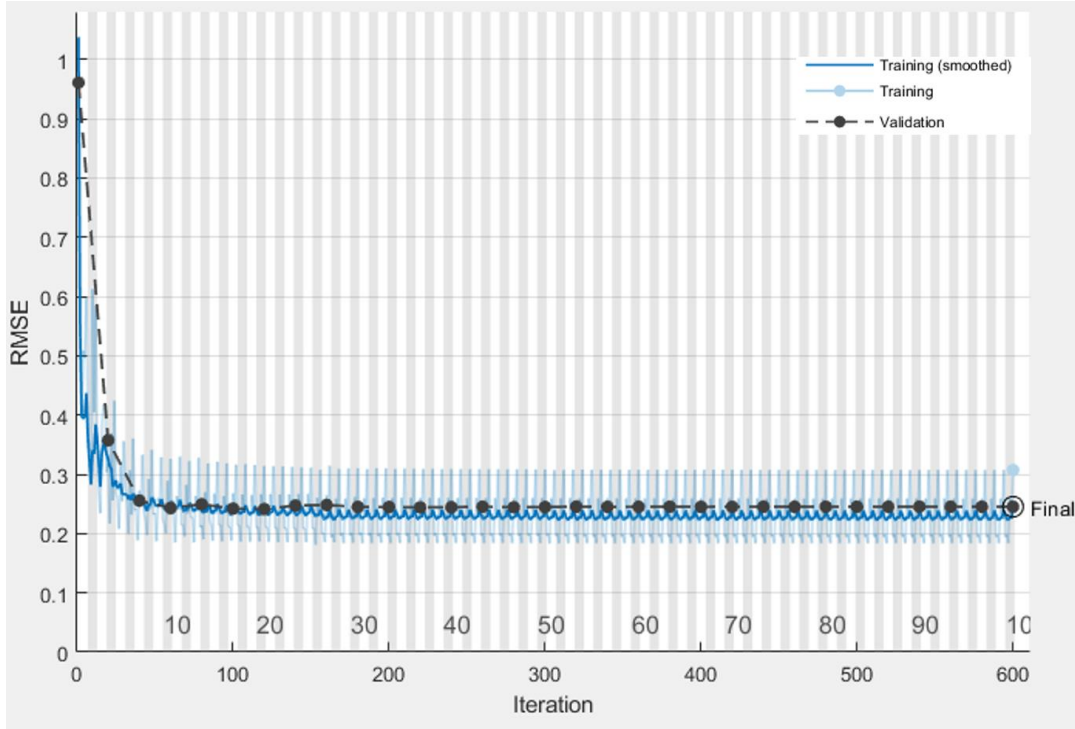
Figure 47 Training process for Bi-LSTM using BS degradation data

From Figure 46, for BP-ANN the training performance begins to become stable after about 300 iterations. From Figure 47, the convergence rate of Bi-LSTM network is faster than BP-ANN, and it will reach a relatively stable level after about 100 iterations. This comparison indicates that compared with BP-ANN, Bi-LSTM network has higher training efficiency. Figure. 48 intuitively shows the Bi-LSTM prediction results for BS in the degradation process, with uncracked concrete, $C=3\%$.

Figure 48 Actual corrosion of BS vs. three step forecasting with uncracked condition, C = 3% (Bi-LSTM)

The forecasted results march the actual degradation data well when giving 3 steps ahead prediction. The notable thing here is, the input and output here used in Bi-LSTM are x_i-E_i, which are the difference between actual or forecasted degradation level and the expected degradation level generated by gamma-gamma two stage degradation model, rather than the simple actual degradation level. Using a difference value as the output is based on the following consideration:

The neural network in this research gives forecast based on the three most recent datapoints. This is a reasonable setting because the datapoints too early ago usually have little power in the forecasting mechanism, besides, this approach can also enlarge the training set. Therefore, when giving long-term forecast, for example, a 15-months ahead forecast, the neural network takes previous predicted datapoints as the input to give the later forecast. This will lead the result that the difference between output data and input data become smaller as the epoch goes. Figure 49

shows the actual corrosion path and long-term forecasted result given by BP-ANN and Bi-LSTM, where BP-ANN directly uses degradation level as the input and output while Bi-LSTM network uses the difference as the input and output.
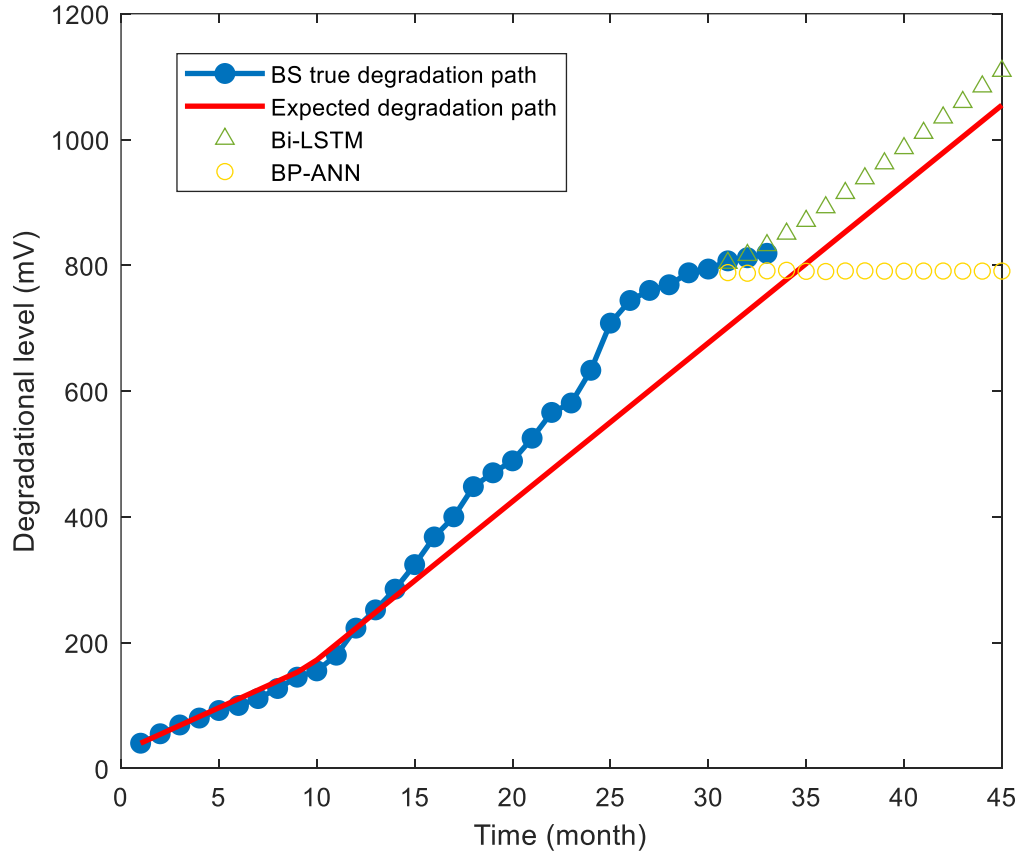

Figure 49 Actual corrosion of BS vs. 15 step forecasting with uncracked condition, C = 3%

In Figure 49, both network work fine at the initial 3 steps of the forecast. However, as the time goes, the difference between output and input of BP-ANN becomes smaller, which makes the forecasted degradation path become flat. Although the difference between input and output of Bi-LSTM network is also smaller as time goes, the E_i, expected degradation level keeps growing up, which raises the forecasted degradation path and makes it following a reasonable degradation rate. The Bi-LSTM forecasted result in Figure 49 meets the actual situation, which is, when giving a short-term forecast, the neural network takes the charge and when giving a long-term forecast, the predicted results follow gamma-gamma two stage degradation model.

6. Conclusion

This research plans to establish a model to describe the degradation process of rebars in concrete under different experiment conditions. Specifically, this study analyzed the degradation data of concrete covered rebars under different test conditions, obtained a gamma degradation process without considering the influence conditions, and analyzed the effects of crack width, crack depth, and chlorine concentration on the degradation rate. In this part, linear regression method was used to identify the effect of various factors in the model on the corrosion rate of rebar.

On this basis, a general rebar degradation model and accelerated testing degradation model are proposed. Various experimental conditions are considered in the general rebar degradation model, and the effects on the model caused by different conditions' combinations are compared. The influence of experimental conditions on the rebar degradation rate is discussed. The conclusion is the same as the actual situation.

Based on the hypothesis of acceleration experiment, the degradation model of acceleration experiment is established. This model selects the degradation process under no crack condition as the benchmark, and introduces a parameter, acceleration ratio, A. According to this model, the crack width and depth only affect the acceleration ratio, A, while the chlorine concentration will affect the degradation process for benchmark conditions. In this research, maximum likelihood estimation is used to obtain the value of parameter A, which is basically consistent with the actual physical scenario.

By observing the result between one-stage model and the actual value, and combining with the actual physical situation, a preliminary two-stage degradation model is proposed. In the first stage, the chloride ions gradually penetrate the concrete layer and the rebar coating, at which time the rebar rusts at a lower rate. In the second stage, enough chloride ions have completely passed through the concrete layer and the steel reinforcement coating, at which time the rebar rusts at a greater rate. By observing the results of the preliminary two-stage degradation model, the hypothesis that the second-stage degradation rate is not affected by the artificial concrete crack

size is proposed.

Based on the preliminary 2-stage degradation model, the advanced 2-stage degradation models are established, which includes a gamma-gamma 2-stage degradation model and a Weibull-gamma 2-stage degradation model. A reasonable assumption, which is, the degradation level is impacted by pre-cracking area and chloride concentration in stage 1 but only chloride concentration in stage 2, is made to improve and make the model more physically reasonable. Gamma-gamma model consists of two gamma process. By applying to the model to the rebars, the degradation rates for different materials under different environmental stress are calculated. The accelerated testing is also applied on the gamma-gamma 2-stage degradation model, and the corresponding accelerate factor are estimated for all four material under different conditions. The Weibull-gamma model consists of a time-to-event model and a gamma process. It assumes the time span of first degradation stage follows Weibull distribution and the second stage of degradation is a gamma process affected by only chloride concentration. The reliability function of Weibull-gamma 2-stage degradation model are derived and applied to BS and MMFX materials as an example to evaluate the impact from environmental stress variables on the rebar reliability performance.

Apart from 2-stage degradation model, the machine learning approaches are also adopted in this research. Using linear regression, the forecast for the degradation level in last five month of each material are generated. For linear regression model, the input delay does not affect much on the regression and forecasting result. The linear regression works better when the degradation level is relatively low. For all materials, the best forecast is made when there is no crack and the chloride percentage is 3%. The linear regression works better on SS and MMFX than BS than EC. 3-layer back propagated network is also used to give forecast to the degradation level in last 3 or 5 month. The number of neurons in two hidden layers is found to be 10 and 3. The interesting thing is, the forecast performance of BP-ANN is better on EC, and BS, then SS, then MMFX. The order happened to be opposite with the linear regression result. Besides, the BP-ANN works better on short-term forecast. For example, the forecast result for degradation level of BS in last 3 month is

better than it in last 5 month. When doing the forecast for degradation level in last 5 month, the 3-month input delay helps the network performs better. However, when doing forecast to last 3-month degradation data, the 5-month input delay helps to improve the forecast performance.

The general BP-ANN has two defects: 1) the ANN cannot take long-term dependent relation into account when giving forecast. 2) the ANN cannot give long-term forecast; it can only perform well when giving a 3- or 5-month future forecast. To solve these problem, Bi-LSTM network with gamma-gamma two stage degradation model related input/output adjustment are applied. The Bi-LSTM can take the long-term dependent relation when giving forecast. It improves the forecast performance, especially for SS and MMFX rebar degradation. On the other hand, the adjustment in input and output combines the Bi-LSTM network and gamma-gamma two stage degradation model. When giving long term forecast, the model can perform as 2-stage degradation models to give a correct degradation tendency. When giving short-term forecast, the model can consider the recent actual degradation levels and give more accurate forecast.

References

[1]   B. Bavarian and L. Reiner, "Migrating corrosion inhibitor protection of steel rebar in concrete," Mater. Performance, vol. 42, no. 2, pp. 3-5, 2003.

[2]   G. H. Koch, M. P. Brongers, N. G. Thompson, Y. P. Virmani, and J. H. Payer, "Corrosion cost and preventive strategies in the United States," United States. Federal Highway Administration2002.

[3]   A. C. 222, "Guide to Design and Construction Practices to Mitigate Corrosion of Reinforcement in Concrete Structures," American Concrete Institute2011, Available: http://dl.mycivil.ir/dozanani/ACI/ACI%20222.3R-11%20Guide%20to%20Design%20and%20Construction%20Practices%20to%20Mitigate%20Corrosion%20of%20Reinforcement%20in%20Concrete%20Structures_MyCivil.ir.pdf.

[4]   Park, Sang-Soon. Kwon, Seung-Jun. and Jung, Sang Hwa. (2012). "Analysis technique for chloride penetration in cracked concrete using equivalent diffusion and permeation." *Construction and Building Materials* **29**: 183-192.

[5]   B. M. Phares, F. S. Fanous, T. J. Wipf, Y.-S. Lee, and M. J. Jolley, "Evaluation of Corrosion Resistance of Different Steel Reinforcement Types," 2006.

[6]   Yuan, Fenghua. Zhang, Qing. and Xia, Xiaozhou. (2019). "Effect of Reinforcement Corrosion Sediment Distribution Characteristics on Concrete Damage Behavior." *Computers, Materials & Continua* **58**(3): 777-793.

[7]   James, A. Bazarchi, E. and Chiniforush, Alireza A. (2019). "Rebar corrosion detection, protection, and rehabilitation of reinforced concrete structures in coastal environments: A review." *Construction and Building Materials* **224**: 1026-1039.

[8]   Mohamed, Nedal. Boulfiza, Mohamed. and Evitts, Richard. (2012). "Corrosion of Carbon Steel and Corrosion-Resistant Rebars in Concrete Structures Under Chloride Ion Attack." *Journal of Materials Engineering and Performance* **22**(3): 787-795.

[9]   Reinforcing Steel Comparative Durability Assessment and 100-year Service Life Cycle Cost Analysis Report, Tourney Consulting Group LLC. June 2016. from https://www.cmc.com/de/americas/our-businesses/performance-steel/chromx/corrosion-resistance

[10]   Tuutti, K. (1982). Corrosion of steel in concrete. Swedish Cement and Concrete Research Institute, Stockholm.

[11]   Z. S. Ye and M. Xie, "Stochastic modelling and analysis of degradation for highly reliable products," Applied Stochastic Models in Business and Industry, vol. 31, no. 1, pp. 16-32, 2015.

[12]   X. Wang, "Wiener processes with random effects for degradation data," Journal of Multivariate Analysis, vol. 101, no. 2, pp. 340-351, 2010/02/01/ 2010.https://doi.org/10.1016/j.jmva.2008.12.007.

[13]   M. Otieno, M. Alexander, and H.-D. Beushausen, "Corrosion in cracked and uncracked concrete–influence of crack width, concrete quality and crack reopening," Magazine of Concrete Research, vol. 62, no. 6, pp. 393-404, 2010.

[14]   N. Yousefi, D. W. Coit, S. Song, and Q. Feng, "Optimization of on-condition thresholds for a system of degrading components with competing dependent failure processes," Reliab. Eng. Syst. Saf., vol. 192, p. 106547, 2019/12/01/ 2019.https://doi.org/10.1016/j.ress.2019.106547.

[15]   N. Chen, Z.-S. Ye, Y. Xiang, and L. Zhang, "Condition-based maintenance using the inverse Gaussian degradation model," European Journal of Operational Research, vol. 243, no. 1, pp. 190-199, 2015/05/16/ 2015.https://doi.org/10.1016/j.ejor.2014.11.029.

[16]   V. R. Joseph and I. T. Yu, "Reliability improvement experiments with degradation data," IEEE Transactions on Reliability, vol. 55, no. 1, pp. 149-157, 2006.10.1109/TR.2005.858096.

[17]   D. Kong, N. Balakrishnan, and L. Cui, "Two-Phase Degradation Process Model With Abrupt Jump at Change Point Governed by Wiener Process," IEEE Transactions on Reliability, vol. 66, no. 4, pp. 1345-1360, 2017.10.1109/TR.2017.2711621.

[18]   J. Feng, Q. Sun, and T. Jin, "Storage life prediction for a high-performance capacitor using multi-phase Wiener degradation model," Communications in Statistics-Simulation and Computation, vol. 41, no. 8, pp. 1317-1335, 2012.

[19]   X. Ni, J. Zhao, W. Song, C. Guo, and H. Li, "Nonlinear degradation modeling and maintenance policy for a two-stage degradation system based on cumulative damage model," Eksploatacja i Niezawodność, vol. 18, 2016.

[20]   M. Fouladirad and A. Grall, "On-line change detection and condition-based maintenance for systems with unknown deterioration parameters," IMA Journal of Management Mathematics, vol. 25, no. 2, pp. 139-158, 2012.10.1093/imaman/dps032.

[21]   J.-X. Zhang, C.-H. Hu, X. He, X.-S. Si, Y. Liu, and D.-H. Zhou, "A novel lifetime estimation method for two-phase degrading systems," IEEE Transactions on Reliability, vol. 68, no. 2, pp. 689-709, 2018.

[22]   P. Wang, Y. Tang, S. J. Bae, and A. Xu, "Bayesian Approach for Two-Phase Degradation Data Based on Change-Point Wiener Process With Measurement Errors," IEEE Transactions on Reliability, vol. 67, no. 2, pp. 688-700, 2018.10.1109/TR.2017.2785978.

[23]   Q. Dong and L. Cui, "A study on stochastic degradation process models under different types of failure thresholds," Reliab. Eng. Syst. Saf., vol. 181, pp. 202-212, 2019.

[24]   Park, C. and W. J. Padgett (2006). "Stochastic Degradation Models with Several Accelerating Variables." *IEEE Transactions on Reliability* **55**(2): 379-390.

[25]   Lawless, J. and Crowder, M. (2004) Covariates and Random Effects in a Gamma Process Model with Application to Degradation and Failure. *Lifetime Data Analysis,* **10***,* 213–227

[26]   Cholette, M. E. Yu, Hongyang. Borghesani, Pietro. Ma, Lin. and Kent, Geoff. (2019). "Degradation modeling and condition-based maintenance of boiler heat exchangers using

gamma processes." *Reliability Engineering & System Safety* **183**: 184-196.

[27]   Ling, Man Ho. Tsui, Kwok Leung. and Balakrishnan, Narayanaswamy. (2015). "Accelerated Degradation Analysis for the Quality of a System Based on the Gamma Process." *IEEE Transactions on Reliability* **64**(1): 463-472.

[28]   M. H. Ling, H. K. T. Ng, and K. L. Tsui, "Bayesian and likelihood inferences on remaining useful life in two-phase degradation models under gamma process," Reliab. Eng. Syst. Saf.*, vol. 184, pp. 77-85, 2019/04/01/ 2019.https://doi.org/10.1016/j.ress.2017.11.017.

[29]   W.-a. Yan, B.-w. Song, G.-l. Duan, and Y.-m. Shi, "Real-time reliability evaluation of two-phase Wiener degradation process," Communications in Statistics - Theory and Methods*, vol. 46, no. 1, pp. 176-188, 2017/01/02 2017.10.1080/03610926.2014.988262.

[30]   X. Wang, P. Jiang, B. Guo, and Z. Cheng, "Real-time reliability evaluation with a general Wiener process-based degradation model," Qual. Reliab. Eng. Int.*, vol. 30, no. 2, pp. 205-220, 2014.

[31]   D. Wang and K.-L. Tsui, "Two novel mixed effects models for prognostics of rolling element bearings," Mechanical Systems and Signal Processing*, vol. 99, pp. 1-13, 2018/01/15/ 2018.https://doi.org/10.1016/j.ymssp.2017.06.004.

[32]   J. Zhou, N. Huang, D. W. Coit, and F. A. Felder, "Combined effects of load dynamics and dependence clusters on cascading failures in network systems," Reliab. Eng. Syst. Saf., vol. 170, pp. 116-126, 2018.

[33]   Dong, Q. and L. Cui (2019). "A study on stochastic degradation process models under different types of failure Thresholds." *Reliability Engineering & System Safety* **181**: 202-212.http://www.sampleurl.com/sampleURL

[34]   Chen, N. & Tsui, K.L. (2013) Condition monitoring and remaining useful life prediction using degradation signals: Revisited, *IIE Trans*., 45(9), 939-952.

[35]   J. Zhou, Z. Li, H. Nassif, and D. W. Coit, "A two-stage Weibull-gamma degradation model with accelerated failure mechanism initiation and propagation", Rutgers, the State

University of New Jersey, Technical Report 2020.

[36] J. Zhou, H. Al-Nawadi, H. Nassif, , Z. Li, and D. W. Coit, "An enhanced corrosion analysis testing method for reinforced concrete bridge deck rebars based on effective pre-cracking," Rutgers, the State University of New Jersey, Technical Report 2020.

[37] Wang, X.L, Jiang, P., Guo, B. & Cheng, Z.J. (2014) Real-time reliability evaluation for an individual product based on change-point Gamma and Wiener process, Qual. Reliab. Engng. Int., 30 (4), 513–525.

[38] Z. Ye, L. Chen, L. C. Tang, and M. Xie, "Accelerated Degradation Test Planning Using the Inverse Gaussian Process," IEEE Transactions on Reliability, vol. 63, no. 3, pp. 750-763, 2014.10.1109/TR.2014.2315773.

[39] E. A. Elsayed, "Reliability Engineering, 1996," Addison Wes-Iey, 1996.

[40] M. Otieno, M. Alexander, and H.-D. Beushausen, "Corrosion in cracked and uncracked concrete–influence of crack width, concrete quality and crack reopening," Magazine of Concrete Research, vol. 62, no. 6, pp. 393-404, 2010.

[41] A. Xu and A. Shayan, "Relationship between reinforcing bar corrosion and concrete cracking," ACI Mater. J., vol. 113, no. 1, p. 3, 2016.

[42] C. Arya and F. Ofori-Darko, "Influence of crack frequency on reinforcement corrosion in concrete," Cem. Concr. Res., vol. 26, no. 3, pp. 345-353, 1996.

[43] K. Tuutti, *Corrosion of steel in concrete*. Cement-och betonginst., 1982.

[44] N. Yousefi, D. W. Coit, and X. Zhu, "Dynamic maintenance policy for systems with repairable components subject to mutually dependent competing failure processes", Computers & Industrial Engineering, vol. 143, 2020